Polytechnic
UNIVERSITY

AD-A194 269

POLY-WRI-1551-88

Wide Band Gyrotron Traveling
Wave Amplifier Analysis

A. Rekiouak and B. R. Cheo

Route 110 Farmingdale, New York

POLY-WRI-1531-88

Wide Band Gyrotron Traveling
Wave Amplifier Analysis

A. Rekiouak and B. R. Cheo

Weber Research Institute
Polytechnic University
Farmingdale, New York 11735

DTIC
ELECTE
APR 1 3 1988
H

88

REPORT DOCUMENTATION PAGE

1a. REPORT SECURITY CLASSIFICATION	1b. RESTRICTIVE MARKINGS
Unclassified	

2a. SECURITY CLASSIFICATION AUTHORITY	3. DISTRIBUTION / AVAILABILITY OF REPORT
2b. DECLASSIFICATION / DOWNGRADING SCHEDULE	Approved for public release; distribution unlimited.

4. PERFORMING ORGANIZATION REPORT NUMBER(S)	5. MONITORING ORGANIZATION REPORT NUMBER(S)
	ARO 23282.1-PH-A

6a. NAME OF PERFORMING ORGANIZATION	6b. OFFICE SYMBOL (If applicable)	7a. NAME OF MONITORING ORGANIZATION
Polytechnic Inst of New York		U. S. Army Research Office

6c. ADDRESS (City, State, and ZIP Code)	7b. ADDRESS (City, State, and ZIP Code)
Farmingdale, NY 11735	P. O. Box 12211 Research Triangle Park, NC 27709-2211

8a. NAME OF FUNDING / SPONSORING ORGANIZATION	8b. OFFICE SYMBOL (If applicable)	9. PROCUREMENT INSTRUMENT IDENTIFICATION NUMBER
U. S. Army Research Office		DAAG29-85-K-0258

8c. ADDRESS (City, State, and ZIP Code)	10. SOURCE OF FUNDING NUMBERS			
P. O. Box 12211 Research Triangle Park, NC 27709-2211	PROGRAM ELEMENT NO.	PROJECT NO.	TASK NO.	WORK UNIT ACCESSION NO.

11. TITLE (Include Security Classification)

Wide Band Gyrotron Graveling Wave Amplifier Analysis

12. PERSONAL AUTHOR(S) A. Reklioak and B. R. Cheo

13a. TYPE OF REPORT	13b. TIME COVERED	14. DATE OF REPORT (Year, Month, Day)	15. PAGE COUNT
Final	FROM 10/15/85 TO 2/29/88		118

16. SUPPLEMENTARY NOTATION The view, opinions and/or findings contained in this report are those of the author(s) and should not be construed as an official Department of the Army position, policy, or decision, unless so designated by other documentation.

17.	COSATI CODES		18. SUBJECT TERMS (Continue on reverse if necessary and identify by block number)
FIELD	GROUP	SUB-GROUP	Gyrotron Amplifier, Waveguide Circuits, Cylindrical Waveguides, Small Signal Analysis, Nonlinear Analysis

19. ABSTRACT (Continue on reverse if necessary and identify by block number)

Linear and non-linear analyses on a gyrotron amplifier with a periodically disc-loaded cylindrical waveguide circuit are performed. The dispersion relation of the circuit allows for wideband interaction with a relativistic beam of moderate power (V_b = 60kV, I_b = 5A). Linear analysis of the interaction with the fundamental mode shows a gain of the

20. DISTRIBUTION / AVAILABILITY OF ABSTRACT	21. ABSTRACT SECURITY CLASSIFICATION
☐ UNCLASSIFIED/UNLIMITED ☐ SAME AS RPT. ☐ DTIC USERS	Unclassified

22a. NAME OF RESPONSIBLE INDIVIDUAL	22b. TELEPHONE (Include Area Code)	22c. OFFICE SYMBOL

DD FORM 1473, 84 MAR   83 APR edition may be used until exhausted.   SECURITY CLASSIFICATION OF THIS PAGE
All other editions are obsolete.

UNCLASSIFIED

order of 50-60dB/m over a bandwidth larger than 22% and a linear phase versus frequency characteristic. Non linear analysis predicts the following saturation characteristics: a 48kW peak output power at 5.3GHz with 16% efficiency. The saturation length of the tube is about 37cm.

These results show that this device is competitive with conventional high power traveling wave devices in performance, and, being simpler in structure, also in cost.

ABSTRACT

WIDE BAND GYROTRON TRAVELING
WAVE AMPLIFIER ANALYSIS

A.Rekiouak and B.R.Cheo

December 1987

Linear and non-linear analyses on a gyrotron amplifier with a periodically disc-loaded cylindrical waveguide circuit are performed. The dispersion relation of the circuit allows for wideband interaction with a relativistic beam of moderate power (V_b = 60kV, I_b = 5A). Linear analysis of the interaction with the fundamental mode shows a gain of the order of 50-60dB/m over a bandwidth larger than 22% and a linear phase versus frequency characteristic. Non linear analysis predicts the following saturation characteristics: a 48kW peak output power at 5.3GHz with 16% efficiency. The saturation length of the tube is about 37cm.

These results show that this device is competitive with conventional high power traveling wave devices in performance, and, being simpler in structure, also in cost.

ACKNOWLEDGEMENT

Accession For	
NTIS GRA&I	☑
DTIC TAB	☐
Unannounced	☐
Justification	
By	
Distribution/	
Availability Codes	
Dist	Avail and/or Special
A-1	

TABLE OF CONTENTS

CHAPTER 1

INTRODUCTION

Gyrotrons belong to a class of vacuum electron devices whose operating principle is based on the relativistic interactions between the transverse rf fields and the gyrating electron beams, [1]-[8]. The basic physical principle underlying the operation of gyrotron devices is sometimes referred to as cyclotron maser instability (CMI). It is generally aknowledged that Twiss [9] in 1958 was the first to recognize it as an amplifying mechanism for free electron gyroradiation. Since then, research in the CMI/gyrotron effect has been very active in understanding the phenomenon, finding applications and tapping this new source of radiation.

Most of the work on gyrotrons has concentrated in the past in achieving high power, efficient MM wave oscillators for plasma heating experiments. Considerable success has been reported in this area. Andronov et al,[10], reported on experiments with gyrotrons that operated at MM wavelength with output power over 1MW within a pulse duration of about 10^{-4}s. In one of the experimental gyrotrons operating at 3mm wavelength, a pulsed ouput power of as much as 2.1MW was reportedly attained, [11] cited in [15]. Other frequencies

were investigated and, in an experiment with a gyromonotron using a TE_{01} circular mode and operating at 35GHz, a peak output power of about 150kW with a 31% efficiency at 100kW was achieved, [12]; a gyrotron operating at the same 35GHz frequency but using a TE_{04} mode, [13], achieved output powers of 320kW with an efficiency of 40%. Boucher et al. [14], achieved 150kW output power at the same frequency (35GHz) using a TE_{02} circular mode. Fix, Flyagin et al. reported in [15] results such as 100kW quasi-CW output power of 3mm wavelength, 150kW with 10% efficiency at 5.6mm, 140kW with 25% efficiency at 9mm. Jory, Friedlander et al., [16], built a pulsed gyrotron which produced 248kW peak output power at 28GHz and 34% efficiency. Symons and Jory, [17], achieved 212kW CW output power at 28GHz.

Although gyrotrons oscillators have had some success as rf sources for plasma heating in fusion devices, their lack of signal coherence and the higher signal quality required for applications in radar and communications has eliminated them as potential sources in those applications. However, another possible application of the CMI effect has been identified: since as an oscillator it is not a source suitable for radar/communication purposes, it is of interest to look into the possibility of achieving high quality amplifier application of the basic CMI effect.

To be regarded as a high quality amplifier, it is well accepted that the device should have large instantaneous bandwidth, and also nearly linear phase versus frequency characteristics. It is in these aspects that the gyrotron amplifier effort has been less than successful. A C-band gyro-TWT experiment at Varian was performed by Symons, Jory, Ferguson and Valier, [18]-[19]. In this experiment, the fundamental electron cyclotron frequency of the beam interacts with the TE_{11} dominant waveguide mode: an output power of 50kW with 16.6% efficiency and 6% bandwidth was achieved, [15]. Higher power outputs or larger bandwidths were achieved using various beam powers. The largest instantaneous bandwidth was 9.3% for 18.8kW peak output power at a 9.8% efficiency for a 40kV-4A beam power. Another experiment by Park, Chu et al., [20], reported a 20kW power output at 6GHz with a 10% efficiency, but a bandwidth no better than 3.7%. Very little information on the phase characteristic was reported in these experiments.

The reason for the narrow bandwidth is well understood: the rapid increase of the group velocity as a function of frequency in a smooth walled waveguide circuit allows the interaction between the beam and the wave to take place over only a very narrow band. Chapter 2 shows that the best operating condition is when the beam mode and waveguide mode are tangent, the so-called grazing condition. In this case,

the frequency band where the instability is excited (i.e., where amplification can occur) is centered at the tangential point, with not much "elbow room" (see figure 1.1). Research to overcome this drawback is very active, and several schemes to improve the bandwidth have been suggested. Barnett, Lau, Chu and Granatstein, [21], used a tapered waveguide circuit in an experiment that achieved a small signal 3-dB bandwidth of 13% with 18-dB gain at midband(35 GHz). The same investigators suggested another structure using a tapered waveguide as well as a tapered external magnetic field profile: they calculated that a saturated bandwidth greater than two octaves is possible for both TE_{01} and TE_{11} modes, [22]. A tapered two-stage structure with a tapered magnetic field was proposed by Ganguly and Ahn, [23]: their calculations showed that a 45% bandwidth at 45dB gain and 25% efficiency is possible if the axial velocity spread of the beam is zero; they found however that both the gain and the bandwidth are very sensitive to the degree of the beam velocity spread, to the external magnetic field profile, and the various beam and circuit parameters; the expression for the efficiency was derived under a quasi-linear approximation. Since these proposals were made several years ago, no experimental results have yet been reported.

Another concept for increasing the bandwidth of the gyro-TWT is to slow down the wave such as to match the beam

axial velocity over a relatively large frequency range. In other words, the idea suggested here is to find a structure capable of maintaining the grazing condition over a large enough frequency range. Several slow wave structures have been proposed, including dielectric loading of the waveguide [24], helix loaded waveguide [25]-[26], and disc-loaded waveguide [26]-[27]. No experimental results on these approaches have been reported either.

Choe and Uhm, [26], investigated the disc loaded waveguide in connection with the gyrotron application. Using the TE_{01} mode, they found that the group velocity of the wave can be adjusted by varying the disc inner and outer radii a and b, and the spacial period L (see figure 1.2 for notation). However, the TE_{01} mode is not the only propagating mode in this structure and hence, mode competition, [28], is a possible shortcoming that has to be addressed. On the other hand, the TE_{01} mode is the only one which excites pure TE modes at the discontinuities, thus simplifying the analysis of the fields in this structure. The only calculation given in [26] on the gain versus frequency showed finite but strongly frequency dependent gain over a larger than usual bandwidth (13%). It is our understanding that this idea is not pursued at NSWC any longer.

In the present effort, we also analyse the periodically disc-loaded cylindrical waveguide for gyro-TWT applica-

tion, but using the hybrid H_{11} mode. The principal goal of this study is not to achieve a MM wave device, but to achieve a device for S to K band range applications of sufficiently high quality that it can compete with conventional TWT's in both performance and cost. The choice of the H_{11} hybrid mode shall be elaborated further later on.

Chapter 2 describes the general approach to the problem. It describes the reasoning leading to the desired circuit dispersion characteristic. In chapter 3, we show that the cold circuit dispersion relation can be accurately described by a polynomial of the form

$$k_o{}^2 = a_4k^4 + a_2k^2 + a_o$$

in the first Brillouin zone. We make use of the polynomial approximation for the cicuit dispersion relation to obtain the gain, small signal bandwidth and the phase characteristics of the gyrotron effect. These results from the small signal (linear) analyses were obtained in the two cases of a spacial growth (complex wavenumber, real frequency) and of a temporal instability (complex frequency, real wavenumber).

In chapter 4, the periodically disc loaded cylindrical waveguide is analyzed. The dispersion relation obtained numerically is compared to the experimental results whenever

possible. The results are then fitted with the polynomial approximation. The circuit analysis was for an $\exp(j\phi)$ azimuthal variation for which the Floquet modes are hybrid.

Chapter 5 is a presentation of the non-linear analysis based on the phase averaging technique developed by Kuo and Cheo, [29]-[30], and adapted to the present structure. Saturated gain, bandwidth, output power and efficiency are presented.

The last chapter compares the results obtained to those published for different configurations, identifies and discusses some pertinent issues for further work.

Two appendices are included for convenience of the readers:

> * Appendix A details the linear dispersion rela-
> tion derivation for TE modes [31] and for TM
> modes;
> * Appendix B is the derivation of the non linear
> integro-differential equation.

A list of references is provided at the end.

Fig. 1.1

Smooth wall waveguide and three beam characteristics

- beam 1 shows two competing interaction points

- beam 2 satisfies the grazing condition
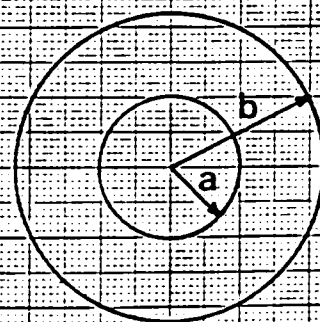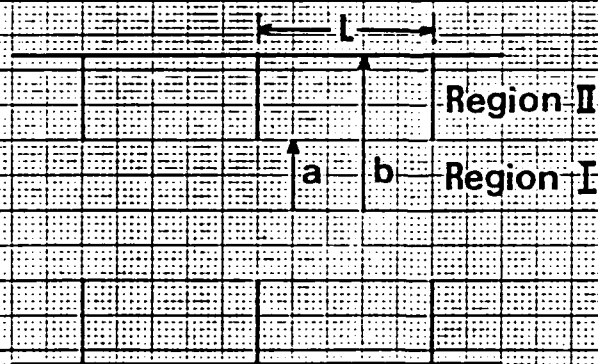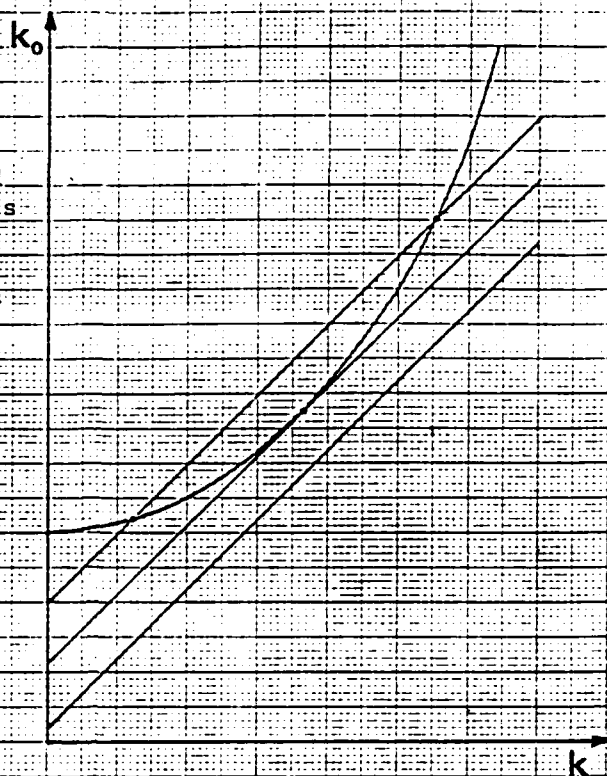
- beam 3 shows minimal or no coupling

Fig. 1.2

Geometry of the periodically disc-loaded waveguide circuit

CHAPTER 2

GENERAL APPROACH

Most of the works on gyro-TWT's done in the past used structures of the smooth wall type, i.e., parallel plate waveguides, rectangular or cylindrical waveguides. All these structures have in common the fact that they support super-luminous waves. The dispersion relation for these structures is the typical hyperbola

$$(\frac{\omega}{c})^2 - (k^2 + k_c^2) = 0 \qquad (2.1)$$

where k_c is the cutoff wave number determined only by the waveguide geometry, and is therefore independant of both the frequency ω and the propagation constant k.

A beam propagating in a helical trajectory along the waveguide will interact with this superluminous wave. The electrons will experience forces that vary as

$$F = F_o e^{j(\omega t - kz)}$$

If the beam is periodic, and its velocity in the

transverse plane varies as

$$v_t = v_o \cos k_b z$$

then the rate of change of the energy of the electrons will be

$$\frac{dE}{dt} = v_o F_o \cos k_b z \, e^{j(\omega t - kz)}$$

$$= \frac{1}{2} v_o F_o \left[e^{j(\omega t - kz - k_b z)} + e^{j(\omega t - kz + k_b z)} \right]$$

The energy exchange shows two components, but only the one traveling slower than the wave is of interest. Indeed, when the slower wave is traveling at about the same speed as the electrons in the longitudinal direction, cumulative bunching and energy extraction can occur. This is described by

$$\omega t - (k + k_b)z = (\omega - kv_z - \Omega)t$$

where $v_z \approx z/t$ is the electron velocity in the z-direction, and $k_b = \Omega/v_z$ describes the periodicity of the beam.

Therefore, when the Doppler shifted wave frequency, $\omega - kv_z$, is equal to the cyclotron frequency Ω, the slower wave of energy exchange is in synchronism with the beam: this is

known as the grazing condition. This description does not explain the need of actually having a slightly higher operating frequency than the Doppler shifted cyclotron frequency, a concept known in the community as $\Delta\omega > 0$. However, the results of computing the hot tube dispersion relation self-consistently shall indeed show that the modes with gain must have also higher operating frequency, fulfilling $\Delta\omega > 0$.

The problem is that this synchronism cannot be maintained over a large frequency band: the rapid increase of the group velocity as a function of frequency in a smooth waveguide circuit allows only a very narrow band interaction. Therefore, for the interaction to be maintained over a larger band, the group velocity should not vary much over all the required band. In fact, the group velocity of the wave should be close to the beam velocity in the longitudinal direction in order to maintain large band interaction. This can be seen through the following:

the beam mode is defined by

$$\omega = kv_z + \Omega \tag{2.2}$$

and the goup velocity of the wave by $d\omega/dk$ which must be equal to v_z to maintain synchronism. That is, the best possible case is to have the beam z-velocity and

the wave group velocity equal over as large a frequency
band as possible.

How can this be achieved?

In a smooth wall waveguide, the transverse wavenumber
k_c is a constant, determined only by the geometry of the
guide, and not by either ω or k. As such, it is not possible
to match the waveguide dispersion relation (eq 2.1) to that
of the beam (eq 2.2). However, if we can make the transverse
wave number ω or k dependant, then we give ourselves the
possibility of having more control over the variations of
the group velocity of the wave.

In the derivation of the smooth wall waveguide disper-
sion relation (eq. 2.1), the left hand side represents the
Helmholtz operator $\nabla^2 + (\omega/c)^2$. If an artificial boundary
can be created such that k_c is no longer a constant but ω or
k dependant, the Helmholtz operator representation on the
LHS of (eq 2.1) is replaced by a different function $f(\omega,k)$;
and $f(\omega,k) = 0$ is the circuit dispersion relation. Moreover,
if this relation can be matched to the beam dispersion
relation (eq 2.2) over a wide frequency range, the operating
bandwidth should then increase accordingly. We need there-
fore to find a slow wave structure so that the group velo-
city of the wave matches the beam velocity down the wavegui-
de. A circuit that can achieve the two stated purposes

(i.e., a transverse wave number ω or k dependant, and a group velocity about constant over a large operating band) may be found in the form of a periodic structure.

Indeed, the dispersion relation of a periodic structure shows (figures 2.1 and 2.2) the existence of a region in the passband where ω versus k is nearly a straight line (we are interested only in the lowest pass band and in the first Brillouin zone in this region). Choosing the beam parameters accordingly (that is, in such a way as to make the two slopes almost equal over the range) should solve our bandwidth problem: gain can be achieved over a larger frequency band.

Before proceeding further, two important points need to be made :

1. In a periodic structure, the rf field, as per Floquet theorem, is given in general by

$$\mathbf{E} = \sum_{p=-\infty}^{\infty} \mathbf{E_p}(r,\phi)\exp(-jk_pz) \qquad (2.3)$$

where

$$k_p = k + (2p\pi/L)$$

L is the spacial period

Representing the Helmholtz operator on the LHS of (2.1) by a simple algebraic function $f(\omega,k)$ can be applied to the

fundamental Floquet mode (the term p = 0) only. It is shown in chapter 4 that, by using the exp(jϕ) mode and properly choosing the dimensions of the structure, it is possible to have the beam interact strongly only with the p = 0 term, and minimally with the other terms which are evanescent, decreasing exponentially toward the axis from r = a. Further more, these other modes, propagating in both directions, all have much slower phase velocity, and hence do not interact effectively with the beam.

2. In addition to TE waves, the periodic discontinuities shall also introduce TM terms which should in principle be taken into account. That is, in $E_p(r,\phi)$ of equation (2.3), there is a TM part as well as a TE part. For the p = 0 term, the combined TE and TM parts form the modal field which interact with the beam. Thus, contained in the linear gyrotron dispersion relation, should also be the contributions by the TM part. However, the TM contribution is negligible and becomes zero when the grazing condition is met[*].
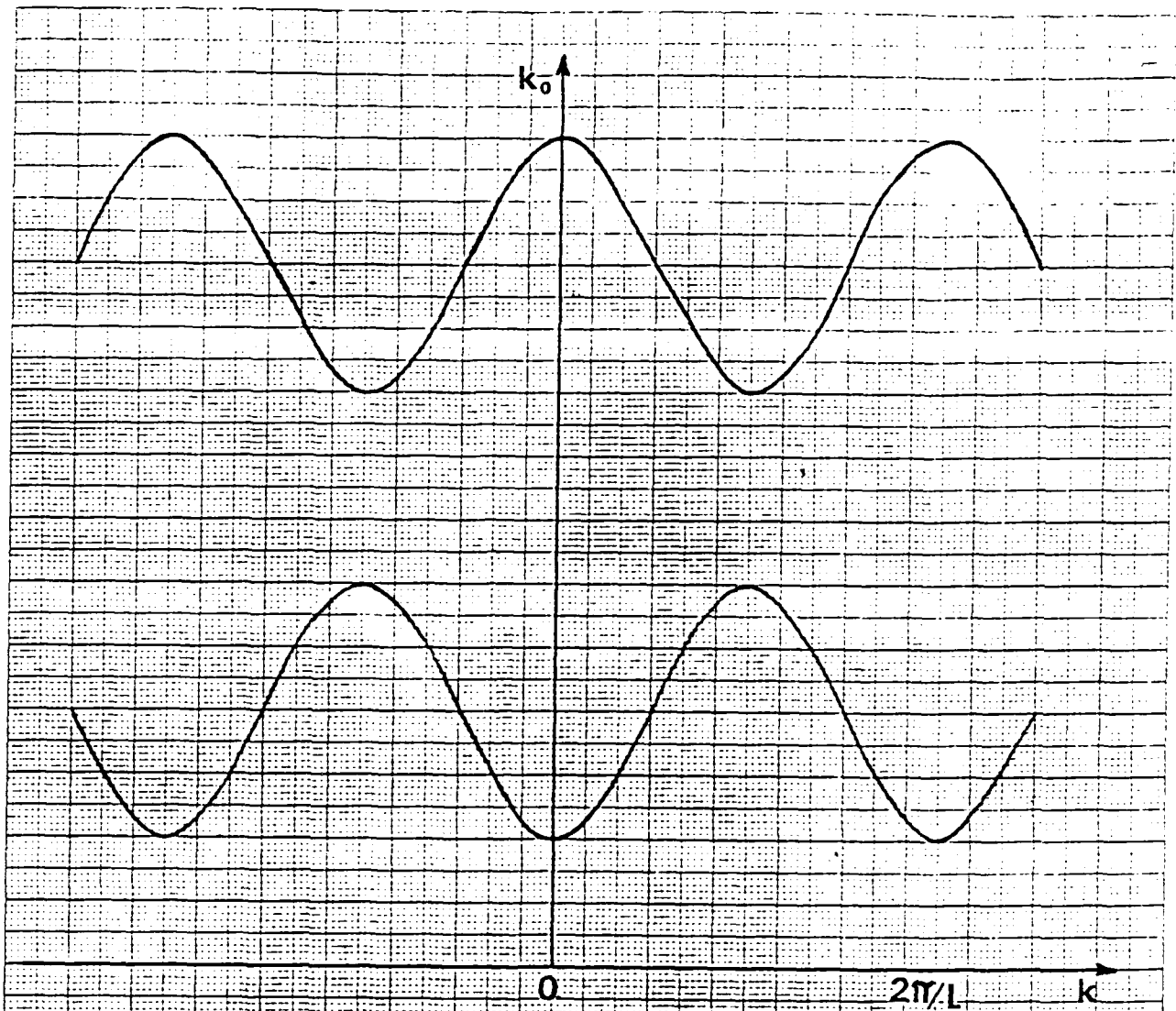
---

[*] S.P.Kuo, private communication.

Fig. 2.1
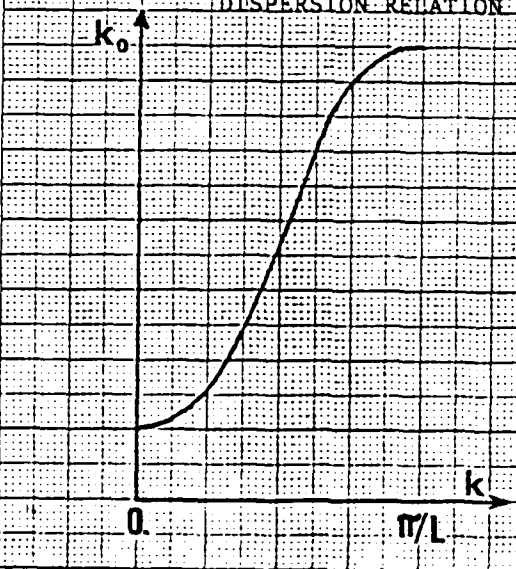DISPERSION RELATION OF A PERIODIC STRUCTURE

Fig. 2.2
FIRST BRILLOUIN ZONE

CHAPTER 3

SMALL SIGNAL ANALYSIS

3.1 The polynomial approximation:

In the previous chapters we explained how it is pos-
sible to overcome the limitation on the bandwidth of a
gyro-TWT by using a periodic structure instead of a smooth
walled structure. The propagating mode in this circuit will
be the fundamental TE_{11} mode since we are interested in the
C/S frequency band. However, the periodically disc-loaded
cylindrical waveguide which we will investigate for gyro-TWT
application will excite all of the Floquet terms of the TE_{1n}
and TM_{1n} modes for an $\exp(j\phi)$ azimuthal variation.

In such a circuit, the higher Floquet modes (that is
for $p \neq 0$) do not interact with the beam, when the latter
is confined near the axis and the higher modes are evanes-
cent, and when the choice of the waveguide dimensions are
properly made. Representation of the Helmholtz operator

$$\nabla^2 + \left(\frac{\omega}{c}\right)^2 \qquad \text{by} \qquad \left(\frac{\omega}{c}\right)^2 - (k^2 + k_t^2)$$

is legitimate when only one single mode is considered. Such
a representation can also be legitimate in this case, except
that the k_t^2 is to be replaced by a function of k given by

the circuit dispersion relation. Over the range (ω, k) of interest, i.e. the first Brillouin zone, this can be well approximated by a polynomial. This polynomial should not only fit the actual dispersion curve of that particuliar circuit, but should also satisfy two basic conditions:

1. It must have the symetry of the system. A periodically loaded cylindrical waveguide show an even symetry; the polynomial must therefore be an even polynomial

2. At $k = \pi/L$, the slope $d\omega/dk$ must be zero. Thus,

$$\left(\frac{\omega}{c}\right)^2 - (a_4 k^4 + a_2 k^2 + a_0)$$

should be a reasonable *form for the polynomial.*

The above discussion led us to a dispersion relation for the periodically loaded cold tube which is simple enough to be used in the analysis of the hot tube, and yet theoretically sound to be reasonably accurate.

The dispersion relation for the cold tube is thus given by

$$k_0{}^2 = \left(\frac{\omega}{c}\right)^2 = a_4 k^4 + a_2 k^2 + a_0 \qquad (3.1)$$

The three constants leading to the approximate circuit dispersion relationship can be found in any appropriate way. Generally, two conditions should be met:

1. $a_o = \omega_c^2/c^2$, where ω_c is the lower cut-off frequency, obtained either analytically or experimentally.

2. $d\omega/dk = 0$ at $k = \pi/L$.

The third relation to determine all three coefficients can be set by some curve fitting to either theoretical results by solving the boundary conditions, or to an experimental curve. If neither is available, any reasonable assumption may be tried, e.g., $d^2\omega/dk^2 = 0$ at $k = \pi/2L$.

The polynomial approximation used in this study is shown in figure 3.4, along with the dispersion curve of a smooth walled waveguide of the same outer radius b.

However, in general, the polynomial approximation is found from the numerical results of the complete dispersion relation described in chapter 4. Experimental plots for different values of a, b, and L are presented at the end of chapter 4, figures 4.1 and 4.2.

3.2 Linear analysis of the hot tube:

In the litterature, the arrangement of the gyro-TWT consists of an annular electron beam propagating inside the waveguide. This arrangement is appropriate when the higher order modes are the ones for which amplification is sought (i.e., the interaction of interest is with the higher harmonics of the electron cyclotron frequency). Indeed, the beam must be positioned in such a way as to interact with

the rf field in the region where the field is maximum, a very delicate arrangement in some cases: figure 3.1 shows the distribution of the field lines for a waveguide in the whispering gallery mode. However, in the case at hand, the fundamental TE_{11} mode, the field is maximum at the center of the guide (figure 3.2); hence, the beam should be positioned at the center. In fact, the positioning of the beam is not as critical as when considering higher order interactions: appendices A and B show that the energy density profile in the cross section of the guide, the geometrical factor $J_1^2(1.84R_0/R_w)$ changes by 16% only when R_0 is changed from 0 to 30% R_w. Therefore, an electron beam located near the center of the waveguide with beamlets of radius R_L (Larmor radius) centered at R_0 (the guiding center radius) equal to R_L should give results not much different from those whose guiding center is the center of the waveguide (actually, R_0/R_w is on the order of 15%). Thus, the arrangement of the gyro-TWT in the fundamental TE_{11} mode is depicted in figure 3.3.

The electrons, guided by a uniform magnetic field $B_0 z_0$, move along helical trajectories. In our model, we assume that the beam is sufficiently tenuous that its space charge electric field can be neglected and the spacial structure of the waveguide mode is unaffected by the presence of the beam. The beam interacts with the single TE_{11} waveguide

mode (appendix A shows that the additional terms due to interaction with the other TE and with the TM modes can be disregarded), and the cold circuit dispersion relation used in the following analysis is the polynomial approximation derived previously (eq. 3.1).

For the disc-loaded circuit, the TE part of the $p = 0$ term has the same field distribution as that of the TE_{11} mode of a smooth walled waveguide: the terms on the RHS can therefore be kept as such.

The small signal (linear) dispersion relation for the hot tube, with the above assumptions (see also the discussion in appendix A) is then:

$$\left(\frac{\omega}{c}\right)^2 - (a_4 k^4 + a_2 k^2 + a_0) =$$

$$- \frac{4\nu}{\tau_0 R_w^2 K_{11}} \left[\beta_t^2 \frac{(k_0^2 - k^2) H_{11}(x,y)}{(k_0 - \beta_z k - k_b)^2} - \frac{(k_0 - \beta_z k) Q_{11}(x,y)}{k_0 - \beta_z k - k_b} \right] \qquad (3.2)$$

where

$$\nu = I_b / 1.707 \times 10^4 \beta_z$$

$$H_{11}(x,y) = \left[J_0(x) J_1'(y) \right]^2$$

$$Q_{11}(x,y) = 2H_{11}(x,y) + y \left[J_0^2(x) J_1'(y) J_1''(y) + \frac{1}{2} J_{-1}^2(x) J_1'(y) J_0'(y) - \right.$$

$$\frac{1}{2}J_1{}^2(x)J_1{}'(y)J_2{}'(y)\Big]$$

$$x = k_t R_o$$

$$y = k_t R_L$$

$$K_{11} = (1 - \frac{1}{1.84^2})J_1{}^2(k_t R_w)$$

$$k_t = \left[(\omega/c)^2 - k^2\right]^{1/2}$$

At this point, one more question needs to be answered. The quantity R_w that appears in equation 3.2 enters into the derivation from the averaging of the beam current over the cross section of the smooth waveguide. It is the boundary where E_ϕ or $J_1{}'(k_t r)$ is zero. Therefore, the periodically disc loaded cylindrical waveguide may be represented by a smooth wall cylindrical waveguide with an artificial conducting boundary at R_w. However, this boundary is not stationary, but function of frequency, with $k_t R_w = 1.84$. Using this value of R_w on the RHS should be a good approximation. Since the per unit length gain of the tube depends weakly (1/3 power) on the multiplying factor on the RHS of equation 3.2, the error introduced should therefore be very minor.

The first term on the right hand side of equation 3.2 gives the gain, and the second term, known as the Weibel term, is a damping term. Both mechanisms are present simul-

taneously and compete rather than reinforce each other. The first term (the one multiplied by H_{11}) drives the instability whereas the second (the one multiplied by Q_{11}) has a stabilizing effect. (<u>Note</u>: when $H_{11} = 0$, we get a cubic equation in ω with 3 stable roots). The Q term leads to a threshhold beam energy beyond which the CMI can be excited:

$$\beta_t(0) > \beta_t(\text{critical})$$

i.e., $\quad \gamma_t(0) > \gamma_t(\text{critical})$

We see that, in order to have gain, the RHS (which represents the coupling) must be negative. Complex roots, whenever they occur, give the gain of the device. Equation 3.2 may be solved for either ω or k. In the first case, k is a real parameter and we solve for complex ω, $\omega = \omega_r - j\omega_i$; whereas in the latter case, the solution is a complex value for $k = k_r + jk_i$, ω being the real parameter. Both approaches were used. Graphs 1 through 8 are plots of the results of the linear analysis. It needs to be pointed out that the polynomial representation of the cold circuit dispersion is a mathematical approximation in the first Brillouin zone of the true dispersion which gives all branches in the entire $k_0 - k$ plane. Thus, it does not contain all the physics of the system. Therefore, in solving equation 3.2 numerically, if any solution found lies near the cold circuit characteristic in the first Brillouin zone, it

it can then be regarded as legitimate. Any solution found away from this neighborhood must then be discarded.

3.3 Discussion of the Numerical Results:

In the following, the polynomial approximation used for the dispersion relation of the cold tube represents the experimental model #8 as described in chapter 4. The reason for using this model is twofold:

1. The dimensions a, b, and L are such that the slope of the dispersion curve (which is equivalent to $v_z = \beta_z c$) over most of the passband is small enough to have positive gain; in other words, the energy of the beam (i.e., γ) is above threshold.

2. With reference to figures 4.1 and 4.2, one can readily understand the compromise one has to make between gain and bandwidth. The ultimate bandwidth is limited by the difference between the lower (at $k = 0$), and the upper (at $k = \pi/L$) cut off frequencies. The larger is this difference, the larger the bandwidth will be. But this also leads to a larger group velocity: less time is available for the wave to grow for a fixed tube length. Further more, the larger the beam parallel velocity leads to less perpendicular beam energy available for the interaction. In the computations done here, a fix beam voltage of 60kV is used. This implies that the initial $\gamma = 1 + 60/511 =$

1.1174 and β_0 = 0.446. The most recent experimental results, models #6 through #8, showed that a very large range of dispersion can be obtained, from $\beta_z \sim$ 0.08 for model #6 (a = 1.016cm, b = 2.93cm, L = 2.7cm) at the most dispersive end, to $\beta_z \simeq$ 1.0 for the earlier models (a = 2.22cm, b = 2.98cm, L = 3.3cm, for model #2), almost the same as the smooth wave guide. A desirable division of perpendicular and parallel velocities is about v_t/c = 0.3 and v_z/c = 0.33. Model #8 has $v_g/c \simeq$ 0.32.

In this analysis, we therefore used the values of experimental model #8:

L = 0.027m

b = 0.0298m

a = 0.5b = 0.01486m

With reference to figure 3.4, note how remarkable is the agreement between the experimental data and the polynomial approximation used. This proves our point: the dispersion relation of this structure represented by an infinite by infinite determinant can be accurately described by equation 3.1.

The coeficients in equation 3.1 are:

a_4 = -2.74x10^{-5}

a_2 = 0.7413

a_0 = 8046.1

The initial parameters for the beam were the following

$V_B = 60kV$

$I_B = 5A$

$\gamma = 1.1174$

$R_O = R_L$

$B_O \approx 1500G$

3.3-3 Numerical Results:

Several beam parameters were used in order to compare the performances of their respective tubes(Fig.3.5). Two beams are then used for further linear and non linear studies: beam B1 which meets the grazing condition over the largest range of frequencies, and beam B3 which achieves the flatest linear gain over the passband(Fig.3.6).

Figure 3.5 shows the cold circuit dispersion curve (WG) along with three straight lines that describe the dispersion curves of the three beams used (B1-B3). These three beams differ by the value of the electron cyclotron frequency Ω, and/or their slope $\Delta k_O/\Delta k$; the beam voltage and the beam current are kept the same for all three beams, i.e., $V_b = 60kV$ and $I_b = 5A$.

Figure 3.6 is a plot of the gain versus frequency for all three interactions WG-B's using the complex ω, real k computer program. The WG-B1 interaction shows the largest

small signal gain of all three interactions.

We are not however interested in getting the largest gain because it may give rise to some absolute instability. What is more desirable is a reasonable high and <u>uniform</u> gain over a large frequency range, that is, we would like to obtain a gain as flat as possible over as large a frequency range as possible. The reason for this is to have the tube output the maximum (or close to the maximum) power over that range of frequencies, hence, to have a tube working at maximum efficiency over a relatively large bandwidth. The plots in figure 3.6 point obviously to B3 to achieve the best performance.

As mentioned earlier, equation 3.2 may be solved by either

      1. Let k be a real parameter, then looking for roots of ω; or

      2. By letting ω be a real parameter while looking for roots of k.

Whenever complex roots occur, gain is indicated. In the first approach, an equivalent per unit length gain (k_i) or phase shift (k_r) may be obtained by letting $k_i = \omega_i/v_g$ and $k_r = \omega_r/v_g$. The equation is 4th degree in ω. It is found that over a large range of k, two complex roots can be obtained. Two other roots are real, and hence are stable modes. The two complex roots are conjugate to each other.

modes. The two complex roots are conjugate to each other. Figures 3.7(for the WG-B1 interaction) and 3.12(for the WG-B3 inteaction) show the k_r solutions versus k as compared with cold circuit characteristics and the beam characteristic. It is of interest to note that:

1. The k_r of the complex mode lies above the beam characteristic, and is almost parallel to it. This shows that $\Delta\omega > 0$, and the group velocity is nearly constant and equal to v_z of the beam.

2. The two stable modes are below the beam characteristic ($\Delta\omega < 0$). The one immediately below is a modified waveguide mode with a smaller phase velocity. The other stable mode is a backward wave; it is however too far from the first Brillouin zone to be taken seriously.

3. Figure 3.12 shows that for low frequencies, no instability is excited: the solution of equation 3.2 shows only stable roots. Then, at some frequency, two of the real roots merge into two complex conjugates whose real part presents the characteristic feature of the instability been excited, i.e., $\Delta\omega > 0$.

Figures 3.8 and 3.9 (for the WG-B1 interaction) and figures 3.13 and 3.14 (for the WG-B3 interaction) show the gain (in dB/m) versus frequency obtained by the two approaches. Figure 3.10 and 3.15 compares the two sets of results:

the agreement is remarkable, especially for the WG-B3 inter-
action.

Figures 3.11 and 3.16 show the per unit length phase
delay versus frequency, showing the linear phase relation so
very important for amplifier applications.

To summarize, the linear analysis of the gyro-TWT shows
that reasonably high and uniform gain, as well as an almost
linear phase shift can be achieved with this design. It also
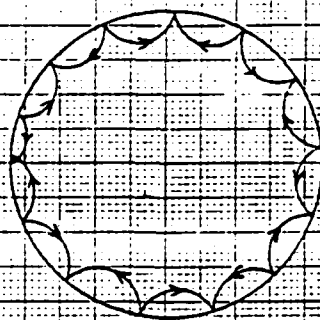predicts a 20.4% bandwidth.
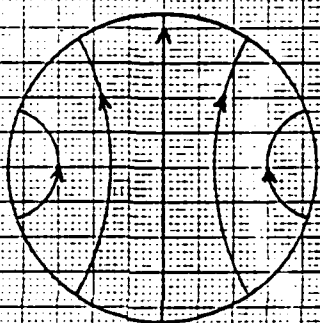
Fig. 3.1

TE_{m1} WHISPERING GALLERY MODE

Fig. 3.2

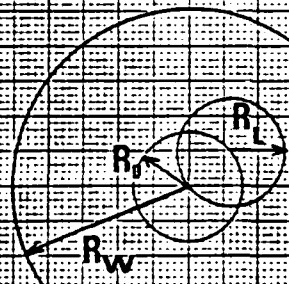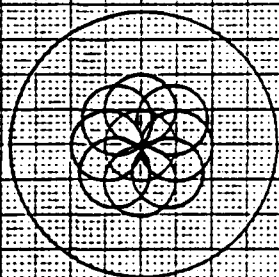TE_{11} MODE ELECTRIC FIELD LINES

Fig. 3.3

BEAM SHAPE AND BEAM LOCATION
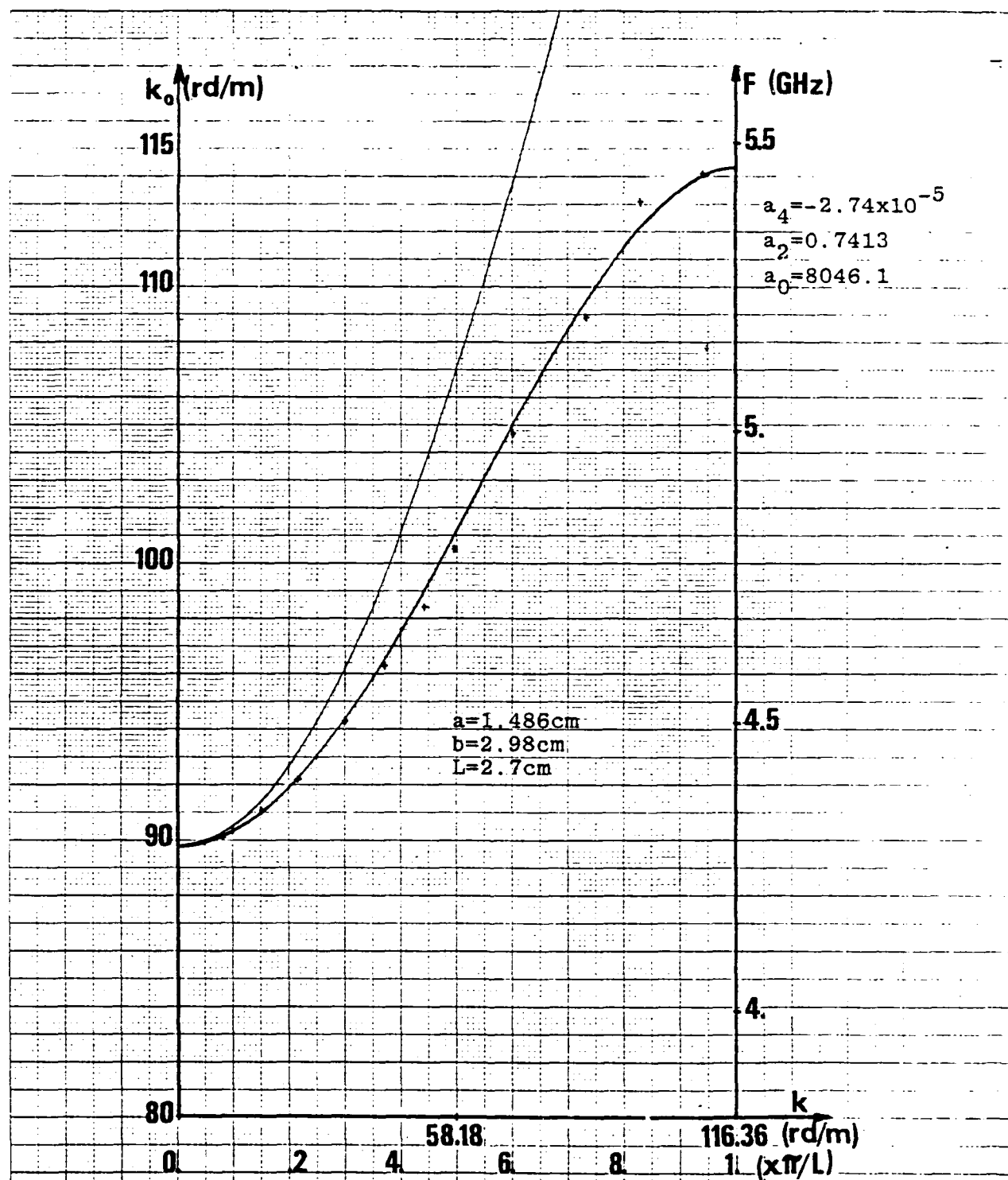
Fig. 3.4

Dispersion Curves
  1. Smooth Walled Waveguide
  2. Disc Loaded Waveguide. Polynomial Approximation
  + Experimental Points

Beam B1: $k_b = 82.8$ rd/m
          $v_z = 0.3163c$
          $v_t = 0.3148c$

Beam B2: $k_b = 81.6$ rd/m
          $v_z = 0.3341c$
          $v_t = 0.2958c$

Beam B3: $k_b = 79.$ rd/m
          $v_z = 0.3615c$
          $v_t = 0.2617c$

Fig. 3.5

Positioning of beam modes relative to the waveguide mode
(WG) represented by the polynomial approximation
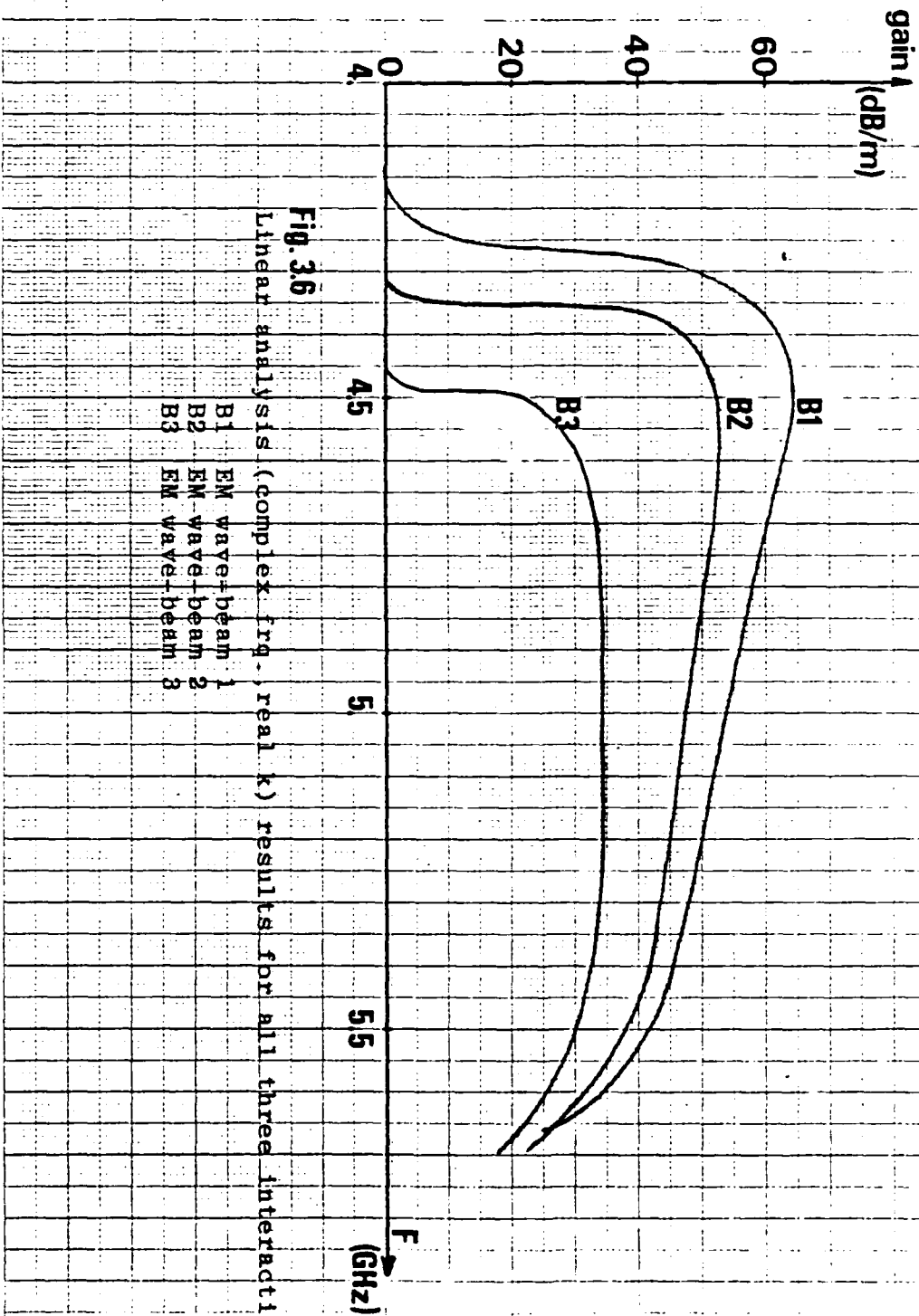
Fig. 3.6
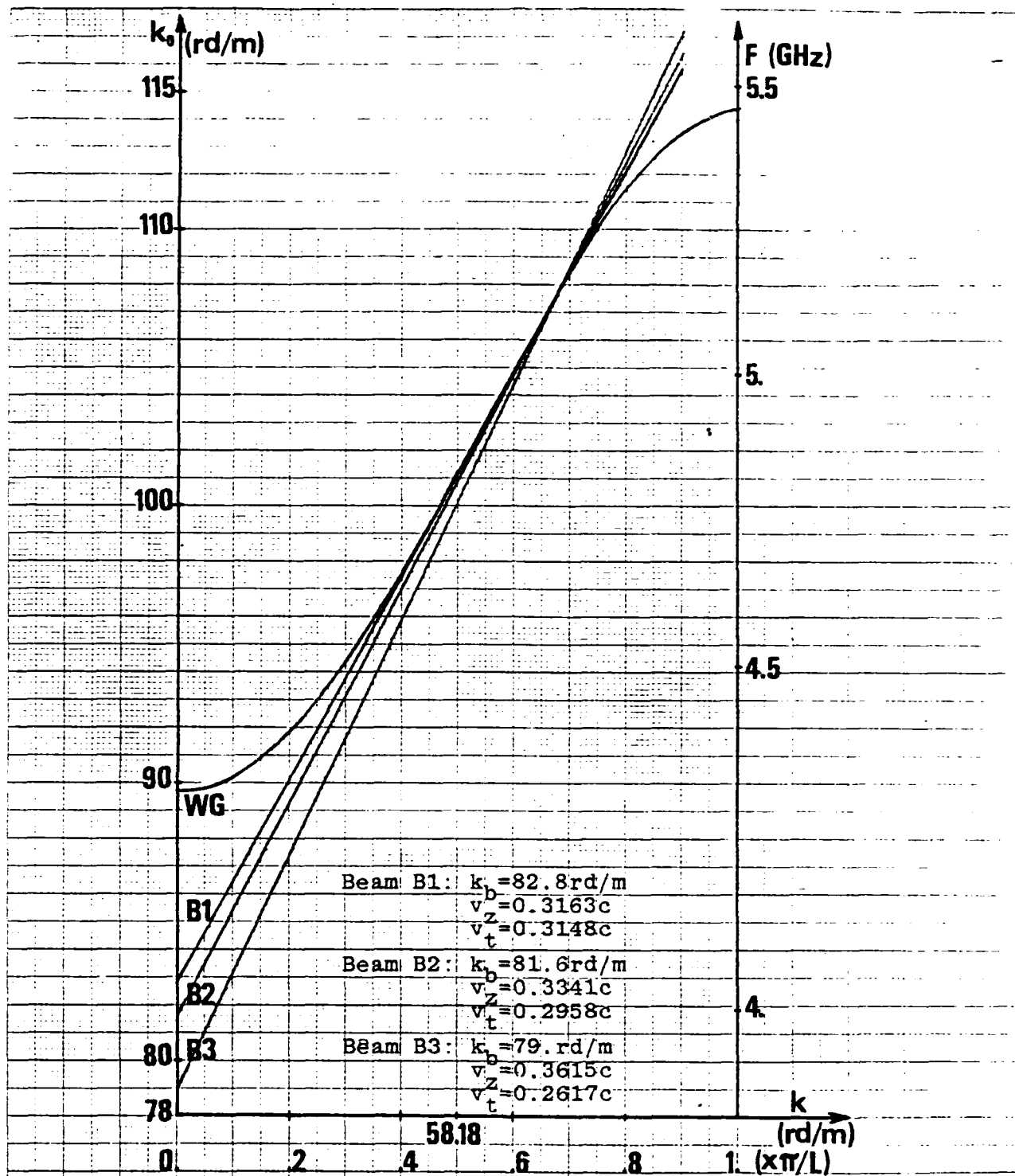Linear analysis (complex frq. real k) results for all three interactions

B1 - EM wave-beam 1
B2 - EM wave-beam 2
B3 - EM wave-beam 3

gain (dB/m): 60, 40, 20, 0

F (GHz): 4, 4.5, 5, 5.5

k_0 (rd/m)

B1

WG

115

110

100

90

80

78

11.64

k
(rd/m)

0.   .25   .5   .75   1.   (x π/L)

Fig. 3.7

Dispersion curves of the hot tube
(WG-B1 interaction)

Fig. 3.8

Linear Analysis (complex freq.,real k) result
WG-B1 interaction

Fig. 3.9

Linear Analysis (complex k,real freq.) result
WG-B1 interaction

Fig.3.10
Figures 3.8 and 3.9 superimposed (WG-B1 interaction)

Fig.3.11
Phase per unit length vs frequency
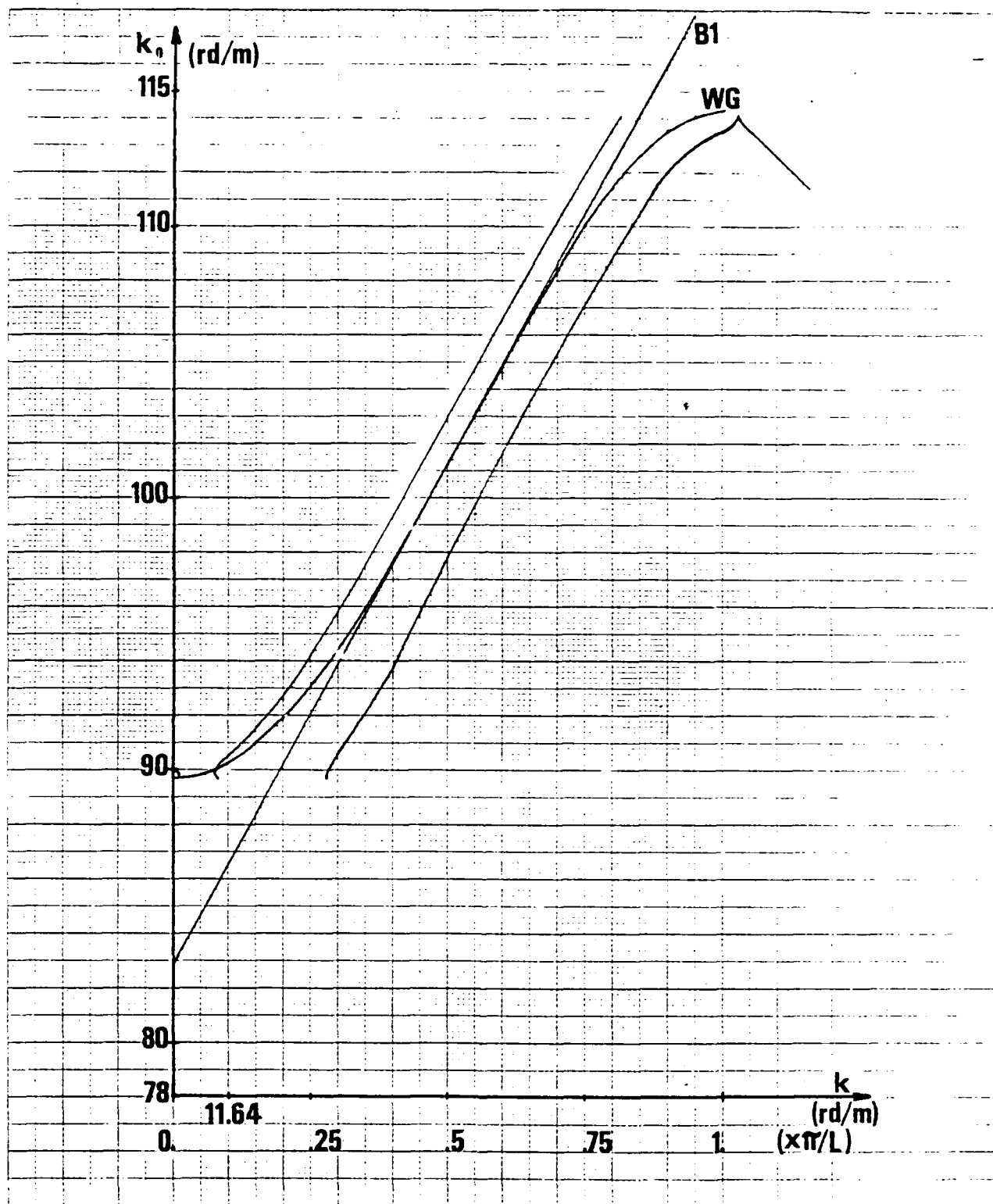WG-B1 interaction

Fig. 3.12
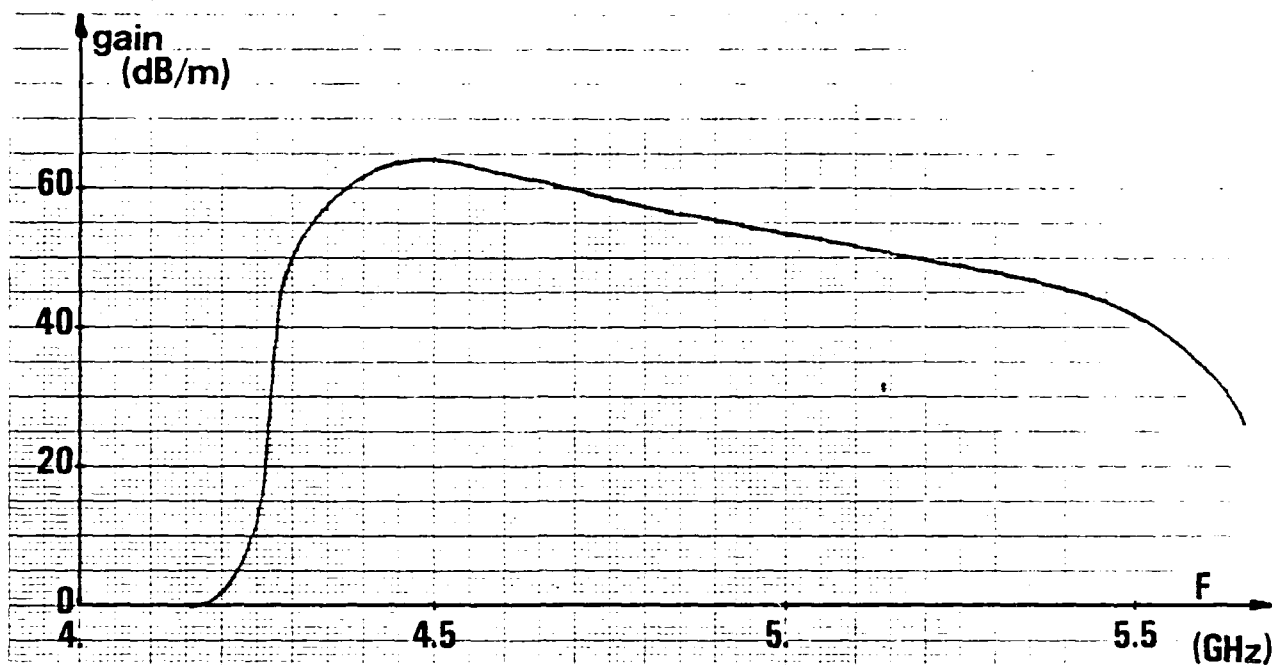Dispersion curves of the hot tube
(WG–B3 interaction)
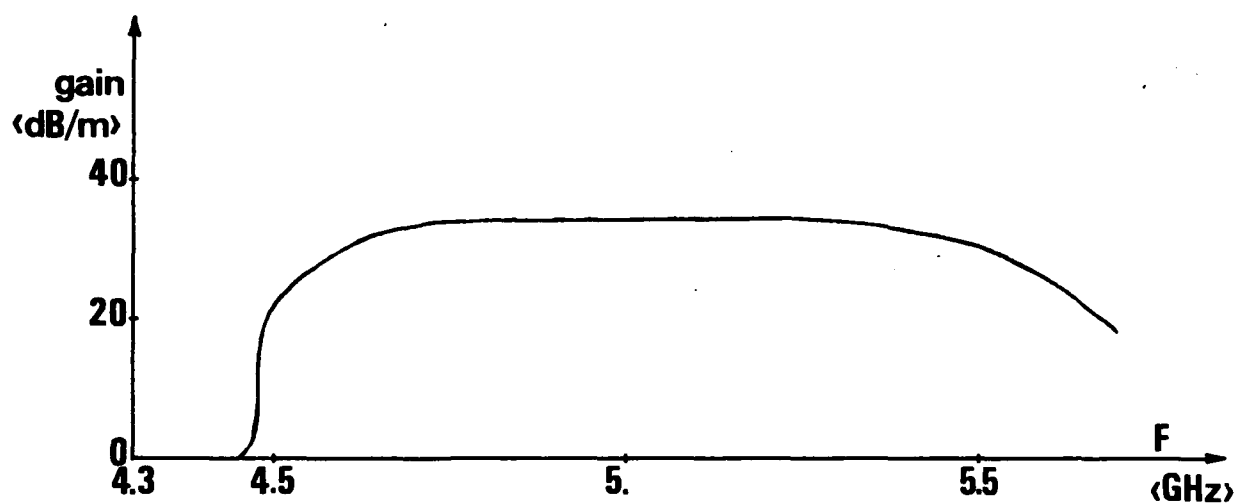
Fig. 3.13
Linear Analysis (complex freq.,real k) result
WG-B3 interaction
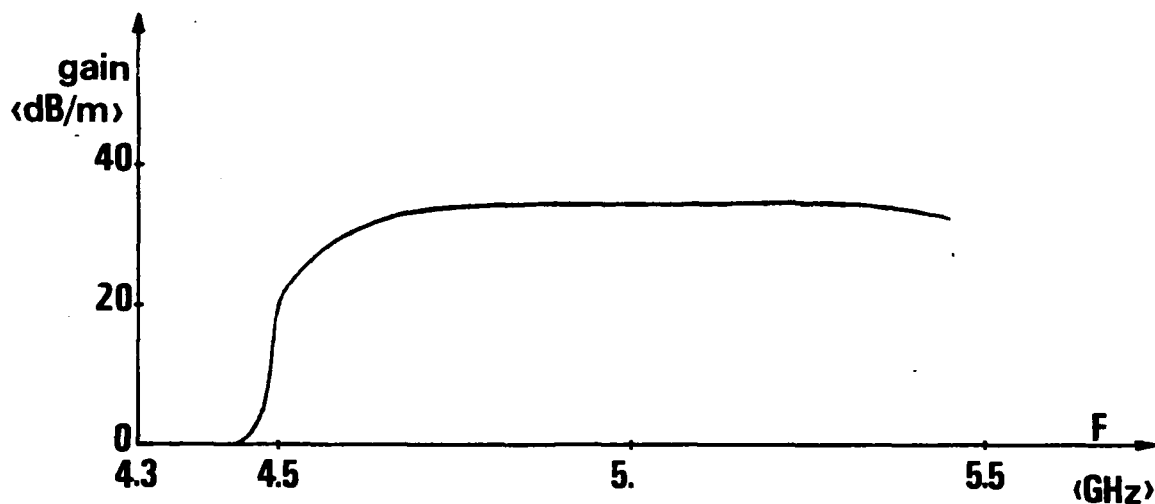
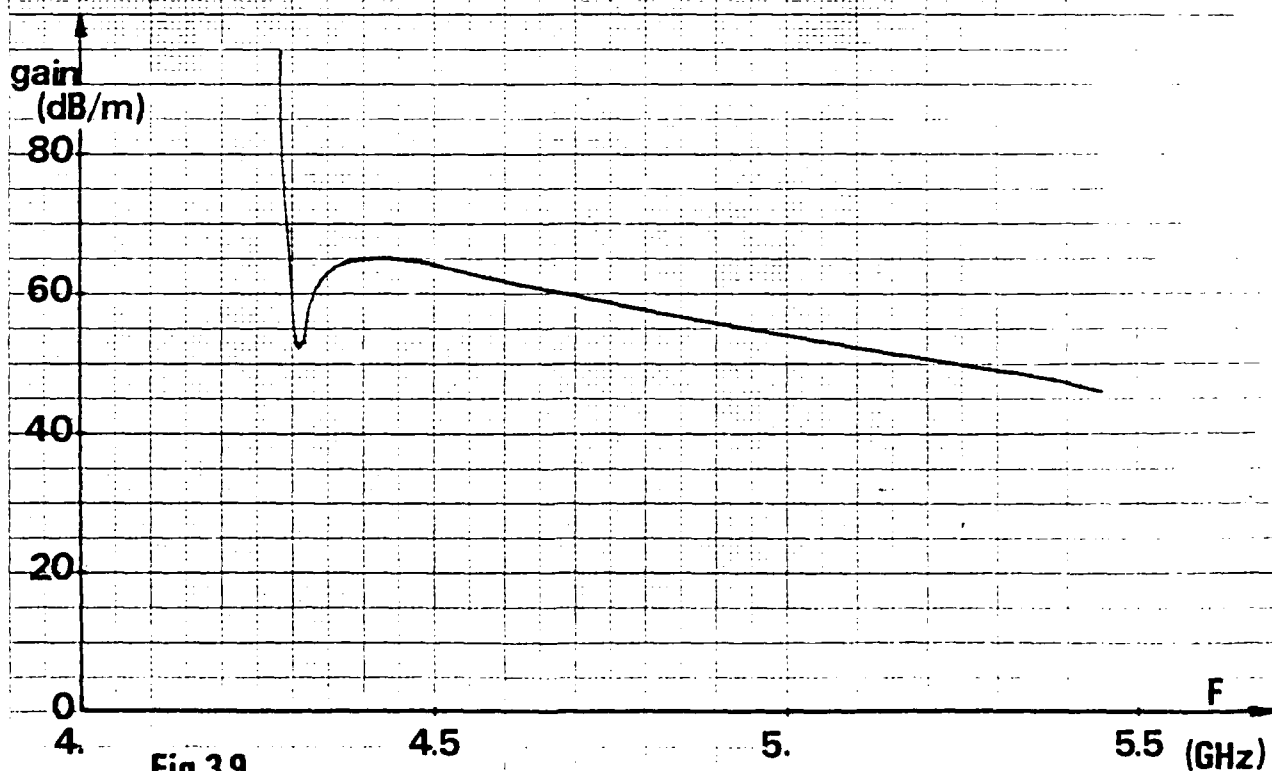**Fig. 3.14**
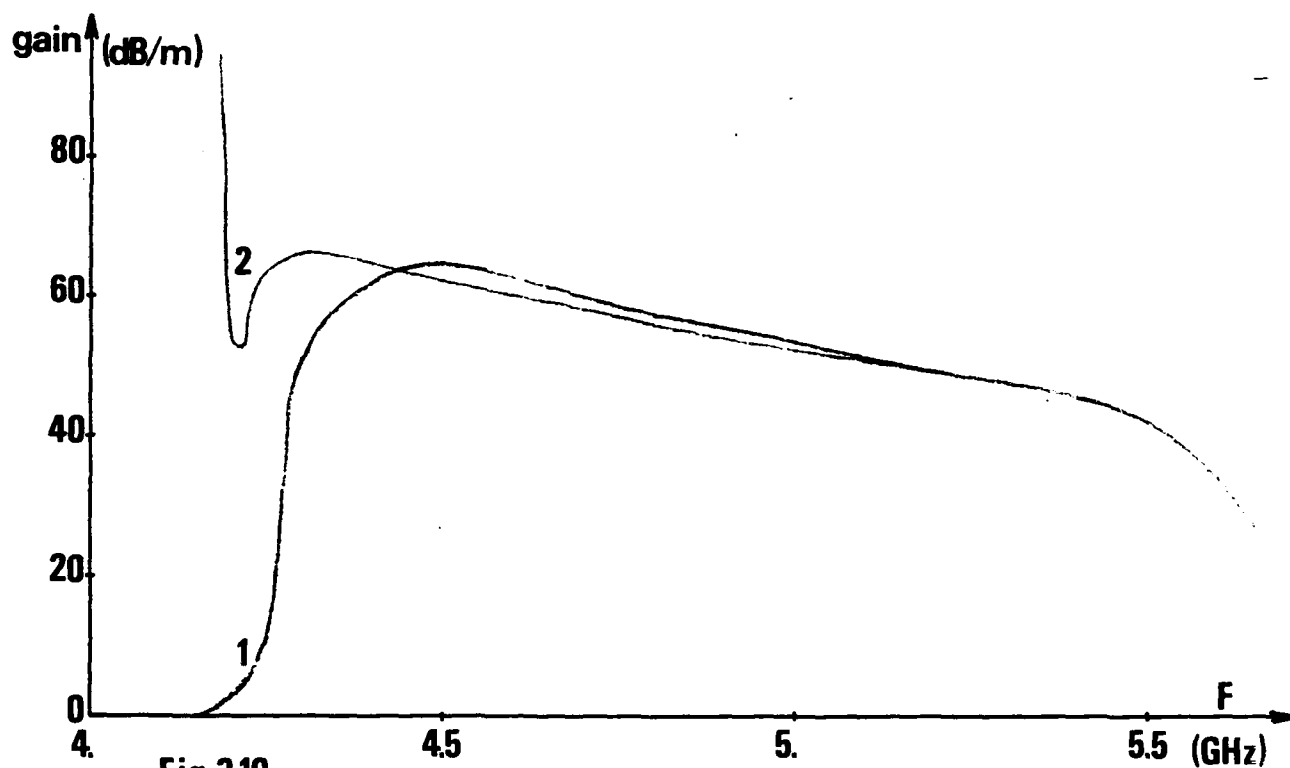Linear Analysis (complex k,real freq.) result
WG-B3 interaction
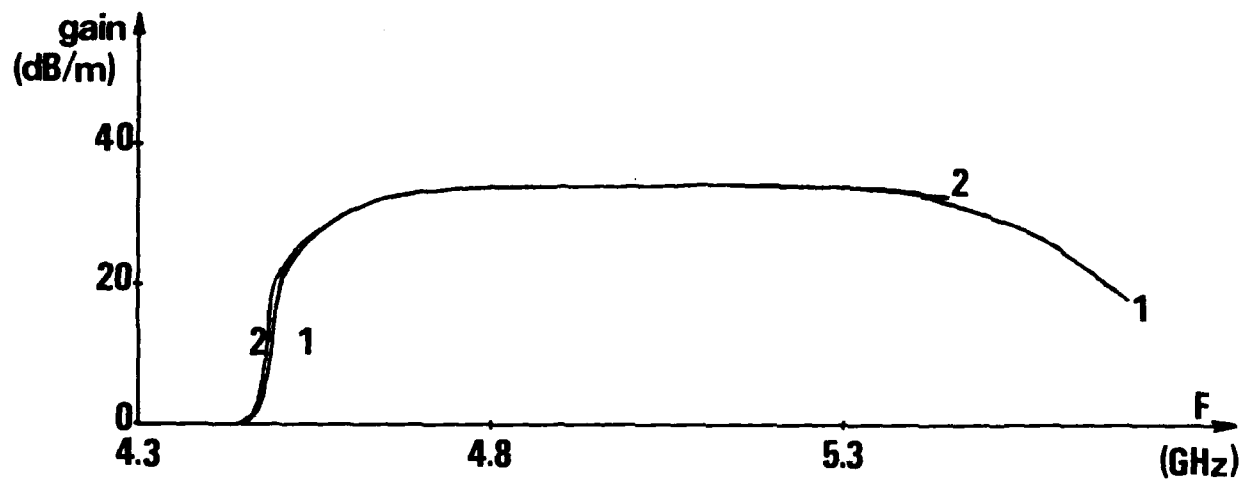
Fig. 3.15
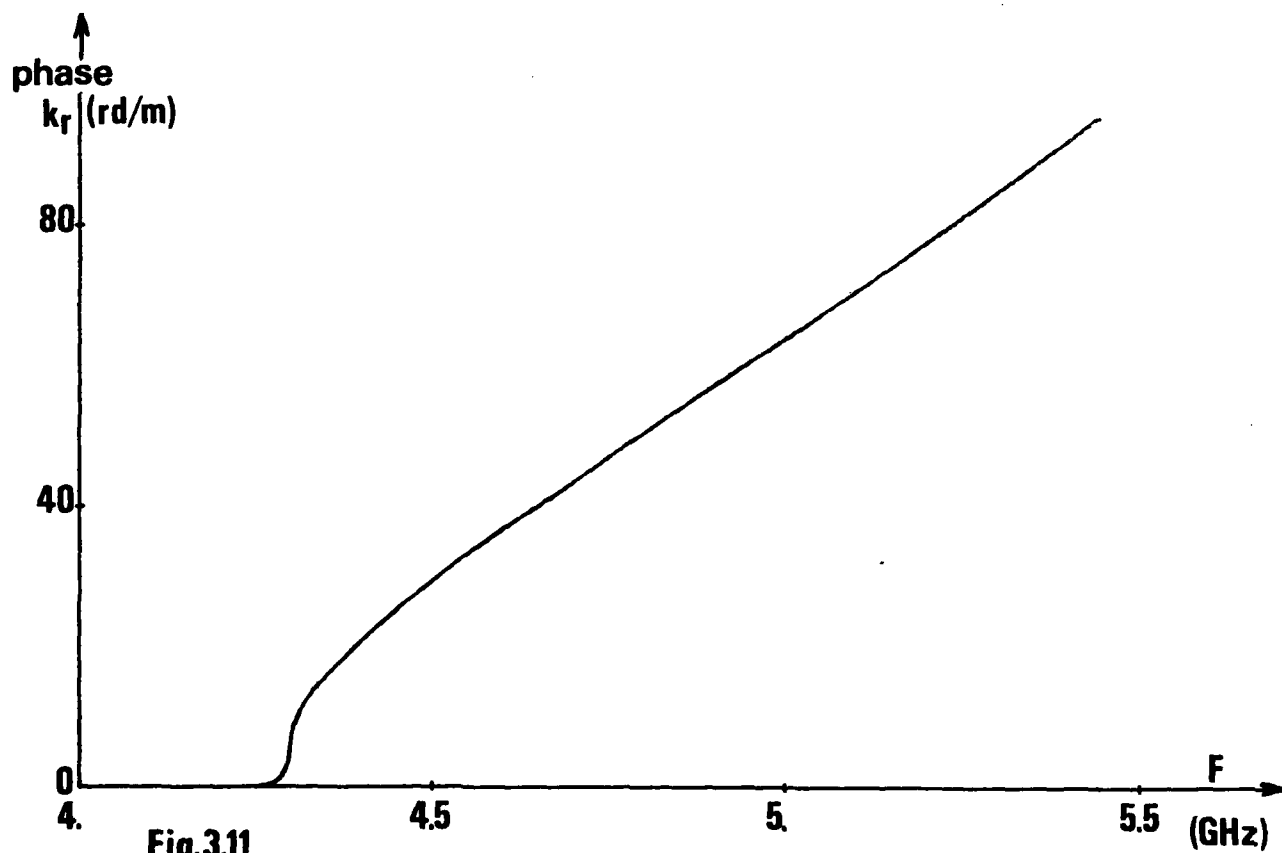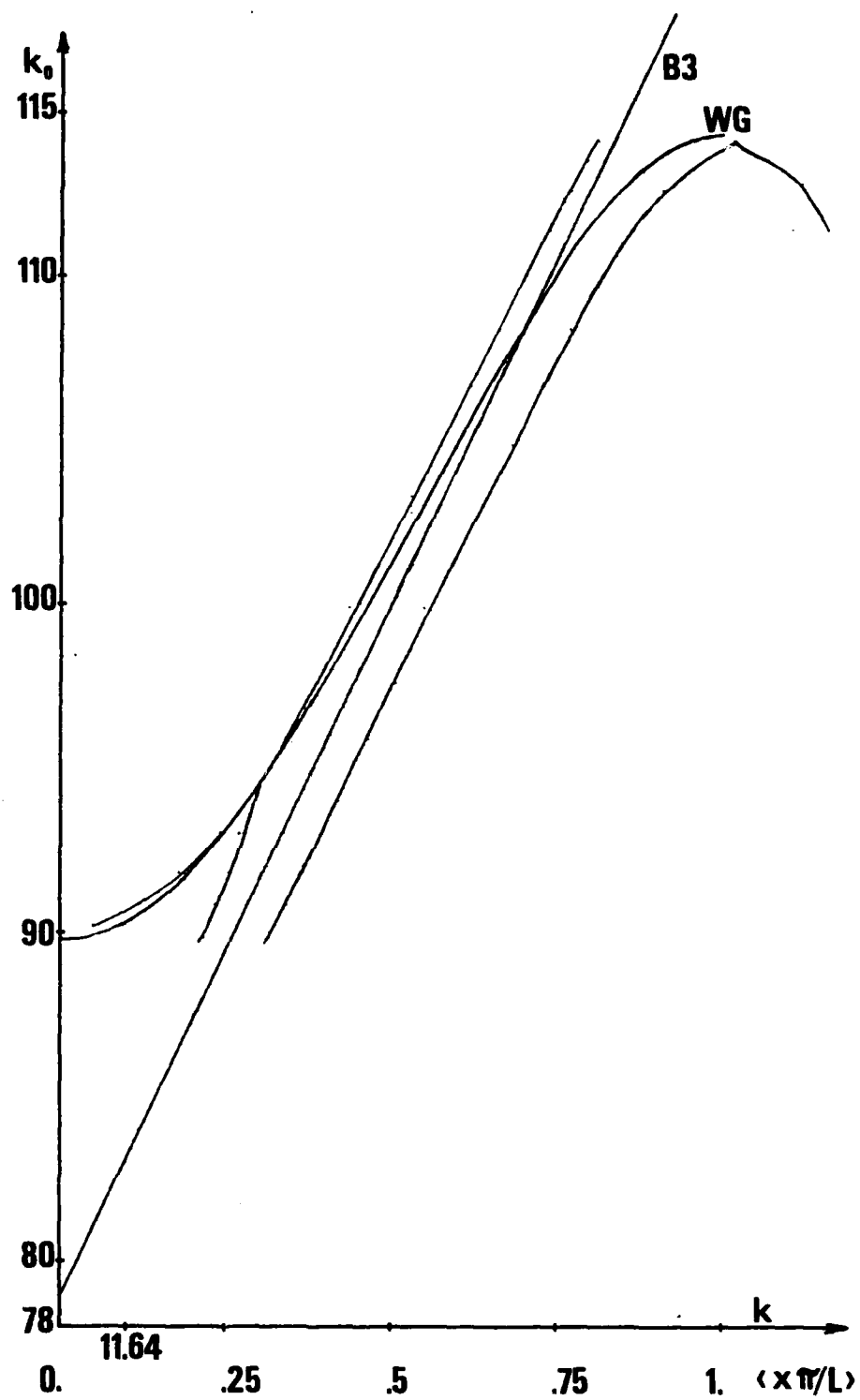Figures 3.13 and 3.14 superimposed
WG-B3 interaction
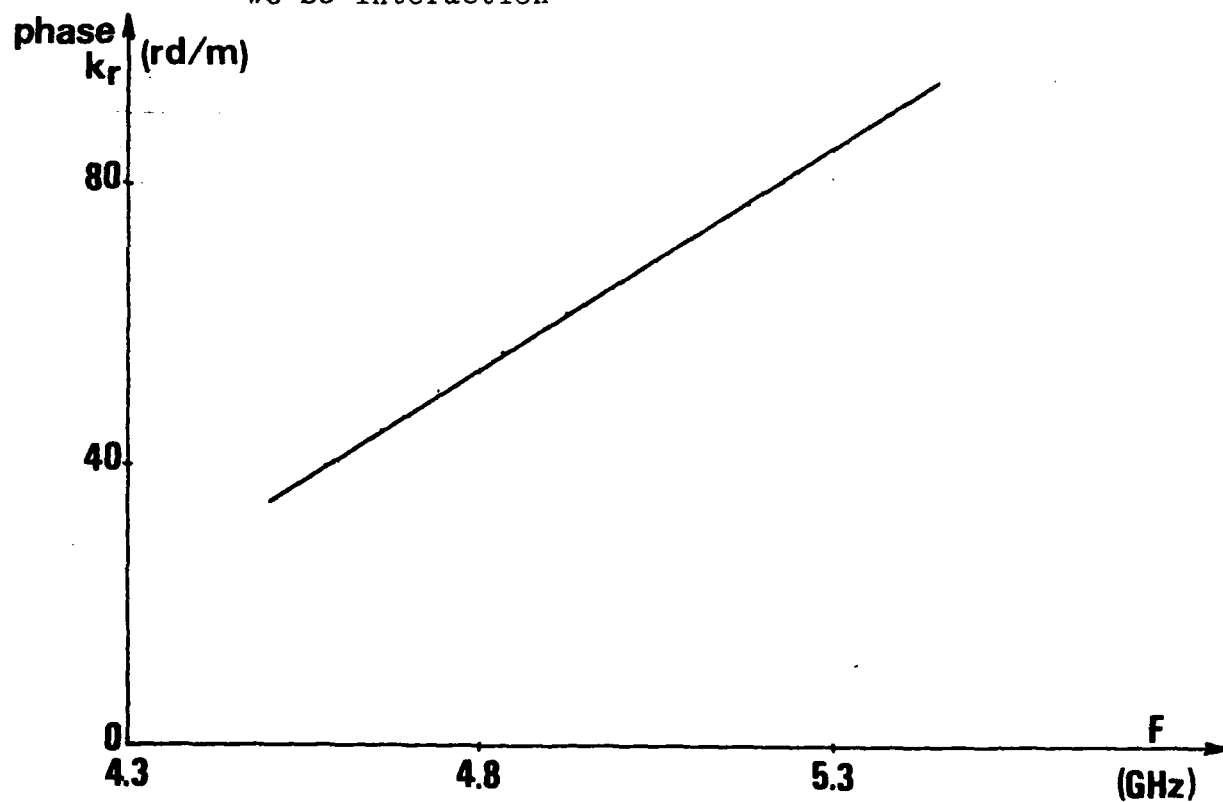
Fig. 3.16
Phase per unit length vs frequency
WG-B3 interaction

CHAPTER 4

THE PERIODICALLY DISC LOADED

CYLINDRICAL WAVEGUIDE

4.1 Derivation of the dispersion relation:

The disc loaded waveguide circuit has been analyzed in the past in connection with studies of the conventional TWT [24]; only azimuthally symmetric TM modes were of interest. Choe and Uhm [23] analyzed the axially symetric TE modes of the structure. These are the only cases where pure TE or pure TM modes are excited. In this section, we solve the boundary value problem of the cold disc loaded circuit, thus leading to the circuit dispersion relation.

The discs in our structure excite all TE_{1n} and all TM_{1n} modes. They are however evanescent, except for the dominant TE_{11} mode. Hence, for a given choice of beam parameters, only the dominant mode will couple to the beam, thus amplified.

The expression for the fields will therefore consist of all the Floquet terms of both TE and TM modes. With respect to figure 1.2, and using the $\exp(j\omega t)$ convention, the fields for an $\exp(j\phi)$ azimuthal variation can be expressed as:

For region I $(r < a)$

$$H_z = \sum_p A_p \, J_1(\chi_p r) \, e^{-jk_p z} \, e^{j\phi}$$

$$E_z = \sum_p C_p \, J_1(\chi_p r) \, e^{-jk_p z} \, e^{j\phi}$$

$$H_r = \sum_p \left[-j \frac{k_p}{\chi_p} A_p \, J_1{}'(\chi_p r) - \frac{\omega\varepsilon}{\chi_p{}^2 r} C_p \, J_1(\chi_p r) \right] e^{-jk_p z} \, e^{j\phi}$$

$$H_\phi = \sum_p \left[\frac{k_p}{\chi_p{}^2 r} A_p \, J_1(\chi_p r) - \frac{j\omega\varepsilon}{\chi_p} C_p \, J_1{}'(\chi_p r) \right] e^{-jk_p z} \, e^{j\phi}$$

$$E_r = \sum_p \left[\frac{\omega\mu}{\chi_p{}^2 r} A_p \, J_1(\chi_p r) - j \frac{k_p}{\chi_p} C_p \, J_1{}'(\chi_p r) \right] e^{j\phi} \, e^{-jk_p z} \, e^{j\phi}$$

$$E_\phi = \sum_p \left[\frac{j\omega\mu}{\chi_p} A_p \, J_1{}'(\chi_p r) + \frac{k_p}{\chi_p{}^2 r} C_p \, J_1(\chi_p r) \right] e^{-jk_p z} \, e^{j\phi}$$

where

$$-\infty < p < \infty$$

For region II $(a < r \quad b)$

$$H_z = \sum_m B_m \sin \frac{m\pi z}{L} Z_E(\eta_m r) \, e^{j\phi}$$

$$E_z = \sum_m D_m \cos \frac{m\pi z}{L} Z_H(\eta_m r) \, e^{j\phi}$$

$$H_r = \sum_m \left[\frac{m\pi/L}{\eta_m} B_m \cos \frac{m\pi z}{L} Z_E{}'(\eta_m r) - \frac{\omega\varepsilon}{\eta_m{}^2 r} D_m \cos \frac{m\pi z}{L} Z_H(\eta_m r) \right] e^{j\phi}$$

$$H_\phi = \sum_m \left[j \frac{m\pi/L}{\eta_m{}^2 r} B_m \cos \frac{m\pi z}{L} Z_E(\eta_m r) - \frac{j\omega\varepsilon}{\eta_m} D_m \cos \frac{m\pi z}{L} Z_H{}'(\eta_m r) \right] e^{j\phi}$$

$$E_r = \sum_m \left[\frac{\omega\mu}{\eta_m{}^2 r} B_m \sin \frac{m\pi z}{L} Z_E(\eta_m r) - \frac{m\pi/L}{\eta_m} D_m \sin \frac{m\pi z}{L} Z_H{}'(\eta_m r) \right] e^{j\phi}$$

$$E_\phi = \sum_m \left[\frac{j\omega\mu}{\eta_m} B_m \sin \frac{m\pi z}{L} Z_E{}'(\eta_m r) - j \frac{m\pi/L}{\eta_m{}^2 r} D_m \sin \frac{m\pi z}{L} Z_H(\eta_m r) \right] e^{j\phi}$$

where

$$1 \quad m < \infty$$

Where χ_p and η_m become imaginary, the Bessel functions are replaced by the modified functions: $J_n(x) \to I_n(x)$, $Y_n(x) \to K_n(x)$.

We define

$$Z_E(\eta_m r) = J_1(\eta_m r) - \frac{J_1{}'(\eta_m b)}{Y_1{}'(\eta_m b)} Y_1(\eta_m r)$$

$$Z_E{}'(\eta_m r) = J_1{}'(\eta_m r) - \frac{J_1{}'(\eta_m b)}{Y_1{}'(\eta_m b)} Y_1{}'(\eta_m r)$$

$$Z_H(\eta_m r) = J_1(\eta_m r) - \frac{J_1(\eta_m b)}{Y_1(\eta_m b)} Y_1(\eta_m r)$$

$$Z_H{}'(\eta_m r) = J_1{}'(\eta_m r) - \frac{J_1(\eta_m b)}{Y_1(\eta_m b)} Y_1{}'(\eta_m r)$$

Also

$$\eta_m^2 = k_o^2 - \left(\frac{m\pi}{L}\right)^2 \tag{4.1}$$

$$k_p^2 = k^2 + \left(\frac{2p\pi}{L}\right)^2 \tag{4.2}$$

$$\chi_p^2 = k_o^2 - k_p^2 \tag{4.3}$$

Both the boundary conditions and Floquet conditions are seen to be satisfied.

Using the continuity condition at r = a:

$$H_z^{\;I} = H_z^{\;II}$$

$$E_z^{\;I} = E_z^{\;II}$$

$$H_\phi^{\;I} = H_\phi^{\;II}$$

$$E_\phi^{\;I} = E_\phi^{\;II}$$

and the orthogonal properties of the trigonometric functions

$$\int_0^L \sin(m\pi z/L)\sin(m'\pi z/L)\,dz = \int_0^L \cos(m\pi z/L)\cos(m'\pi z/L)\,dz$$

$$= \frac{L}{2}\,\delta_{mm'}$$

one can eliminate B_m and D_m, and arrive at:

$$k_o \sum_p \frac{1}{(k_p L)^2-(m\pi)^2}\left[\frac{J_1{}'(\chi_p a)}{\chi_p} - \frac{Z_E{}'(\eta_m a)}{Z_E(\eta_m a)}\frac{J_1(\chi_p a)}{\eta_m}\right]A_p =$$

$$\frac{a}{L}\sum_p \frac{k_p L}{(k_p L)^2-(m\pi)^2}\left[\left(\frac{1}{\eta_m a}\right)^2 - \left(\frac{1}{\chi_p a}\right)^2\right]J_1(\chi_p a)C_p{}'$$

$$\frac{a}{L}\sum_p \frac{1}{(k_p L)^2-(m\pi)^2}\left[\left(\frac{k_p L}{\chi_p a}\right)^2 - \left(\frac{m\pi}{\eta_m a}\right)^2\right]J_1(\chi_p a)A_p =$$

$$k_o \sum_p \frac{k_p L}{(k_p L)^2-(m\pi)^2}\left[\frac{Z_H{}'(\eta_m a)}{Z_H(\eta_m a)}\frac{J_1(\chi_p a)}{\eta_m} - \frac{J_1{}'(\chi_p a)}{\chi_p}\right]C_p{}'$$

where

$$C_p{}' = -\frac{j\omega\varepsilon}{k_o}\,C_p = -j\sqrt{\varepsilon/\mu}\;C_p$$

Equation (2.10) is seen to be of the following matrix form

$$\begin{bmatrix} \overline{\overline{W}}_{mp} & -\overline{\overline{X}}_{mp} \\ \overline{\overline{Y}}_{mp} & -\overline{\overline{V}}_{mp} \end{bmatrix} \begin{bmatrix} \underline{A}_p \\ \underline{C}_p{}' \end{bmatrix} = 0$$

where the elements $\overline{\overline{W}}_{mp}$ etc are matrices whose elements are:

$$W_{mp}= k_o\;\frac{1}{(k_pL)^2-(m\pi)^2}\left[\frac{J_1{}'(\chi_p a)}{\chi_p} - \frac{Z_E{}'(\eta_m a)}{Z_E(\eta_m a)}\frac{J_1(\chi_p a)}{\eta_m}\right]$$

$$X_{mp}= \frac{a}{L}\;\frac{k_pL}{(k_pL)^2-(m\pi)^2}\left[\left(\frac{1}{\eta_m a}\right)^2 - \left(\frac{1}{\chi_p a}\right)^2\right]J_1(\chi_p a)$$

$$Y_{mp}= \frac{a}{L}\;\frac{1}{(k_pL)^2-(m\pi)^2}\left[\left(\frac{k_pL}{\chi_p a}\right)^2 - \left(\frac{m\pi}{\eta_m a}\right)^2\right]J_1(\chi_p a)$$

$$V_{mp}= k_o\;\frac{k_pL}{(k_pL)^2-(m\pi)^2}\left[\frac{Z_H{}'(\eta_m a)}{Z_H(\eta_m a)}\frac{J_1(\chi_p a)}{\eta_m} - \frac{J_1{}'(\chi_p a)}{\chi_p}\right]$$

and $\underline{A}_p$, $\underline{C}_p{'}$ are column vectors representing the amplitudes of the fields.

For non trivial solution ($\underline{A}_p$, $\underline{C}_p{'}$), the determinant of the matrix must be zero: this is then the dispersion relation of the cold circuit for the entire Brillouin diagram.

We would like to emphasize here the fact that the interaction between the beam and the hybrid H_{11} wave is equivalent to the interaction between the beam and a TE_{11} smooth walled waveguide. Indeed, equation 4.3 shows that a beam located near the axis will interact mostly with the p = 0 term of the wave fields, the other terms having but a small effect on the fields near the axis. This is so because the Bessel functions will have real argument only for the p = 0 term, and imaginary argument for all the other terms; meaning that the field distribution near the axis will look very much like the one for the TE_{11} mode since the modified Bessel function goes to 0 towards the axis. Another reason is that the phase velocity of the p $\neq$ 0 waves is much less than the beam velocity, hence, even if some interaction takes place, it cannot sustain an instability. The hybrid H_{11} field distribution at the beam location is therefore about the same as that of a TE_{11} smooth walled waveguide mode, a fact that allows us to use the RHS of the linear

dispersion relation (eq. 3.2) as such, adjusted for this case (i.e., substituting k_t^2 by $k_o^2 - k^2$).

Of course, this is not the only possible approach. Other approaches are possible, and indeed are used. They however have the disadvantage that, although they give correct results, the physical picture is not self-evident, imbedded too deeply in the mathematics.

4.2 Discussion:

The dispersion relation in this case is very involved: it is the solution of a double infinite determinant equal to zero, which is of course impossible to compute. Truncating this determinant to some manageable size will undoubtedly introduce some error which has to be minimized. The justification, if at all, for truncation is that the modes above a certain level are of minimal influence to the results. However, by doing so, it actually means that the modes discarded are of _no_ importance, while those kept are of _equal_ importance. Unfortunately, neither of this is true. Not all lower modes are of equal importance to the dominant first TE mode. Meanwhile, the sharp edges at the discs are expected to cause slow convergence at the higher modes. On the other hand, very often, using only one mode is sufficient to give reasonable results, such as in magnetron cavity analysis. Which means that the determinant should not be truncated by just eliminating the higher order term.

This and other similar problems of truncation have faced the electromagnetic community for decades. Numerous methods for dealing with this problem have been devised, none of them however giving satisfactory results for all cases. In this analysis, very often an error of 10% compared to experiment is regarded as satisfactory. Whereas in this study, whenever we can devise an approach, the error is of the order of 1%. We were fortunate however that a parallel effort was undertaken in which the dispersion characteristic of disc-loaded circuits were experimentally measured [*]: eight models were built and measurements were performed. Figures 4.1 and 4.2 are the plots obtained.

With regard to the numerical approach used, since we have no way of knowing a priori which terms are of lesser influence, a trial and error approach was used, the results compared to those given by the experiments. As we mentioned earlier, by properly choosing the value of the axial period L, it is possible to have the beam interact strongly with the fundamental (p = 0) Floquet mode only. All the other forward Floquet terms are evanescent, decreasing exponentially towards the axis from r = a. The choice for L is therefore dictated by

---

[*] Experiments were performed by G. Wurthmann, J. Heary and C. Bates of Electronic Device and Technology Laboratory (ETDL) at Fort Monmouth. The results were communicated to us privately.

$$\chi_p^2 = k_o^2 - k_p^2 \begin{cases} > 0 \text{ for } p = 0 \\ < 0 \text{ for } p \neq 0 \end{cases} \tag{4.5}$$

where k_p is given by equation 4.2.

For a fixed range of frequencies, the value for L can be determined from equations 4.5 and 4.2. For the frequency range of interest, i.e., such that the lower cutoff frequency 3.GHz < fc < 4.GHz, it is found that L < .025 m.

The value for b is determined by the lower cut-off frequency such that $k_t b = 1.84$, k_t being the wave number corresponding to a 3.GHz smooth wall WG cut-off frequency.

By changing the size of the discs, the slope of the dispersion curve can be adjusted, as can be seen in graphs 9 and 10. With a choice of $k_t = 62.83$, the value for b will be 2.93cm.

It turns out that the value for L is also of paramount importance to the numerical analysis: for the value of L such that equation 4.5 is satisfied, we always have $\eta_m^2 < 0$. In this case, whatever we do, the numerical results are erroneous: we get a complete dispersion curve well above where it should be. In fact, the numerical simulation yields results only when η_1 is real, that is, when

$$\eta_1{}^2 = k_o{}^2 - (\pi/L)^2 > 0$$

If we choose L such that $k_o > \pi/L$ for part of the dispersion curve, then we get very accurate results for that portion: indeed, in this case, the piece of the dispersion curve above $k_o = \pi/L$ matches almost perfectly the experimental curve[*]. For the piece below $k_o = \pi/L$, the results are however far off, well below what the measurements give us. So far, we do not have any satisfactory explanation for this numerical problem. We do however believe that we are not far from reaching a solution. For example, Galerkin's approach is now being looked into.

---

[*] Note that, when $k_o > \pi/L$, the $p = -1$ backward traveling wave is not evanescent inward from $r = a$.
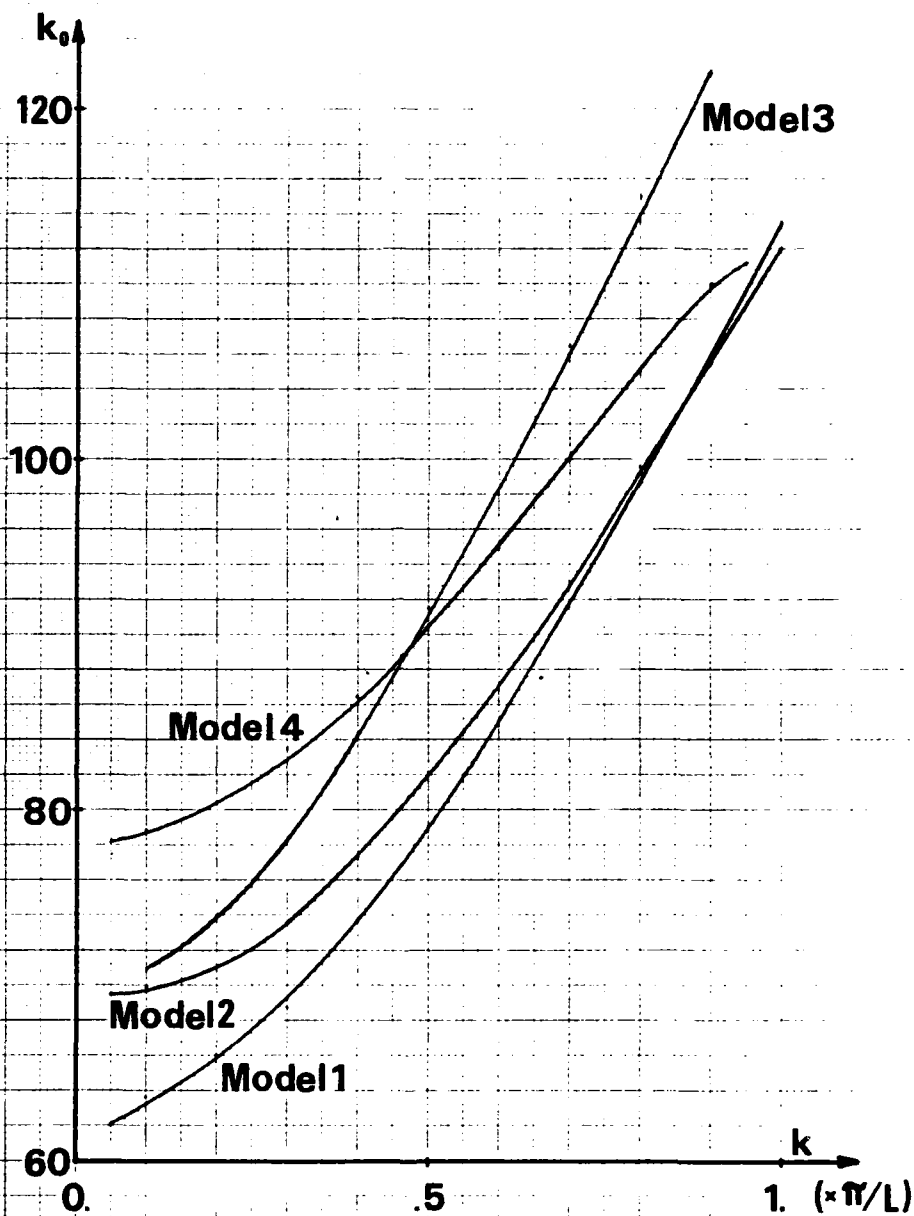
Fig. 4.1

EXPERIMENTAL DISPERSION CURVES FOR EARLIER MODELS

For all models: b = 2.98cm

Model 1: a/b = 0.91 and L = 3.3cm
Model 2: a/b = 0.75 and L = 3.3cm
Model 3: a/b = 0.75 and L = 2.54cm
Model 4: a/b = 0.6 and L = 3.3cm

Fig. 4.1

EXPERIMENTAL DISPERSION CURVES FOR EARLIER MODELS

For all models: b = 2.98cm

Model 1: a/b = 0.9 and L = 3.3cm

Model 2: a/b = 0.75 and L = 3.3cm

Model 3: a/b = 0.75 and L = 2.54cm

Model 4: a/b = 0.6 and L = 3.3cm
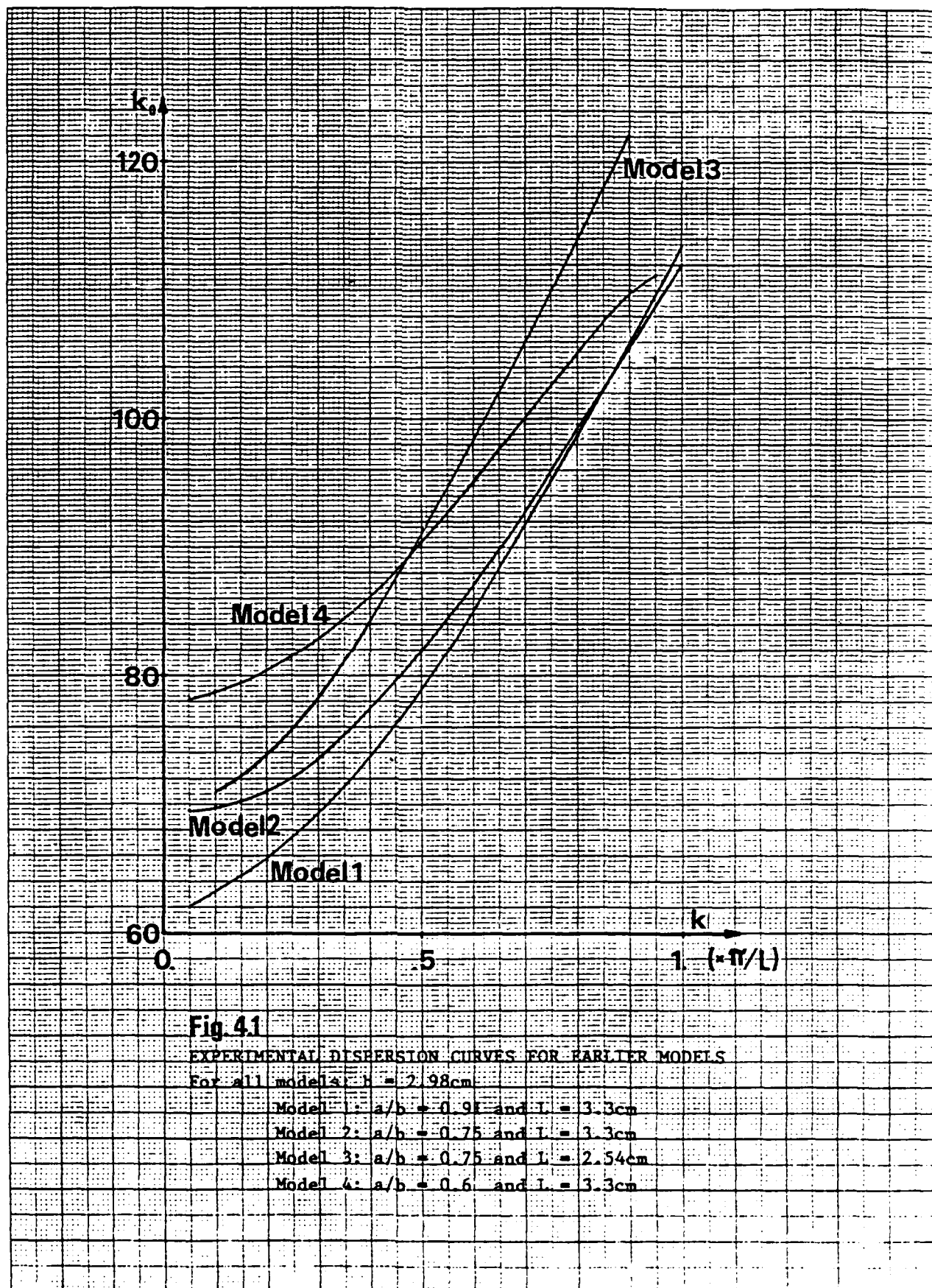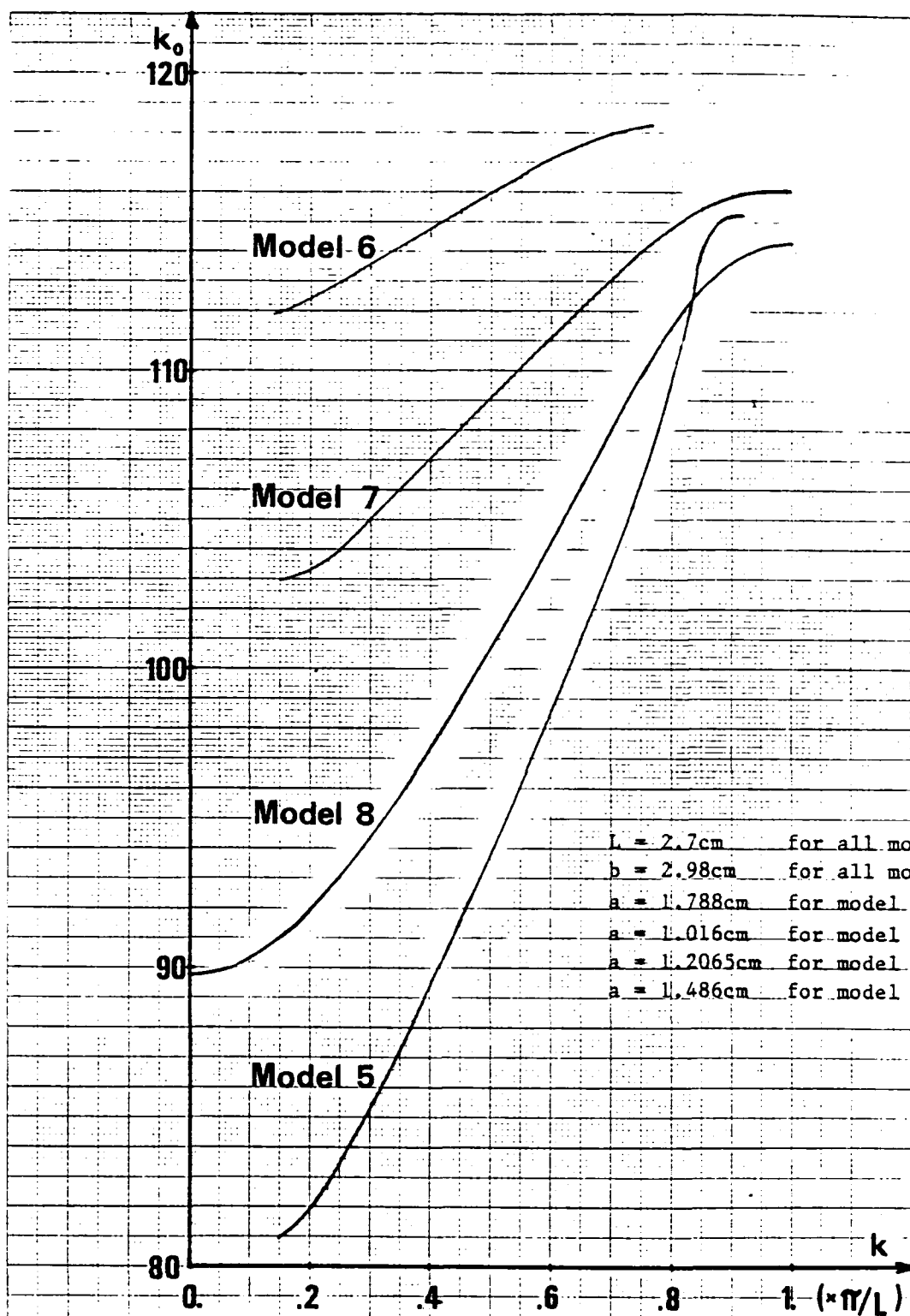
Fig.4.2

EXPERIMENTAL DISPERSION CURVES FOR LATER MODELS

The following parameters appear within the figure:

$L = 2.7cm$ for all models
$b = 2.98cm$ for all models
$a = 1.788cm$ for model 5
$a = 1.016cm$ for model 6
$a = 1.2065cm$ for model 7
$a = 1.486cm$ for model 8

Curve labels: Model 6, Model 7, Model 8, Model 5

Vertical axis: k_0 with values 80, 90, 100, 110, 120

Horizontal axis: k with values 0, .2, .4, .6, .8, 1. $(\times \pi/L)$

CHAPTER 5

NON LINEAR ANALYSIS

5.1 Background:

The linear analysis provides us with a wealth of information with regard to the small signal performance of the tube. However, according to the linear theory, if the wave is gaining energy, it will keep on gaining energy forever. Indeed, there is no provision in the linear theory for any kind of saturation mechanism that the wave must experience. In reality, some mechanism is always present to limit the output. To assess the performance of a power amplifier, a non linear theory must then be developed, which must predict the saturation level, as well as all the other important performance results such as the saturation length, the power output, the efficiency of the tube.

Two different but simultaneously present (in the fundamental interaction) mechanisms are responsible for the saturation :

- Depletion of free energy
- Loss of phase synchronism (phase trapping)

Depletion dominates when the beam energy is slightly above threshhold. Saturation occurs as soon as the beam loses a small amount of energy and the system becomes line-

arly stable. This effect becomes also apparent when the electrons have lost enough energy to the wave so that β_t is no longer high enough to cause amplification. Phase trapping occurs when the beam energy is well above threshold: an average electron loses so much energy that its relativistic cyclotron frequency no longer matches the wave's to favor unstable interaction.

Both mechanisms are important for the fundamental cyclotron harmonic interaction. However, the dominant mechanism depends on the initial choice of the beam parameters: the maximum free energy per particle available to the wave is

$$E = \left[\gamma(0) - \gamma(\text{critical}) \right] m_o c^2 \quad .$$

Non-linear behavior of the gyrotron mechanism has mostly been done by particle simulation [37]-[38], and a combination of both analytic and simulation in part [34]. These approaches need large computers and are hence expensive if large amounts of data is needed for trial and error design work. In the present effort, we adapt the phase averaging technique by Kuo and Cheo [29], and by Kuo et al. [30] to the present structure. In [29] and [30] a single third order ordinary differential-integral equation was derived for the slow varying amplitude. The approach is less

accurate than the particle simulation but readily solvable on a personal computer. Thus it is most convenient for estimating the ultimate performance of a power amplifier. Appendix B gives the essence of the efforts in [29] and [30]. The basic equation is given by:

$$\left[\frac{d^3}{dt^3} + 2S\frac{d^2}{dt^2} + (\Delta\omega_1^2 + c_1)\frac{d}{dt}\right] E_O =$$

$$a_O\left\{1 - \frac{\sigma\varepsilon_O(\omega - kv_z)}{2\gamma_O\Delta\omega_O n_O m_O c^2}\left[E_O^2(t) - E_O^2(0)\right]\right\}$$

$$\int_O^t E_O(t')\cos<\Delta\phi(t - t')>dt' - S\left[2c_1 E_O + \right.$$

$$\left.\frac{a_O}{\Delta\omega_O}\int_O^t E_O(t')\sin<\Delta\phi(t - t')>dt'\right] \qquad (5.1)$$

where

$$<\Delta\phi(t - t')> = -\Delta\omega_O\int_{t'}^t\left\{1 - \frac{\sigma\varepsilon_O(\omega - kv_z)}{2\gamma_O n_O m_O c^2}\right.$$

$$\left.\left[E_O^2(\tau) - E_O^2(0)\right]\right\}d\tau$$

$$a_O = GA_O\Delta\omega_O$$

$$\Delta\omega_O = \omega - \omega_O$$

$$\omega_O = N\frac{\Omega_O}{\gamma_O} + kv_{zo}$$

$$G = \frac{\omega_p^2}{\sigma\omega} \frac{\alpha_o}{\gamma_o} J_N'(\alpha) J_{m-N}^2(k_t R_o)$$

$$\omega_p^2 = \frac{n_o e^2}{\varepsilon_o m_o}.$$

$$A_o = \left(\frac{\Omega_o}{\gamma_o k_t c}\right)^2 (\omega^2 - k^2 c^2)\alpha_o J_N'(\alpha_o)$$

$$\alpha_o = k_t R_L \qquad \text{and} \qquad k_t = (k_o^2 - k^2)^{1/2}$$

$$c_1 = G\left[D_o - A_o \frac{\omega}{2(\omega^2 - k^2 c^2)}\right]$$

$$D_o = (\omega - kv_{zo})\frac{1}{\alpha_o} \frac{d}{d\alpha_o}\left[\alpha_o J_N'(\alpha_o)\right]$$

$$\Delta\omega_1^2 = \Delta\omega_o^2 - a^2\left\{D_1^2 + \left[D_o - 3A_o \frac{\omega}{2(\omega^2 - k^2 c^2)}\right]^2\right\} +$$

$$\frac{3}{4} a(A_o^2 \frac{\omega}{\omega^2 - k^2 c^2})I_s$$

$$a = (-1)^N \frac{B_{zo}}{B_o} J_{m-N}(k_t R_o)$$

$$D_1^2 = (\omega - kv_{zo})^2 J_N'(\alpha_o)\frac{d}{d\alpha_o}\left\{\frac{1}{\alpha_o} \frac{d}{d\alpha_o}\left[\alpha_o J_N'(\alpha_o)\right]\right\}$$

$$S = \frac{3}{8} \frac{aA_o^2\omega}{\Delta\omega_o(\omega^2 - k_z^2 c^2)}I_c$$

$$I_c = \int_0^t dt'\, a(t')\cos\langle\Delta\phi(t - t')\rangle$$

$$I_S = \int_o^t dt' \; a(t') \; \sin<\Delta\phi(t - t')>$$

Note that linearizing equation 5.1, we find that in order to have gain, we need to have

$$(\omega^2 - k^2c^2)\beta_t^2 H_{11}(x,y) -$$
$$(\omega - kv_z - \Omega)(\omega - kv_z)Q_{11}(x,y) > 0$$

i.e., the linear condition.

The output power of the tube was derived through the integration of the Poynting vector over the cross-section of the tube.

$$S = \frac{1}{2} \; ExH^*$$

$$S_z = \frac{1}{2} \; (E_r H_\phi^* - E_\phi H_r^*) = \frac{1}{2\mu_o} \; (E_r B_\phi^* - E_\phi B_r^*)$$

$$S_z = \frac{k}{2\omega\mu_o}(E_r E_r^* + E_\phi E_\phi^*)$$

$$P_z = \frac{k}{2\omega\mu_o} \int_o^{2\pi} \cos^2\phi \, d\phi$$

$$\int_o^{R_w} E_o^2 \left\{ \left[(\frac{1}{k_t r}) J_1(k_t r) \right]^2 + J_1'^2(k_t r) \right\} r \, dr$$

$$P_z = \frac{k}{2\omega\mu_0} \frac{1}{2} E_0^2 \int_0^{R_W} [\{\frac{1}{2}[J_0(k_t r) + J_2(k_t r)]\}^2 +$$

$$\{\frac{1}{2}[J_0(k_t r) - J_2(k_t r)]\}^2] \, rdr$$

$$P_z = \frac{1}{8} \frac{k}{\omega\mu_0} E_0^2 \int_0^{R_W} [J_0^2(k_t r) + J_2^2(k_t r)] \, rdr$$

Using the following relationship

$$\int_0^{R_W} r J_m^2(k_t r) dr =$$

$$\frac{R_W^2}{2}[J_m^2(k_t R_W) - J_{m-1}(k_t R_W) J_{m+1}(k_t R_W)]$$

and substituting, we finally get:

$$P_z = \frac{1}{8} \frac{k}{\omega\mu_0} E_0^2 R_W^2 (1 - \frac{1}{k_t^2 R_W^2}) J_1^2(k_t R_W) \qquad (5.2)$$

5.2 Numerical Results

For a homogeneous cylindrical waveguide (refer to equation 5.1),

$$o = (1 - \frac{m^2}{k_t^2 R_W^2}) J_m^2(k_t R_W)$$

This term, which comes from

$$\int_0^{R_W} r J_m^2(k_t r) dr$$

is a geometrical factor that represents the way the power density is distributed over the cross-section. For the geometry considered, this term should not be very much different from the one of the cylindrical-guide (see chapter 3 for a discussion about R_w).

The above integral-differential equation was then integrated using the solution k and ω of the linear problem. Figures 5.1 (for the WG–B1 interaction) and 5.6 (for the WG–B3 interaction) show the wave amplitude E_O versus the interaction length for several frequencies[*]. The wave amplitude at the input of the tube was the same in both cases, and chosen very small so that the results of the linear analysis apply at the tube entrance. Several conclusions can be inferred from these two figures:

> 1. In the WG–B1 case, the growth rate of the wave is approximately linear, except near the saturation point, and the gain per unit length in the pass-band is about the same as the small signal gain derived in the linear analysis, which proves the consistency of this approach. This also means that the linear approach can be used even for large values of the wave intensity, as long as we are far enough from the saturation level of the tube.

---

[*]The complex ω, real k results were used

The WG-B3 case is different in the sense that the growth rate, although linear, is different from the one obtained in the linear analysis. The reason is that the beam and the wave are far apart, and therefore the nonlinear relationship is different from the one derived in [29] & [30]. However, when the two dispersion relations get closer to each other, i.e., near the higher cut off frequency, both analyses yield the same results.

2. The saturation value of the electric field intensity (i.e., the value of E_0 at saturation) decreases as the frequency is increased. Also, the saturated electric field intensity decreases monotonically as the frequency is increased, then sharply near the higher cut off frequency.

3. The higher the frequency, the longer it takes the wave to reach saturation.

4. The maximum value of the saturated electric field intensity always occurs at the lowest frequency [*].

---

[*] This relates to the experimentally observed fact that the largest linear gain is obtained when the electron cylotron frequency is closest to the lower cut off frequency of the guide.

Figure 5.2 (WG-B1 case) is a plot of the maximum output power available, i.e., the saturation power, versus frequency. This power increases as frequency is increased and shows a sharp drop near the higher cut off frequency.

Figure 5.3 show the saturation efficiency η_S versus frequency. We defined this efficiency η_S as the ratio of the wave power to the dc power of the beam (the $V_B I_B$ product). The saturation efficiency

$$\eta_S = \frac{\gamma - \gamma_0}{\gamma_0 - 1}$$

used by many authors is meaningless in this case because it is greater than 1. This is due to the averaging process used to derive the integral-differential equation. Taking more terms into consideration when averaging the initial phases of the electrons would certainly be more accurate, at the expense however of having to solve a 5th order differential-integral equation at least.

For a complete final picture of the gyrotron amplifier, several choices have to be made: indeed, a trade-off between bandwidth, output power and tube length is required.

For example (see figure 5.1), a 20dB tube at 4.497GHz "center frequency" (defined as the one with a saturated output electric field) will be 37cm long; for the same input electric field, a wave at another frequency would have either passed the saturation point or would still be gaining

energy from the beam. In this example, all the frequencies below 4.497GHz will be at the saturation point and the higher frequencies are close to it. This therefore represents the best operating conditions for the tube since the power output will be maximum (or close to the maximum), and we also get a substantial 24.9% bandwidth (see figures 5.4 and 5.5). The bandwidth can be defined as the range of frequencies such that:

1. the output electric field $E_O \geq E_O max/\sqrt{2}$
2. the output power $P_O \geq P_O max/2$.

In this case, they do not represent the same thing.

Another example would be to choose the "center frequency" of the 20dB tube to be 5.259GHz. But then, the tube would be 42cm long with most of the lower frequencies past the saturation point, hence a lower power output and a smaller bandwidth. This situation arises if one chooses maximum saturation power frequency as the "center frequency" of the tube.
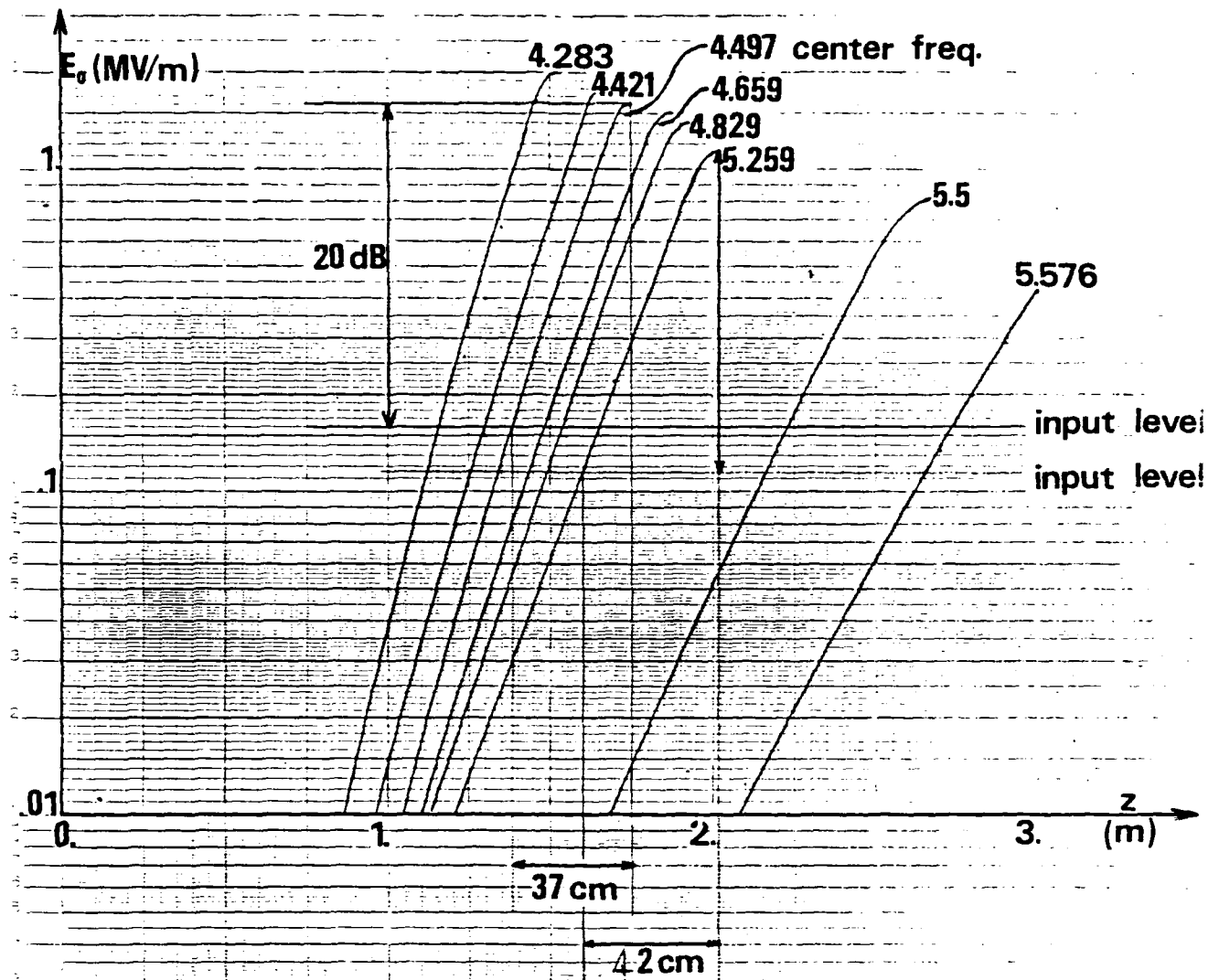
Fig. 5.1

Electric Field Intensity vs interaction length
for several hot tube frequencies
(WG-B1 interaction)

Fig. 5.2
Saturation Power vs frequency
WG–B1 interaction

Fig. 5.3
Saturation Efficiency vs frequency
WG–B1 interaction

Fig. 5.4

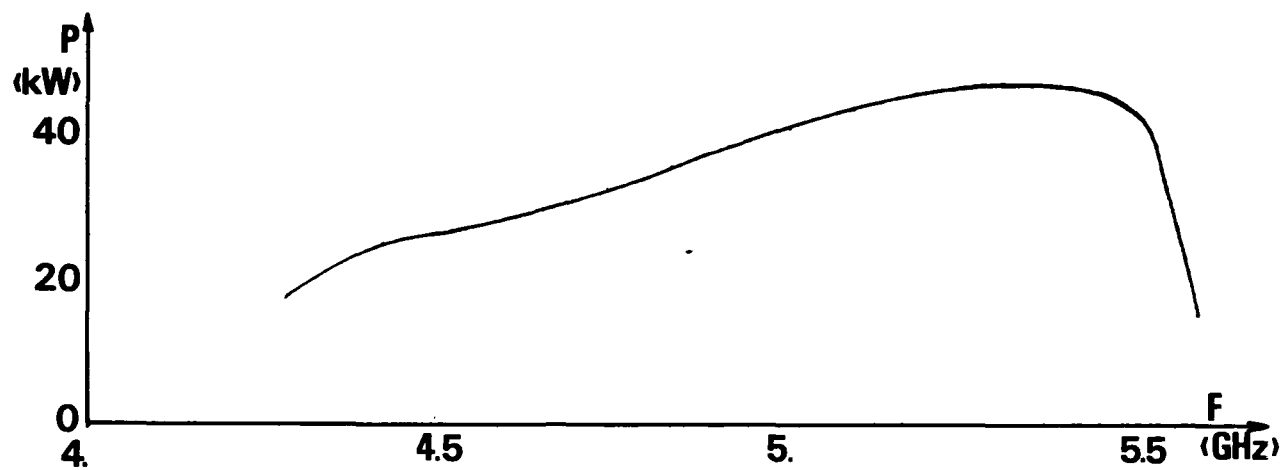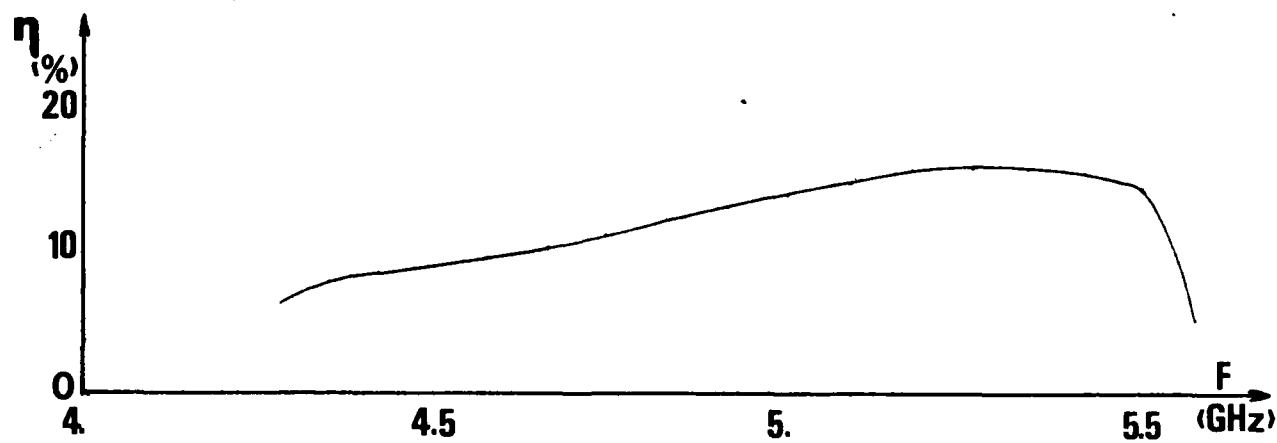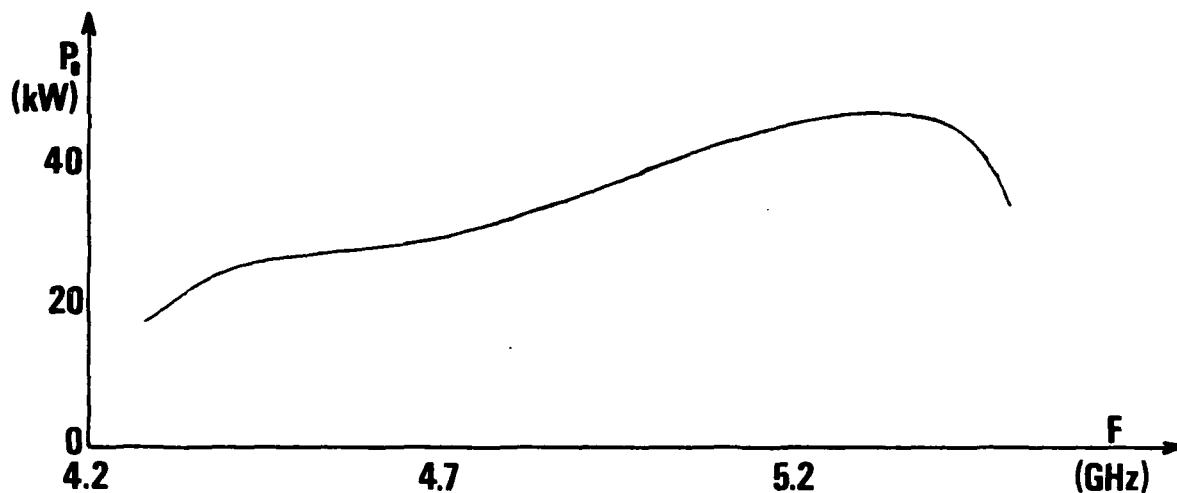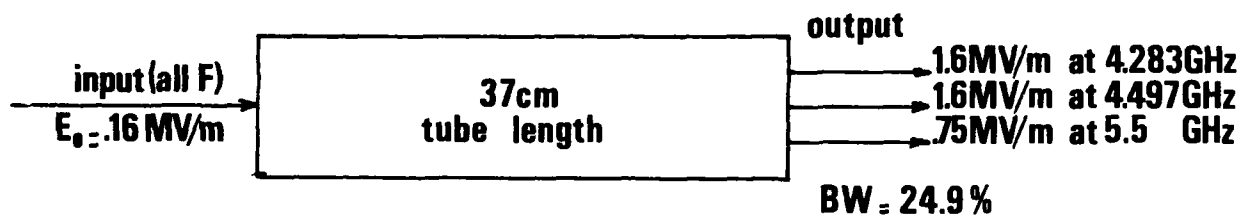Output Power vs frequency for the 37cm long tube

Fig. 5.5
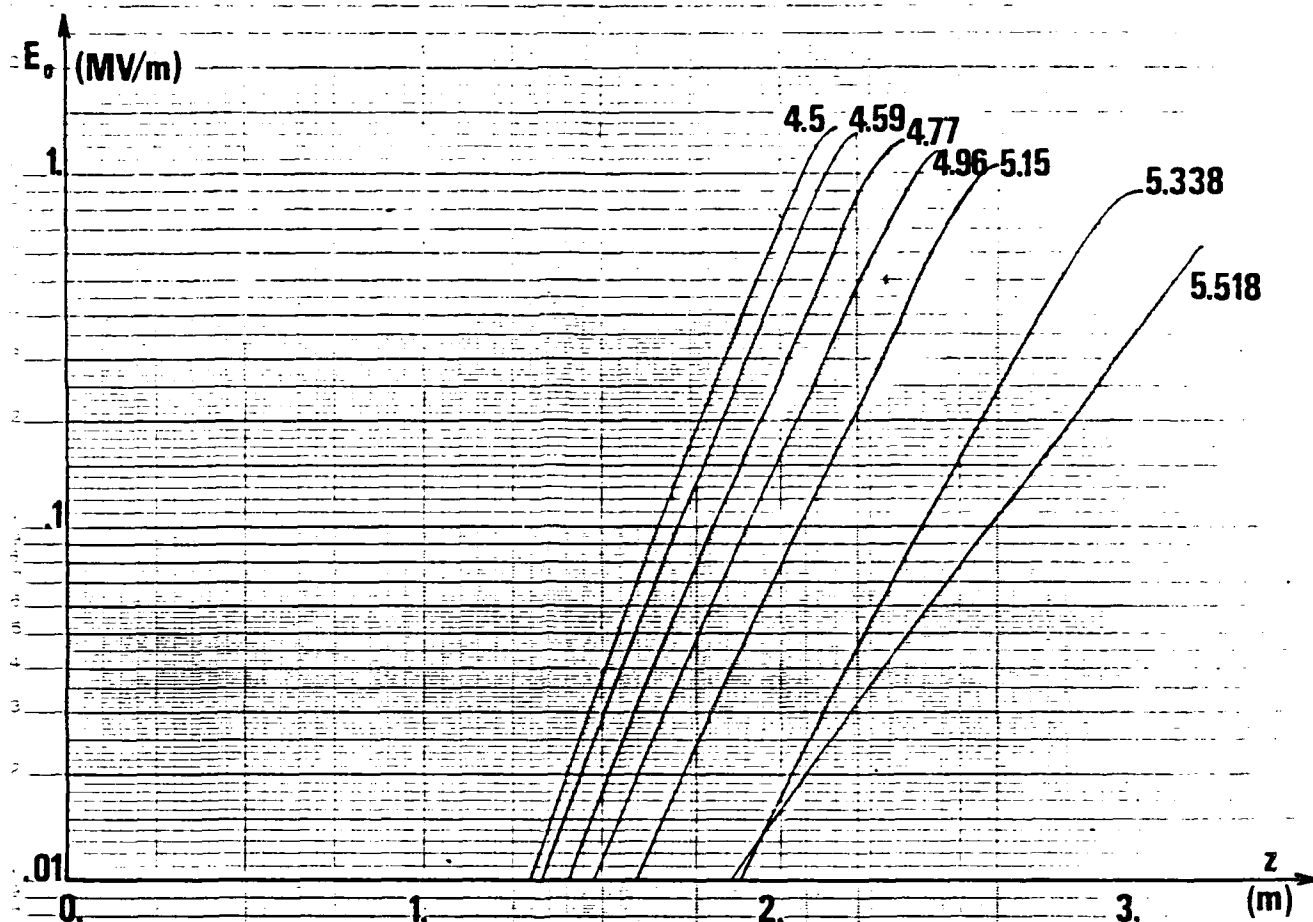
The 20dB tube characteristics (WG-B1 case)

Fig. 5.6

Electric Field Intensity vs interaction length for several hot tube frequencies WG-B3 interaction

CHAPTER 6

CONCLUSION

The results of the linear and non-linear analyses show that a periodically disc-loaded cylindrical waveguide design can be a good contender for gyrotron amplifier applications.

A 37cm long tube (20dB saturated gain) can deliver a peak output power of about 48kW at 5.3GHz with a 18% efficiency. A nearly straight line phase characteristic, a bandwidth of about 25% and the fact that the structure is non-dispersive make it suitable for wide band power amplification in communication /radar.

The only tubes that have been experimentally tested in the same frequency band, are two Varian tubes, [18]-[19]. They were both of a smooth wall cylindrical design; however, the magnetic field profile in the second tube was not uniform, varying from 1800G at the input of the tube to 1900G at the output, and also some distributed losses were included in this second tube. The first tube operated at a beam voltage V_b = 60kV and a beam current I_b = 5A, whereas the second operated at V_b = 65kV and I_b = 8A. Both tubes were 43cm long, for an 18dB saturated gain for the first tube and 20dB saturated gain for the second. The small signal gain was approximately the same in both cases, 24dB/m for the first tube, 26dB/m for the second. The peak power

output achieved was 50kW at 5GHz (with 16.6% efficiency) for the first tube, and 128kW at 5.2GHz (with 24% efficiency for the second tube; the bandwidths were respectively 6% and 8.8%. Phase linearity for the second tube was within $\pm 26^{o}$; it was not reported for the first tube.

In all the work performed for this study, the beam was assumed to be monoenergetic, the space charge effect and the velocity spread were both neglected. Chen and Chu, [44], show that the gain is insensitive to the velocity spread in the longitudinal direction for monoenergetic electrons, for $\Delta p_z/p_{zo}$ = 0, 25%, 50%; also, according to their study, in regions where the growth rate is small, a spread in v_z can enhance the growth rate. These results contradict previous ones (Caplan, Lin, Chu, 1982 as reported by Feinstein and Felch, 1987, [43]) stating that the output efficiency is degraded by a factor of 2 from that achievable with an ideal beam when $\Delta p_z/p_{zo}$ = 15%.

In that same paper, Chen and Chu confirm the existence of a space charge instability, and show that it is an electro-static cyclotron instability that exists in the beam, independently of the circuit. It can lead to significant noise enhancement in gyrotrons and gyrotrons amplifiers. The noise level was measured by Ferguson et al. to be in 44-52dB range above thermal, comparable to the small signal gain.

These problems have not been addressed in this work, which was primarily concerned with the feasability and characteristics of a high quality gyro-TWT using a slow wave structure as its circuit. The upcoming experiments at Fort Monmouth with a hot tube based on this design should yield a wealth of reliable information.

NOTE ABOUT THE APPENDICES

In appendix A, the derivation of the linear dispersion relation is presented in detail. The result has been published first in [37] and subsequently used by several investigators. The derivation has never, however, been published. It has been included here for the benefit of the newcomer to this field and for the sake of completeness.

The detailed derivation of the non-linear equation describing the evolution of the radiation fields has been included in appendix B for similar reasons. It was first derived by S.P. Kuo and B.R. Cheo [29].

APPENDIX A

DERIVATION OF THE LINEAR DISPERSION RELATION

A.1 General:

We have seen that electrons subjected to rapidly fluctuating electromagnetic field will deviate from their unperturbed orbits. The new motion can be resolved into a quasistatic term plus a rapidly oscillating term. It is the slowly varying part of the motion which is responsible for the instability and subsequent nonlinear behavior.

The arrangement of the gyro-TWT consists of an annular electron beam propagating inside the disc loaded waveguide. The electrons, guided by a uniform magnetic field $B_0 z_0$, move along helical trajectories. In this model, we assume that the beam is sufficiently tenuous so that its space charge electric field can be neglected and the spacial structure of the waveguide mode is unaffected by the presence of the beam. The beam interacts with a single TE_{mn} waveguide mode, where m and n are respectively the azimuthal and radial eigen mode numbers. The dynamics of the electron beam is described by the Vlasov equation.

In this appendix, we start with the derivation of the linear dispersion relation of the gyrotron first for a beam

interacting with a TE_{mn} mode, then for a beam interacting
with a TM_{mn} mode, combining at the end the two for a general
linear dispersion relation.

It is then shown that the term due to the interaction
beam-TM_{mn} is much smaller than the one due to the beam-TE_{mn}
interaction and hence, can be discarded without losing much
information regarding the behavior of the hot tube. Similarily, the terms due to the non-fundamental interaction beam-
TE_{mn} have a much smaller contribution than the one due to
the dominant mode.

A.2 Derivation of the linear dispersion relation:

Let's start with Vlasov equation

$$\left[\frac{\partial}{\partial t} + \frac{p}{\gamma m} \cdot \nabla - e(E + v \times B) \cdot \nabla_p \right] f = 0$$

where f is the electron distribution function, and let's
define in the linear approximation $f = f_0 + f_1$, where f_0 is
the initial and f_1 the perturbed distribution functions
respectively, with $f_1 \ll f_0$. Then

$$\left[\frac{\partial}{\partial t} + \frac{p}{\gamma m} \cdot \nabla - e(v \times B_0 z_0) \cdot \nabla_p \right] f_1 = e(E_1 + v \times B_1) \cdot \nabla_p f_0 \quad (A.1)$$

where we have neglected on the right hand side the second
order small term $\left[e(E_1 + v \times B_1) \cdot \nabla_p \right] f_1$; E_1 and B_1 represent
respectively the wave electric field and magnetic displacement.

To solve Vlasov equation, we use the Lagrangian coordinate system, and define an unperturbed trajectory

$$\frac{d\mathbf{r}}{dt} = \frac{\mathbf{p}}{\gamma m_0}$$

$$\frac{d\mathbf{p}}{dt} = - e \ \mathbf{v} \times \mathbf{z}_0 = - e \ \frac{\mathbf{p}}{\gamma m_0} \times B_0 \ \mathbf{z}_0 = - \Omega \ \mathbf{p} \times \mathbf{z}_0$$

(A.2)

where $\Omega = eB_0/\gamma m_0$ is the relativistic electron cyclotron frequency.

Then, along the trajectory:

$$\frac{\partial}{\partial t} + \frac{\mathbf{p}}{\gamma m_0}.\nabla - e \ (\mathbf{v} \times B_0 \ \mathbf{z}_0) = \frac{\partial}{\partial t} + \frac{d\mathbf{r}}{dt}. \ \nabla + \frac{d\mathbf{p}}{dt}. \ \nabla_{\mathbf{p}} = \frac{d}{dt}$$

Equation A.1 then becomes

$$\frac{df_1}{dt} = e(\mathbf{E}_1 + \mathbf{v} \times B_1).\nabla_{\mathbf{p}} f_0$$

(A.3)

We now have only one variable, t, whereas in Euler's coordinate system, we would have three independent variables.

The perturbed electron distribution function is then given by:

$$f_1(t) = e \int_{-\infty}^{t} \left[\mathbf{E}_1(t') + \mathbf{v}(t') \times \mathbf{B}_1(t') \right] \cdot \nabla_{\mathbf{p}'} f_0 \, dt' \qquad (A.4)$$

Along the unperturbed tragectory, γ is a constant and the only force here is the magnetic force due to the uniform and constant background magnetic field $B_0 \mathbf{z}_0$. The solution is therefore a uniform motion along z and a circular motion in the perpendicular plane, i.e.

$$v_z(t) = v_z(t')$$
$$p_t(t) = p_t(t') \qquad (A.5)$$
$$\gamma(t) = \gamma(t')$$

Hence,

$$\nabla_{\mathbf{p}} = \left(\frac{\partial}{\partial p_t} , \frac{\partial}{\partial p_z} \right) = \nabla_{\mathbf{p}'} \left(\frac{\partial}{\partial p_t'} , \frac{\partial}{\partial p_z'} \right) \qquad (A.6)$$

and therefore

$$\nabla_{\mathbf{p}} f_0 = \frac{\partial f_0}{\partial p_x} \mathbf{x}_0 + \frac{\partial f_0}{\partial p_y} \mathbf{y}_0 + \frac{\partial f_0}{\partial p_z} \mathbf{z}_0$$

$$\nabla_{\mathbf{p}} f_0 = \frac{\partial f_0}{\partial p_t} \frac{\partial p_t}{\partial p_x} \mathbf{x}_0 + \frac{\partial f_0}{\partial p_t} \frac{\partial p_t}{\partial p_x} \mathbf{y}_0 + \frac{\partial f_0}{\partial p_z} \mathbf{z}_0 \qquad (A.7)$$

$$\nabla_{\mathbf{p}} f_0 = \frac{\partial f_0}{\partial p_t} \cos\theta \, \mathbf{x}_0 + \frac{\partial f_0}{\partial p_t} \sin\theta \, \mathbf{y}_0 + \frac{\partial f_0}{\partial p_z} \mathbf{z}_0$$

A.2-1 Dispersion Relation for TE modes

The electromagnetic wave fields can be described by:

$$\mathbf{E}_1 = E_r \ \mathbf{r_o} + E_\phi \ \boldsymbol{\phi_o}$$

$$\mathbf{B}_1 = B_r \ \mathbf{r_o} + B_\phi \ \boldsymbol{\phi_o} + B_z \ \mathbf{z_o}$$

Then:

$$\mathbf{E}_1 + \mathbf{v} \times \mathbf{B}_1 = (E_r + v_\phi B_z - v_z B_\phi) \ \mathbf{r_o} +$$

$$(E_\phi + v_z B_r - v_r B_z) \ \boldsymbol{\phi_o} + (v_r B_\phi - v_\phi B_r) \ \mathbf{z_o} \qquad (A.8)$$

For a TE wave,

$$B_\phi = \frac{k}{\omega} \ E_r$$

$$\qquad (A.9)$$

$$B_r = - \frac{k}{\omega} \ E_\phi$$

Also,

$$v_r = v_t \ \cos(\theta - \phi)$$

$$\qquad (A.10)$$

$$v_\phi = v_t \ \sin(\theta - \phi)$$

Substituting equations A.9 and A.10 into equation A.8 we get

$$\mathbf{E}_1 + \mathbf{v} \times \mathbf{B}_1 = \left[(1 - \frac{kv_z}{\omega}) E_r + v_t B_z \ \sin(\theta - \phi) \right] \ \mathbf{r_o} +$$

$$\left[(1 - \frac{kv_z}{\omega}) E_\phi - v_t B_z \ \cos(\theta - \phi) \right] \ \boldsymbol{\phi_o} +$$

$$\frac{v_t k}{\omega} \left[E_r \cos(\theta - \phi) + E_\phi \sin(\theta - \phi) \right] z_O \qquad (A.11)$$

Taking the dot product of equation A.11 with A.7, we get

$$(E_1 + v \times B_1) \cdot \nabla_p f_O = \left[(1 - \frac{k v_z}{\omega}) \frac{\partial f_O}{\partial p_t} + \frac{v_t \kappa}{\omega} \frac{\partial f_O}{\partial p_z} \right]$$

$$\left[E_r \cos(\theta - \phi) + E_\phi \sin(\theta - \phi) \right] \qquad (A.12)$$

where we have used the following relationships:

$$r_O \cdot x_O = \phi_O \cdot y_O = \cos \phi$$

$$r_O \cdot y_O = - \phi_O \cdot x_O = \sin \phi$$

(refer to figure A.1 for notation).

Now, the solution of the wave equation for the TE electric field is given by:

$$E_r = - \frac{\omega}{k_t} B_{zo} \frac{m}{k_t r} J_m(k_t r)\ e^{j(\omega t - kz - m\phi)}$$

$$\qquad (A.13)$$

$$E_\phi = j \frac{\omega}{k_t} B_{zo} J_m{}'(k_t r)\ e^{j(\omega t - kz - \dot{m}\phi)}$$

With the help of Bessel's recursion equations

$$\frac{m}{k_t r} \, J_m(k_t r) = \frac{1}{2}\left[J_{m-1}(k_t r) + J_{m+1}(k_t r) \right]$$

$$J_m{}'(k_t r) = -\frac{1}{2}\left[J_{m-1}(k_t r) - J_{m+1}(k_t r) \right]$$

and Bessel's addition theorem

$$J_m(k_t r) = e^{-jm(\phi_0 - \phi)} \sum_{p=-\infty}^{\infty} J_{m+p}(k_t r_0) \, J_p(k_t R_L)$$

$$e^{jp(\frac{\pi}{2} - \phi_0 + \theta)}$$

where we have used the geometrical relationships

$$r^2 = r_0{}^2 + r_L{}^2 - 2\, r_0 \, r_L \cos \alpha$$

and $\qquad \alpha = \frac{\pi}{2} - \phi_0 + \theta$

we find that

$$E_r \cos(\theta - \phi) + E\phi \sin(\theta - \phi) = j\, \frac{\omega}{k_t}\, B_{zo}\, e^{j(\omega t - kz)}\, e^{-jm\phi_0}$$

$$\sum_{p=-\infty}^{\infty} J_{m+p}(k_t r_0)\, J_p{}'(k_t R_L)\, e^{jp(\frac{\pi}{2} - \phi_0 + \theta)} \qquad\qquad (A.14)$$

and hence, by substituting A.14 into A.12 and the result into equation A.3, we get:

$$\frac{df_1}{dt} = j\frac{eB_{zo}}{k_t}\Big[(\omega - kv_z)\ \frac{\partial f_o}{\partial p_t} + v_t k\ \frac{\partial f_o}{\partial p_z}\Big]\ e^{j(\omega t\ -\ kz)}\ e^{-jm\phi_o}$$

$$\sum_{p=-\infty}^{\infty}\ J(k_t r_o)\ J_p{}'(k_t R_L)\ e^{jp(\frac{\pi}{2}\ -\ \phi_o\ +\ \theta)} \tag{A.15}$$

Note that the only time-dependent functions in the above expression (equation A.15) are

$$e^{j(\omega t - kz)} \quad \text{and} \quad e^{jp(\frac{\pi}{2}\ -\ \phi_o\ -\ \theta)}$$

Integrating equation A.15 with respect to time (from $t' = -\infty$ to t), we get:

$$f_1^{\cdot}(t) = \frac{eB_{z_o}}{\kappa_\tau}\ e^{j(\omega t\ -\ kz)}\ e^{-jm\phi_o}\ \Big[(\omega\ -\ kv_z)\ \frac{\partial f_o}{\partial p_t} + v_t k\ \frac{\partial f_o}{\partial p_z}\Big]$$

$$\sum_{p=-\infty}^{\infty}\ \frac{J_{m+p}(k_t r_o)\ J_p{}'(k_t R_L)}{\omega\ -\ kv_z\ +\ p\Omega_o}\ e^{jp(\frac{\pi}{2}\ -\ \phi_o\ +\ \theta)} \tag{A.16}$$

Equation A.16 represents the response of the beam to the perturbation introduced by the wave field.

This perturbation in the electron distribution function gives rise to a perturbed beam current which will be the source of the perturbation in the wave field. Hence, in the wave equation, this source term must be included to find the response of the field to the perturbation in the beam, i.e.,

$$\left[k_o^2 - (k^2 + k_t^2)\right] B_z = -\mu (\nabla \times J)_z$$

where

$$J_{r,\phi} = -e \int f_1 v_{r,\phi} d^3 p$$

that is

$$\left[k_o^2 - (k^2 + k_t^2)\right] Bz = -\frac{\mu}{r} - \left[\frac{\partial}{\partial r}(rJ_\phi) - \frac{\partial J_r}{\partial \phi} \right] \qquad (A.17)$$

A rigorous solution would be to find the Green's function for a δ-source and then integrate over the source. A good approximation is to take the average over the cross-section.

Since

$$B_z = B_{zo} J_m (k_t r) e^{j(\omega t - kz - m\theta)}$$

we get by substituting the expression for B_z into equation A.17

$$\int_0^{R_w} \left[k^2 - (k_t^2 + k^2)\right] B_{zo} r J_m^2 (k_t r) \, dr =$$

$$- \mu \int_0^{R_w} \left[\frac{\partial}{\partial r}(rJ_\phi) - \frac{\partial J_r}{\partial \theta}\right] J_m(k_t r) e^{-j(\omega t - kz - m\phi)} \, dt \qquad (A.18)$$

The left hand side is easily integrated into:

$$\int_0^{R_w} r J_m^2 (k_t r) dr = \frac{R_w^2}{2} \left[J_m'^2 (k_t R_w) + \right.$$

$$\left. (1 - \frac{m^2}{k_t^2 R_w^2}) J_m^2(k_t R_w) \right]$$

and $J_m'^2(k_t R_w) = 0$ because of the boundary conditions.

Substituting into equation A.18, we get the following

$$k_o^2 - (k^2 + k_t^2) = - \frac{2\mu}{B_{zo} R_w^2 K_{mn}} \int \left[\frac{\partial}{\partial r}(r J_\phi) - \frac{\partial J_r}{\partial \phi} \right] J_m(k_t r)$$

$$e^{-j(\omega t - kz - m\phi)} dr \qquad\qquad (A.19)$$

where

$$K_{mn} = (1 - \frac{m^2}{k_t^2 R_w^2}) J_m^2(k_t R_w)$$

The integration on the right hand side needs more work. For self consistency, the current perturbation must have the same time dependance as the field that created it, i.e.

$$J_{r,\phi} = J_{r,\phi} \, e^{j(\omega t - kz - m\phi)}$$

hence,

$$\frac{\partial J_r}{\partial \phi} = -jm J_r$$

Also, we get through integration by parts:

$$\int \frac{\partial}{\partial r}(rJ_\phi)J_m(k_tr)dr = - \int \alpha_{mn}rJ_\phi J_m{}'(k_tr)dr$$

Hence, the terms in equation A.18 to be integrated with respect to r can be written as:

$$\int \left[-k_trJ_\phi J_m{}'(k_tr) + jmJ_rJ_m(k_tr)\right]dr \qquad (A.20)$$

With the help of the following identities,

$$J_m{}'(k_tr) = -\frac{1}{2}\left[J_{m-1}(k_tr) - J_{m+1}(k_tr)\right]$$

$$\frac{m}{k_tr}J_m(k_tr) = -\frac{1}{2}\left[J_{mn}(k_tr) + J_{m+1}(k_tr)\right]$$

the integral A.20 becomes:

$$-\frac{k_t}{2} \int_O^{R_w}\left[(J_\phi - jJ_r)J_{m-1}(\alpha_{mn}r) - (J_\phi + jJ_r)J_{m+1}(\alpha_{mn}r)\right]dr (A.21)$$

Using

$$J_r = - e\int v_r f_1 d^3p \qquad \text{and} \qquad J_\phi = - e\int v_\phi f_1 d^3p$$

and also

$$v_r = v_t \cos(\theta - \phi) \qquad \text{and} \qquad v_\phi = v_t \sin(\theta - \phi)$$

we get:

$$J_\phi - jJ_r = je\int \frac{p_t}{\gamma m_o} e^{j(\theta - \phi)} f_1 p_t dp_t d\theta dp_z$$

$$(A.22)$$

$$J_\phi + jJ_r = -je\int \frac{p_t}{\gamma m_o} e^{-j(\theta - \phi)} f_1 p_t dp_t d\theta dp_z$$

Using Bessel's addition theorem :

$$J_m(k_t r) = e^{jm(\phi_o - \phi)} \sum_{p'=-\infty}^{\infty} J_{m+p'}(k_t r_o) J_{p'}(k_t R_L) e^{-jp'(\frac{\pi}{2} - \phi_o + \theta)}$$

we find that

$$J_{m-1}(k_t r)e^{j(\theta - \phi)} + J_{m+1}(k_t r)e^{-j(\theta - \phi)} =$$

$$2je^{jm(\phi_o - \phi)} \sum_{p'=-\infty}^{\infty} J_{m+p'}(k_t r_o)$$

$$J'_{p'}(k_t R_L)e^{-jp'(\frac{\pi}{2} - \phi_o + \theta)}$$

$$(A.23)$$

Substituting equations A.22 and A.23 into A.21, and the result into equation A.19, we come up with :

$$k_o^2 - (k^2 + k_t^2) =$$

$$-2\frac{\mu e k_t}{R_w^2 K_{mn}} e^{-j(\omega t - kz - m\phi)}$$

$$\int_0^{R_w} r\,dr \int_{-\infty}^{\infty} dp_z \int_0^{\infty} dp_t \int_0^{2\pi} d\theta \frac{p_t^2}{\gamma m_o} f_1 e^{jm(\phi_o - \phi)}$$

$$\sum_{p'=-\infty}^{\infty} J_{m+p'}(k_t r) J'_{p'}(k_t R_L) e^{-jp'(\frac{\pi}{2} - \phi_o + \theta)} \qquad (A.24)$$

The integration with respect to θ is simple since everything is constant with respect to θ except for the terms

$$\sum_{p'=-\infty}^{\infty} e^{-jp'(\frac{\pi}{2} - \phi_o + \theta)}$$

$$\sum_{p=-\infty}^{\infty} e^{jp(\frac{\pi}{2} - \phi_o + \theta)}$$

which are in the expression for f_1. Hence, we have

$$\int_o^{2\pi} \sum_{p=-\infty}^{\infty} \sum_{p'=-\infty}^{\infty} e^{jp(\frac{\pi}{2} - \phi_o + \theta)} e^{-jp'(\frac{\pi}{2} - \phi_o + \theta)}$$

$$= \sum_{p,p'} e^{j(p - p')(\frac{\pi}{2} - \phi_o)} \int_o^{2\pi} e^{j(p - p')\theta} d\theta$$

Since $\int_o^{2\pi} e^{j(p - p')\theta} d\theta = 2\pi \delta_{pp'}$ where $\delta_{pp'}$ is the kronecker delta, i.e.,

$$\delta_{pp'} = \begin{cases} 0 & p \neq p' \\ 1 & p = p' \end{cases}$$

we get upon substitution into equation (A.24)

$$k_o^2 - (k^2 + k_t^2) = - \frac{4\pi\mu e^2}{R_w^2 K_{mn}} \int_o^{R_w} rdr \int_{-\infty}^{\infty} dp_z \int_o^{\infty} dp_t \frac{p_t^2}{\gamma m_o}$$

$$\left[(\omega - kv_z)\frac{\partial f_o}{\partial p_t} + v_t k \frac{\partial f_o}{\partial p_z} \right] \sum_p \frac{J_{m+p}^2(k_t R_o) J_p'^2(k_t R_L)}{\omega - kv_z + p\Omega} \qquad (A.25)$$

Let's choose the unperturbed distribution function to be

$$f_O = \frac{N_O}{2\pi r}\delta(r_O - R_O)g(p_t,p_z) \qquad (A.26)$$

where N_O is the number of electrons per unit length of the wave guide, the Dirac function $\delta(r_O - R_O)$ means that all the electrons have the same guiding center located on a cylindrical surface defined by $r = R_O$, and $g(p_t,p_z)$ is an arbitrary function of p_z satisfying $\int gd^3 = 1$.

Then (A.25) becomes :

$$k_O{}^2 - (k^2 + k_t{}^2) =$$

$$- \frac{2\mu e^2 N_O}{R_w{}^2 K_{mn}} \int_{-\infty}^{\infty} dp_z \int_O^{\infty} dp_t \frac{p_t{}^2}{\gamma m_O} \left[(\omega - kv_z)\frac{\partial}{\partial p_t} + v_t k_z \frac{\partial}{\partial p_z} \right]$$

$$g(p_t,p_z) \sum_{p=-\infty}^{\infty} \frac{J_{m+p}{}^2(k_t R_O) J_p{}'^2(k_t R_L)}{\omega - kv_z + p\Omega} \qquad (A.27)$$

Now, we need to integrate the right hand side, i.e.

$$\int_{-\infty}^{\infty} dp_z \int_O^{\infty} dp_t \frac{p_t{}^2}{m_O}\left[(\omega - \frac{kp_z}{\gamma m_O})\frac{\partial}{\partial p_t} + \frac{p_t}{\gamma m_O} k \frac{\partial}{\partial p_z} \right]$$

$$g(p_t,p_z) \sum_{p=-\infty}^{\infty} \frac{J_{m+p}{}^2(k_t R_O) J_p{}'(k_t R_L)}{\gamma\omega - \dfrac{k}{m_O}p_z + p\Omega_O} \qquad (A.28)$$

where we have let

$$\omega - kv_z + p\Omega = \frac{\gamma\omega - \dfrac{k}{m_O}p_z + p\Omega_O}{\gamma}$$

$$v_z = p_z/\gamma m_o \qquad \text{and} \qquad v_t = p_t/\gamma m_o$$

Integration by parts of (A.28) yields :

$$k_o^2 - (k^2 + k_t^2) = - \frac{2\mu e^2 N_o}{R_w^2 K_{mn}} \sum_{p=-\infty}^{\infty} \int_{-\infty}^{\infty} dp_z \int_{o}^{\infty} dp_t \frac{p_t}{\gamma m_o}$$

$$\left[\beta_t^2 \frac{(\omega^2 - k^2 c^2) H_{mp}(x,y)}{(\omega - kv_z + p\Omega)^2} - \frac{(\omega - kv_z) Q_{mp}(x,y)}{\omega - kv_z + p\Omega} \right] g(p_t, p_z)$$

where

$$x = k_t R_o$$

$$y = k_t R_L$$

$$H_{mp}(x,y) = \left[J_{p-m}(x) J_p{}'(y) \right]^2$$

$$Q_{mp}(x,y) = 2H_{mp}(x,y) + y \left[J_{p-m}{}^2(x) J_p{}'(y) J_p{}''(y) + \right.$$

$$\frac{1}{2} J_{p-m-1}{}^2(x) J_p{}'(y) J_{p-1}{}''(y) -$$

$$\left. \frac{1}{2} J_{p-m+1}{}^2(x) J_p{}'(y) J_{p+1}{}''(y) \right]$$

Let us now choose

$$g(p_t, p_z) = \frac{1}{2\pi p_t} \delta(p_t, p_{to}) \delta(p_z - p_{zo})$$

that is, the momentum distribution function of the electrons is the one for an idealized cold electron beam (the energy spread is very small). The integration is then easily carried out. The dispersion relation of the TE modes for a gyrotron is then :

$$k_o^2 - (k^2 + k_t^2) =$$

$$- \frac{\mu e^2 N_o}{\gamma m_o \pi R_w^2 K_{mn}} \left[\frac{\beta_t^2(\omega^2 - k^2 c^2) H_{mN}(x,y)}{(\omega - k v_z - N\Omega)^2} - \frac{(\omega - k v_z) Q_{mN}(x,y)}{\omega - k v_z - N\Omega} \right]$$

where we have introduced the grazing condition,

$$\omega = k v_z + N\Omega \qquad (i.e., \ p \rightarrow -N)$$

that is, the only electron cyclotron harmonic that interacts strongly with the wave is the lowest.

We can rewrite the common factor on the right hand side as

$$\frac{\mu e^2 N_o}{\gamma m_o \pi R_w^2 K_{mn}} = \frac{\omega_p^2}{\gamma K_{mn} c^2}$$

$$= \frac{4\nu}{\gamma R_w^2 K_{mn}}$$

ω_p = average non relativistic plasma frequency

$$\omega_p^2 = \frac{N_o e^2}{\varepsilon m_o \pi R_w^2}$$

ν = Budker constant

$$\nu = \frac{N_o \mu_o e^2}{4\pi m_o} \qquad \alpha \qquad I_b \ (the \ beam \ current)$$

A.2-2 Dispersion Relation for TM Modes

Following the same procedure, we derive now the dispersion relation for TM modes

$$E_1 = E_r \ r_o + E_\phi \ \phi_o + E_z \ z_o$$

$$\mathbf{B}_1 = B_r \, \mathbf{r}_o + B_\phi \, \boldsymbol{\phi}_o$$

Then

$$\mathbf{E}_1 + \mathbf{v} \times \mathbf{B}_1 = (1 - \frac{v_z}{c}\frac{\omega}{kc})(E_r \, \mathbf{r}_o + E_\phi \, \boldsymbol{\phi}_o) +$$

$$\left\{ E_z + \frac{v_t}{c}\frac{\omega}{kc} \left[E_r \cos(\theta - \phi) + E_\phi \sin(\theta - \phi) \right] \right\} \mathbf{z}_o$$

and

$$(\mathbf{E}_1 + \mathbf{v} \times \mathbf{B}_1) \cdot \nabla_p f_o =$$

$$(1 - \frac{v_z}{c}\frac{\omega}{kc}) \left[E_r \cos(\theta - \phi) + E_\phi \sin(\theta - \phi) \right] \frac{\partial f_o}{\partial p_t} +$$

$$\left\{ E_z + \frac{v_t}{c}\frac{\omega}{kc} \left[E_r \cos(\theta - \phi) + E_\phi \sin(\theta - \phi) \right] \right\} \frac{\partial f_o}{\partial p_z}$$

But now

$$E_r = - j\frac{k}{k_t} E_{zo} J_m{}'(k_t r) e^{j(\omega t - kz - m\phi)}$$

$$E_\phi = - \frac{m}{k_t}\frac{k}{k_t r} E_{zo} J_m(k_t r) e^{j(\omega t - kz - m\phi)}$$

After substitution, and using Bessel's addition theorem

we get

$$\frac{df_1}{dt} = eE_{zo} \sum_{p=-\infty}^{\infty} \left\{ \frac{p}{R_L k_t{}^2} \left[(k - \frac{\omega}{c}\frac{v_z}{c})\frac{\partial f_o}{\partial p_t} + \frac{v_t}{c}\frac{\omega}{c}\frac{\partial f_o}{\partial p_z} \right] + 1 \right\}$$

$$J_p(k_t R_L) e^{j(\omega t - kz)} J_{m+p}(k_t r_o) e^{-jm\phi_o} e^{jp(\frac{\pi}{2} - \phi_o + \theta)}$$

and, upon integration,

$$f_1(t) = -jeE_{zo}e^{j(\omega t - kz)}e^{-jm\phi_o}\frac{k}{k_t\omega}$$

$$\left\{\left[\omega - (k^2 + k_t^2)\frac{v_z}{k}\right]\frac{\partial f_o}{\partial p_t} + (k^2 + k_t^2)\frac{v_t}{k}\frac{\partial f_o}{\partial p_z}\right\}$$

$$\sum_{p=-\infty}^{\infty}\frac{(\frac{p}{k_tR_L} + 1)\, J_{m+p}(k_tr_o)J_p(k_tR_L)}{\omega - kv_z + p\Omega}e^{jp(\frac{\pi}{2} - \phi_o + \theta)}$$

where we substituted ω^2/c^2 by $k^2 + k_t^2$.

After integration with respect to θ where

$$\int_0^{2\pi} e^{jp\theta}e^{-jp'\theta}\,d\theta = 2\pi\delta_{pp'}$$

and integration with respect to r for the same unperturbed distribution function as we used for TE modes, the dispersion relation for TM modes becomes

$$\frac{\omega^2}{c^2} - (k^2 + k_t^2) = j\frac{\mu N_o e^2}{R_w^2 K_{mn}}\frac{E_{zo}}{B_{zo}}$$

$$\sum_{p=-\infty}^{\infty}\int_{-\infty}^{\infty}dp_z\int_0^{\infty}dp_t\frac{pt^2}{\gamma m_o}\frac{k}{\omega}\left\{\left[\omega - (k^2 + k_t^2)\frac{v_z}{k}\right]\frac{\partial g}{\partial p_t} + \right.$$

$$\left. (k^2 + k_t^2)\frac{v_t}{k}\frac{\partial g}{\partial p_z}\right\}(\frac{p}{k_tR_L} + 1)$$

$$\frac{J_{m+p}^2(k_tR_o)J_p'(k_tR_L)J_p(k_tR_L)}{\omega - kv_z + p\Omega} \tag{A.31}$$

We can substitute

$$j \; \frac{N_0 \mu e^2}{R_w^2 K_{mn}} \qquad \text{by} \qquad j \; \frac{\omega_p^2}{2c^2 K_{mn}}$$

Integration by parts of equation A.31 yields

$$\left(\frac{\omega}{c}\right)^2 - (k^2 + k_t^2) = - \frac{4\nu}{\gamma K_{mn} R_w^2} \left(- j \; \frac{k}{\omega}\right) \frac{E_{zo}}{B_{zo}}$$

$$\left\{ \beta_t^2 \; \frac{\left[\omega^2 - (k^2 + k_t^2)c^2\right] G_{mN}(x,y)}{(\omega - kv_z - N\Omega)^2} - \right.$$

$$\frac{\left[\omega - (k^2 + k_t^2)\frac{v_z}{k}\right] R_{mN}(x,y)}{\omega - kv_z - N\Omega} \qquad (A.32)$$

where

$$x = k_t R_O$$

$$y = k_t R_L$$

$$G_{mN}(x,y) = - J_{m-N}^2(x) \; \frac{N}{y} \; J_N(y) J_N{}'(y)$$

$$R_{mN}(x,y) = 2G_{mN}(x,y) - J_{m-N}^2(x) \; y \; \frac{\partial}{\partial y} \left[\frac{N}{y} \; J_N(y) J_N{}'(y)\right]$$

A.2-2 General linear dispersion relation

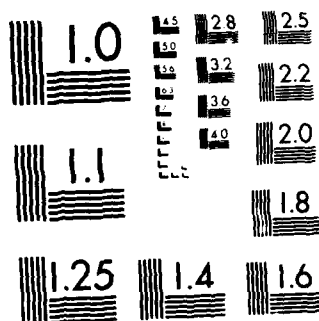Combining the results of the interaction with TE modes (equation A.30) and the result of the interaction with TM

END
DATE
FILMED
5 88

MICROCOPY RESOLUTION TEST CHART
NATIONAL BUREAU OF STANDARDS-1963-A

modes (equation A.32), we finally get the general dispersion relation :

$$\frac{\omega^2}{c^2} - (k^2 + k_t^2) = - \frac{\omega_p^2}{\gamma K_{mn} c^2}$$

$$\left\{ \beta_t^2 \frac{(\omega^2 - k^2 c^2) H_{Nm}(x,y) - j\frac{k}{\omega} \frac{E_{zo}}{B_{zo}} \left[\omega^2 - (k^2 + k_t^2)c^2\right] G_{Nm}(x,y)}{(\omega - kv_z - N\Omega)^2} \right.$$

$$\left. - \frac{(\omega - kv_z)Q_{Nm}(x,y) - j\frac{k}{\omega} \frac{E_{zo}}{B_{zo}} \left[\omega - (k^2 + k_t^2)\frac{v_z}{k}\right] R_{Nm}}{\omega - kv_z - N\Omega} \right\} (A.33)$$

If we substitute E_{zo}/B_{zo} by jcC/A, we then get a real dispersion relation

$$\frac{Ez_o}{Bz_o} = \frac{C}{A} = j\ c\ \frac{C'}{A}$$

The first term in the curled brackets on the RHS represents the contribution from the instability, the second term is the attenuation due to the Weibel instability.

A.3 Simplification of the dispersion relation

The linear theory allows us to derive the small signal dispersion relation (eq. A.33) for all types of beam-TE and beam-TM interactions. It may, however be possible to make
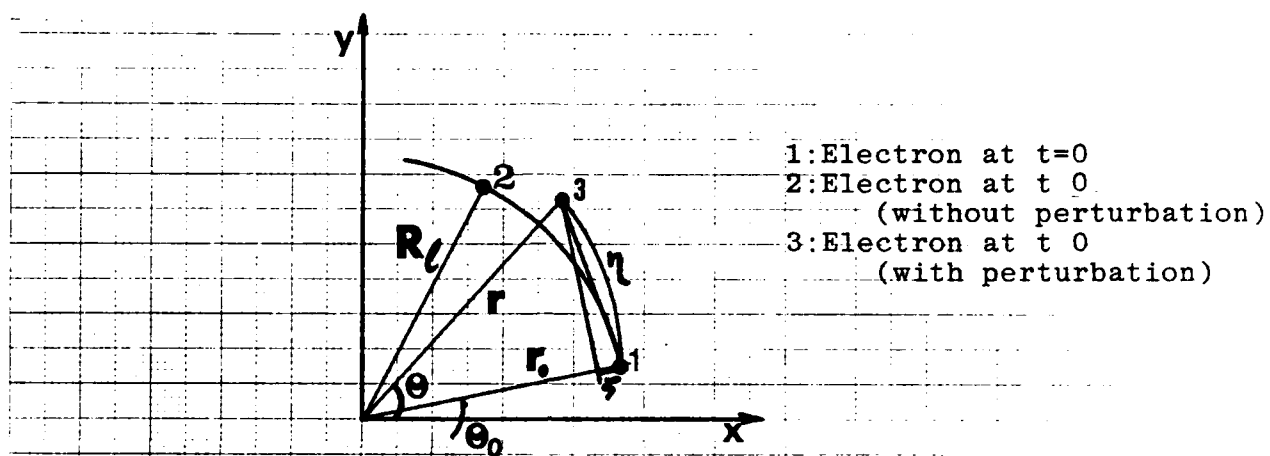
some approximations in order to have a simpler equation to work with. To achieve this purpose, we should compare the contributions from each interaction to the one which is dominant (i.e., the TE_{11}-beam interaction). We know that the magnitudes A_p/A_o and C_p'/A_o are small numbers since only the fundamental mode is propagating, the higher order modes being small and evanescent.

However, this is not enough to neglect the TM terms. Indeed, we need to know what is the contribution of the TM modes to the coupling. To do this, let's calculate the ratios of the TM to the TE contributions for each term on the right hand side of the dispersion relation (equation A.33) :

$$E_G = \frac{TM}{TE}\bigg|_{Gain} \simeq -\frac{2}{\beta_t^2}\left(\frac{k}{k_o}\right)^2 \frac{\Delta k}{k_o(1 - k^2/k_o^2)} \frac{G_{Nm}}{H_{Nm}} \frac{C_p'}{A_o}$$

$$E_W = \frac{TM}{TE}\bigg|_{Weibel} \simeq \frac{k}{k_o} \frac{1 - \beta_z k_o/k - 2\beta_z\Delta k}{(1 - k/k_o)\beta_z} \frac{R_{Nm}}{Q_{Nm}} \frac{C_p'}{A_o}$$

For a given (ω, k), these contributions are negligibly small. We can therefore disregard the contribution of the TM Modes to the dispersion relation, the error thus introduced being small.

FIG A1: Electron trajectory
Symbols used in the text

1:Electron at t=0
2:Electron at t 0
   (without perturbation)
3:Electron at t 0
   (with perturbation)

APPENDIX B

DERIVATION OF THE NON-LINEAR

EVOLUTION OF THE RADIATION FIELDS

B.1 General background:

The investigation of the non-linear evolution of the CMI starts with solving the equation of the single electron motion in the radiation fields. It is assumed that the phase trapping of the bunching electrons in the wave fields is the mechanism responsible for the saturation. The relations that determine the collective response of the electrons to the radiation fields are derived following the averaging of the results over the initial random phase distribution of the electron transverse velocity. The response of the radiation fields to the current induced by the electron bunching is then analyzed using the equation of conservation of energy. This self-consistant approach leads to the derivation of a single non-linear equation that describes the evolution of the radiation field intensity.

B.2 Characteristic equations:

The motion of the electrons in an electromagnetic field superimposed on a d.c. magnetic field is governed by the following set of coupled non-linear equations

$$\frac{d\mathbf{r}}{dt} = \frac{\mathbf{p}}{\gamma m_o} \tag{B.1}$$

$$\frac{d\mathbf{p}}{dt} = -e\left[\mathbf{E} + \mathbf{v} \times (\mathbf{B} + B_o\mathbf{z_o})\right] \tag{B.2}$$

The equation for the conservation of energy is defined by

$$m_o c^2 \frac{d\gamma}{dt} = -e\mathbf{E}.\mathbf{v} \tag{B.3}$$

where

$$\gamma = (1 + \frac{p^2}{m_o^2 c^2})^{1/2}$$

$$\mathbf{p} = \gamma m_o \mathbf{v}$$

The wave fields $\mathbf{E}$ and $\mathbf{B}$ of the TE_{mn} mode in a circular wave guide of radius Rw are given by

$$B_z = B_{zo} J_m(k_t r)\ e^{-jkz}\ e^{-jm\phi}$$

$$E_r = -\frac{\omega}{k_t}\ B_{zo}\ \frac{m}{k_t r}\ J_m(k_t r)\ e^{-jkz}\ e^{-jm\phi}$$

$$E_\phi = j\ \frac{\omega}{k_t}\ B_{zo}\ J_m{}'(k_t r)\ e^{-jkz}\ e^{-jm\phi} \tag{B.4}$$

$$B_r = -\ ^k/_\omega\ E_\phi$$

$$B_\phi = \ ^k/_\omega\ E_r$$

where k_t is the n-th root of the equation $J_m{}'(k_t R_w) = 0$.

Referring to figure A.1 for notation, the spatial coordinates (R, ϕ) of the electron can be expressed in terms of the coordinates (R_o, ϕ_o) of the guiding center of the elec-

tron and the coordinates (R_L, θ) of the motion of the electron about the guiding center, i.e.,

$$r^2 = R_O{}^2 + R_L{}^2 - 2R_O R_L \cos(\frac{\pi}{2} - \phi_O + \theta)$$
$$\phi = \phi_O - \sin^{-1} (R_L/R_O)\cos(\phi_O - \theta)$$

where $R_L = v_t/\Omega = p_t/m_O \gamma_O$ is the Larmor radius of the electron.

If the wave frequency ω is near one of the Doppler shifted harmonics, i.e., $\omega = kv_z + N\Omega$, the slowest term of the forces experienced by the gyrating electrons has the dominant influence on the orbit evolution of the electrons. Retaining this term only in equation B.1, we first define a self consistent trajectory

$$R_L = R_L(t)$$

$$\theta = \theta(t) = \theta_O + \psi(t) + \int_O^t \Omega(t')dt'$$

prior to express B.1 explicitly.

$R_L(t)$ and $\psi(t)$ are to be determined self-consistently and represent respectively the time dependant Larmour radius and that term in the phase that varies slowly in response to the slow time varying force.

We then substitute these relations and the expressions for the fields (eq. B.4) into B.1 and B.2 and neglect all the fast oscillating terms.

With the help of the addition theorem of the Bessel functions, the following results are derived

$$J_m(k_t R) = e^{jm(\phi_o - \phi)} \sum_{l=-\infty}^{\infty} J_{m+l}(k_t R_o) J_l(k_t R_L)$$

$$e^{-jl(\pi/2 - \phi_o + \theta)}$$

(B.5)

$$J_{m+1}(k_t R) = e^{\pm j(m\pm 1)(\phi_o - \phi)}$$

$$\sum_{l=-\infty}^{\infty} J_{+1+l}(k_t R_o) J_l(k_t R_L) e^{\pm jl(\pi/2 - \phi_o + \theta)}$$

Using B.5 and

$$e^{jx\sin\phi} = \sum_{l=-\infty}^{\infty} J_l(x) e^{jl\phi}$$

a set of self consistent characteristic equations for the slow varying functions γ, R_L, ψ and, v_z are derived

$$\frac{d}{dt}\alpha = a(\omega - kv_z) J_N'(\alpha)\cos\phi \qquad (B.6)$$

$$\frac{d}{dt}\phi = - \Delta\omega\left[1 + aJ_N(\alpha)\sin\phi\right] -$$

$$a(\omega - kv_z)\left\{-\frac{1}{\alpha}\frac{d}{d\alpha}\left[\alpha J_N'(\alpha)\right]\right\}\sin\phi \qquad (B.7)$$

$$\frac{d}{dt}\gamma = a\frac{\Omega_o^2\omega}{\gamma k_t^2 c^2}\alpha J_N'(\alpha)\cos\phi \qquad (B.8)$$

$$\frac{d}{dt}v_z = -a\frac{\Omega_0^2\omega}{\gamma^2 kk_t^2 c^2}(kv_z - \frac{k^2c^2}{\omega})\alpha J_N'(\alpha)\cos\phi \qquad (B.9)$$

where

$$\alpha = k_t R_L$$

$$\Omega_0 = \gamma\Omega = \frac{eB_0}{m_0 c}$$

$$\phi = (m - N)\phi_0 - \int_0^t \Delta\omega(t')dt' + N(\psi + \theta_0 + \frac{\pi}{2}) + kz_0 + \frac{\pi}{2}$$

$$\Delta\omega = \omega - N\Omega - kv_z = \Delta\omega_0 + (\omega_0 - \frac{k^2c^2}{\omega})\frac{\gamma - \gamma_0}{\gamma}$$

$$\Delta\omega_0 = \omega - \omega_0$$

$$\omega_0 = \frac{N\Omega_0}{\gamma_0} + kv_{zo}$$

$$a = (-1)^N\frac{B_{zo}}{B_0}J_{m-N}(k_t R_0)$$

Under the grazing condition, $v_z = kc^2/\omega = v_g$, equation B.9

reduces to $\frac{dv_z}{dt} = 0$ and thus $v_z = v_{zo}$

To close the system of equations, it is necessary to include a field equation that takes into account the dynami-

cal effects of the medium on the fields. The energy conser-
vation equation B.3 is used for this purpose, and under
grazing conditions it becomes

$$n_o m_o c^2 \frac{d\gamma}{dt} + \frac{\sigma \varepsilon_o}{2} \frac{d}{dt} E_o^2 = 0 \qquad (B.10)$$

n_o is the electron beam density averaged over the
cross-section of the guide.

< > stands for an average over the random initial phase
distribution of the electron beam.

$$E_o = \frac{\omega}{k_t c} B_{zo}$$

$$\sigma = (1 - \frac{m^2}{k_t^2 R_w^2}) J_m^2 (k_t R_w) \text{ is the filling factor and}$$

represents the energy distribution over the cross-section of
the guide.

The integration of equation B.10 leads to

$$n_o m_o c^2 (<\gamma> - <\gamma_o>) = \frac{\sigma \varepsilon_o}{2} \left[E_o^2(t) - E_o^2(0) \right] \qquad (B.11)$$

B.3 derivation of the NL field equation:

From the equation of conservation of energy, we can
find the polarization current density, i.e.,

$$n_o m_o c^2 \frac{d\gamma}{dt} + J.E = 0 \qquad (B.12)$$

yields

$$J_p = - a n_o m_o c^2 \frac{\Omega_o^2 \omega}{\gamma k_t^2 c^2} \alpha \frac{J_N'(\alpha)}{E_o} \cos\phi$$

But, since,

$$a = (-1)^N \frac{B_{zo}}{B_o} J_{m-N}(k_t R_o)$$

and

$$E_o = \frac{\omega}{k_t} B_{zo}$$

the expression for a becomes

$$a = (-1)^N \frac{k_t}{\omega} \frac{E_o}{B_o} J_{m-N}(k_t R_o)$$

and the expression for J_p, the polarization current density, is then

$$J_p = - (-1)^N \frac{e n_o \Omega_o}{\gamma k_t} J_{m-N}(k_t R_o) \alpha J_N'(\alpha) \cos\phi \qquad (B.13)$$

Also, using equations B.10 and B.12, we have

$$J_p = \sigma \varepsilon_o \frac{dE_o}{dt} \qquad (B.14)$$

We assume in the present analysis that the effect of depletion of the electron rotational free energy to be insignificant. Then, $E_0(t)$ and $\phi_0(t)$ are expected to vary with time much faster than the other variables α, γ, and v_z. We can then neglect the slow time variation of α and γ and make $\alpha \simeq \alpha_0$ in equation B.6 and $\gamma \simeq \gamma_0$ in equation B.8.

The averaged (over the random initial phase distribution) polarization current density will then be

$$\langle J_p \rangle = - (-1)^N \frac{e n_0 \Omega_0}{k_t} J_{m-N}(k_t R_0) \langle -\frac{\alpha}{\gamma} J_N'(\alpha) \cos\phi \rangle$$

$$\langle J_p \rangle = - (-1)^N \frac{e n_0 \Omega_0}{k_t} J_{m-N}(k_t R_0) -\frac{\alpha_0}{\gamma_0} J_N'(\alpha_0) \langle \cos\phi \rangle \qquad (B.15)$$

Using equation B.14 and writing equation B.15 as

$$\langle J_p \rangle = - (-1)^N P \langle \cos\phi \rangle$$

we get

$$\langle \cos\phi \rangle = - \frac{\sigma \varepsilon_0}{(-1)^N P} \frac{dE_0}{dt}$$

$$\langle \cos\phi \rangle = (-1)^{N+1} \frac{\sigma \varepsilon_0}{P} \frac{dE_0}{dt} \qquad (B.16)$$

where

$$P = \frac{e n_0 \Omega_0}{k_t} J_{m-N}(k_t R_0) -\frac{\alpha_0}{\gamma_0} J_N'(\alpha_0)$$

Equation B.8, with the simplifying assumptions $\alpha \simeq \alpha_O$ and

$\gamma \simeq \gamma_O$, can now be integrated to obtain

$$\gamma - \gamma_O \simeq \frac{\Omega_O{}^2 \omega}{k_t{}^2 c^2} \frac{\alpha_O}{\gamma_O} J_N{}'(\alpha_O) \int_0^t dt' a(t') \cos\phi' \qquad (B.17)$$

We can also approximate the expression for $\Delta\omega$ (using $\gamma \simeq \gamma_O$) to give

$$\Delta\omega \simeq \Delta\omega_O + \frac{\gamma - \gamma_O}{\gamma_O}(\omega_O - \frac{k^2 c^2}{\omega}) \qquad (B.18)$$

which, upon substituting equation B.17, yields

$$\Delta\omega \simeq \Delta\omega_O + A_O \int_0^t dt' a' \cos\phi'$$

where

$$A_O = (\frac{\Omega_O}{\gamma_O k_t c})^2 (\omega^2 - k^2 c^2) \alpha_O J_N{}'(\alpha_O)$$

$$a' = a(t')$$

$$\phi' = \phi(t')$$

Using equations B.16 and B.17, the average of $\Delta\omega$ can be expressed as

$$\langle \Delta\omega \rangle = \Delta\omega_O - (\omega - \frac{k^2 c^2}{\omega}) \frac{\sigma\varepsilon_O}{2\gamma_O n_O m_O c^2} [E_O{}^2(t) - E_O{}^2(0)] \qquad (B.19)$$

Taking into account only the resonant processes, the averaged polarization current density will be shown to obey a second order differential equation.

From the definition of J_p, we get

$$\frac{d^2 J_p}{dt^2} = P\left\{ \left[\frac{d\phi^2}{dt} - \frac{\frac{d^2}{dt^2}\left[\frac{\alpha}{\gamma}-J_N{'}(\alpha)\right]}{\alpha/\gamma \ J_N{'}(\alpha)}\right]\cos\phi + \right.$$

$$\left[\frac{d^2}{dt^2} + 2\frac{\delta\phi v}{dt} \frac{\frac{d}{dt}\left[\frac{\alpha}{\gamma}-J_N{'}(\alpha)\right]}{\alpha/\gamma \ J_N{'}(\alpha)}\right]\sin\phi \Big\}$$

$$\left\langle\frac{d^2 J_p}{dt^2}\right\rangle = P\left\{ \left\langle\frac{d\phi^2}{dt}\cos\phi\right\rangle - \left\langle\frac{\frac{d^2}{dt^2}\left[\frac{\alpha}{\gamma}-J_N{'}(\alpha)\right]}{\alpha/\gamma \ J_N{'}(\alpha)}\cos\phi\right\rangle + \right.$$

$$\left. + \left\langle\frac{d^2\phi}{dt^2}\sin\phi\right\rangle + 2\left\langle\frac{d\phi}{dt}\frac{\frac{d}{dt}\left[\frac{\alpha}{\gamma}-J_N{'}(\alpha)\right]}{\alpha/\gamma \ J_N{'}(\alpha)}\sin\phi\right\rangle \right\} \qquad (B.20)$$

In the following, we are going to derive the explicit expressions of functions averaged over the random initial phase distribution of the electron beam. Only the linear terms, and the non-linear terms of lowest order are retained.

Using equation B.6 through B.8, we get

$$\left\langle 2 \frac{d\phi}{dt} \frac{\frac{d}{dt}\left[\frac{\alpha}{\gamma} J_N{}'(\alpha)\right]}{\alpha/\gamma \; J_N{}'(\alpha)} \sin\phi \right\rangle = \left\langle \frac{d\phi}{dt} a\left(D_O - \frac{A_O \omega}{\omega^2 - k^2 c^2}\right)\sin 2\phi \right\rangle \tag{B.21}$$

$$\left\langle \frac{\frac{d^2}{dt^2}\left[\frac{\alpha}{\gamma} J_N{}'(\alpha)\right]}{\alpha/\gamma \; J_N{}'(\alpha)} \cos\phi \right\rangle =$$

$$(D_O{}^2 + D_1{}^2)a^2 \langle \cos^3\phi\rangle + \left(D_O - \frac{A_O\omega}{\omega^2 - k^2 c^2}\right)$$

$$\left[\frac{da}{dt}\langle\cos\phi\rangle + \frac{1}{2}a\langle\Delta\omega\sin2\phi\rangle + a^2 D_O\langle\sin2\phi\cos\phi\rangle\right.$$

$$\left. - 3\frac{A_O\omega}{\omega^2 - k^2 c^2}a^2\langle\cos^3\phi\rangle\right] \tag{B.22}$$

where

$$D_O = (\omega - kv_z)\frac{1}{\alpha_O}\frac{d}{d\alpha_O}\left[\alpha_O J_N{}'(\alpha_O)\right]$$

$$D_1{}^2 = (\omega - kv_z)^2 J_N{}'(\alpha_O)\frac{d}{d\alpha_O}\left\{\frac{1}{\alpha_O}\frac{d}{d\alpha_O}\left[\alpha_O J_N{}'(\alpha_O)\right]\right\}$$

and we have neglected $2A_O\omega/(\omega^2 - k^2 c^2)$ compared to $D_O{}^2 + D_1{}^2$ and also $a^2\Delta\omega J_N(\alpha)\sin^2\phi$ since this term is high order non-linear.

We also have

$$\frac{d\phi}{dt} = - \Delta\omega\left[1 + aJ_N(\alpha)\sin\phi\right] - aD_O\sin\phi \qquad (B.23)$$

$$\frac{d\phi^2}{dt} = (\Delta\omega_O)^2 + A_O(\Delta\omega + \Lambda\omega_O)$$

$$\int_O^t dt'a'\cos\phi' + a^2D_O^2\sin^2\phi + 2aD_O\Delta\omega\sin\phi \qquad (B.24)$$

$$\frac{d^2\phi}{dt^2} = - aA_O\cos\phi - D_O(\frac{da}{dt}\sin\phi - a\Lambda\omega\cos\phi) +$$

$$\frac{a^2}{2}\left[D_O^2 - D_1^2 - A_OJ_N(\alpha)\right]\sin2\alpha \qquad (B.25)$$

Then,

$$\langle\frac{d\phi^2}{dt}\cos\phi\rangle = (\Delta\omega_O)^2\langle\cos\phi\rangle + a^2D_O^2\langle\sin^2\phi\cos\phi\rangle +$$

$$aD_O\langle\Delta\omega\sin2\phi\rangle + A_O\langle(\Lambda\omega + \Delta\omega_O)\cos\phi$$

$$\int_O^t dt'a'\cos\phi'\rangle \qquad (B.26)$$

$$\langle\frac{d^2\phi}{dt^2}\sin\phi\rangle = - \frac{1}{2}aA_O\langle\sin2\phi\rangle - \frac{1}{2}\frac{da}{dt}D_O + \frac{1}{2}aD_O\langle\Delta\omega\sin2\phi\rangle$$

$$+ \frac{1}{4}a^2(D_O^2 - D_1^2)\langle\cos\phi\rangle \qquad (B.27)$$

The following simplifications

$$\langle\sin2\phi\rangle \simeq 0$$

$$\langle \sin^2\phi\cos\phi \rangle = \frac{1}{4}\langle \cos\phi \rangle - \frac{1}{4}\langle \cos3\phi \rangle \simeq \frac{1}{4}\langle \cos\phi \rangle$$

$$\langle \cos^3\phi \rangle = \frac{3}{4}\langle \cos\phi \rangle + \frac{1}{4}\langle \cos3\phi \rangle \simeq \frac{3}{4}\langle \cos\phi \rangle$$

can be substituted into equations B.21, B.22, B.26 and B.27, and the result into equation B.20 which then becomes:

$$\langle \frac{d^2 J_p}{dt^2} \rangle = P\left\{ \langle \cos\phi \rangle \left[3a^2 \frac{A_0\omega}{\omega^2 - k^2 c^2}(D_0 - \frac{3}{4}\frac{A_0\omega}{\omega^2 - k^2 c^2}) - \right.\right.$$

$$\left. (D_0{}^2 + D_1{}^2)a^2 + (\Delta\omega_0)^2 \right] - \frac{da}{dt}(D_0 - \frac{1}{2}\frac{A_0\omega}{\omega^2 - k^2 c^2}) +$$

$$\frac{3}{4}\langle \Delta\omega\sin2\phi \rangle a \frac{A_0\omega}{\omega^2 - k^2 c^2} +$$

$$A_0 \langle (\Delta\omega + \Delta\omega_0)\cos\phi \int_0^t dt' a'\cos\phi' \rangle \qquad (B.28)$$

We still need to find the explicit expressions for

$$\langle \Delta\omega\sin^2\phi \rangle \quad \text{and} \quad \langle (\Delta\omega + \Delta\omega_0)\cos\phi \int_0^t dt' a'\cos\phi' \rangle$$

$$\langle \Delta\omega\sin2\phi \rangle \simeq A_0 \langle 2\sin\phi\cos\phi \int_0^t dt' a'\cos\phi' \rangle$$

$$\simeq A_0 \left\{ \langle \sin\phi \int_0^t dt' a'\cos\phi\cos\phi' \rangle + \right.$$

$$\langle\cos\phi\int_0^t dt'a'\cos\phi'\sin\phi\rangle\Big\}$$

$$\simeq \frac{1}{2}A_0\Big\{\langle\sin\phi\int_0^t dt'a'\cos(\phi - \phi')\rangle +$$

$$\langle\sin\phi\int_0^t dt'a'\cos(\phi + \phi')\rangle +$$

$$\langle\cos\phi\int_0^t dt'a'\sin(\phi - \phi')\rangle +$$

$$\langle\cos\phi\int_0^t dt'a'\sin(\phi + \phi')\rangle\Big\}$$

We make the following approximations

$$\langle\sin\phi\int_0^t dt'a'\cos(\phi - \phi')\rangle \simeq \langle\sin\phi\rangle\int_0^t dt'a'\langle\cos(\phi - \phi')$$

$$\simeq \langle\sin\phi\rangle\int_0^t dt'a'\cos\langle\phi - \phi'\rangle$$

$$\langle\cos\phi\int_0^t dt'a'\sin(\phi - \phi')\rangle \simeq \langle\cos\phi\rangle\int_0^t dt'a'\langle\sin(\phi - \phi')\rangle$$

$$\simeq \langle\cos\phi\rangle\int_0^t dt'a'\sin\langle\phi - \phi'\rangle$$

$$\langle\sin\phi\int_0^t dt'a'\cos(\phi + \phi')\rangle \simeq \langle\sin\phi\rangle\int_0^t dt'a'\langle\cos2\phi\rangle \simeq 0$$

$$\langle\cos\phi\int_0^t dt'a'\sin(\phi + \phi')\rangle \simeq \langle\cos\phi\rangle\int_0^t dt'a'\langle\sin2\phi\rangle \simeq 0$$

These approximations are legitimate if only the linear and the lowest order non-linear terms are taken into consideration.

With the help of these approximations, we get

$$\langle \Lambda \omega \sin 2\phi \rangle \simeq \frac{1}{2}A_0 \left\{ \langle \sin\phi \rangle \int_0^t dt'a'\cos\langle \phi - \phi' \rangle + \right.$$

$$\left. \langle \cos\phi \rangle \int_0^t dt'a'\sin\langle \phi - \phi' \rangle \right\}$$

Integrating equation B.23, we get

$$\phi - \phi' = -\int_{t'}^t d\tau \Delta\omega(\tau) - a\int_{t'}^t d\tau \left[\Delta\omega J_N(\alpha) + D_0 \right] \sin\phi$$

So that

$$\langle \phi - \phi' \rangle \simeq -\int_{t'}^t \langle \Lambda\omega(\tau) \rangle d\tau$$

The other expression we still need can be expressed as

$$\langle (\Delta\omega + \Delta\omega_0)\cos\phi \int_0^t dt'a'\cos\phi' =$$

$$= \langle \Delta\omega\cos\phi \int_0^t dt'a'\cos\phi' \rangle + \Delta\omega_0 \langle \cos\phi \int_0^t dt'a'\cos\phi' \rangle$$

$$\simeq \frac{1}{2}\Delta\omega_0 \int_0^t dt'a'\cos\langle \phi - \phi' \rangle + \frac{1}{2}\langle \Delta\omega \rangle \int_0^t dt'a'\cos\langle \phi - \phi' \rangle$$

$$\simeq \frac{1}{2}(<\Delta\omega> + \Delta\omega_o)\int_o^t dt'a'\cos<\phi - \phi'>$$

Also, from the definition of J_p, we have

$$\frac{dJ_p}{dt} = - \frac{en_o\Omega_o}{k_t}J_{m-N}(k_tR_o)$$

$$\left\{\cos\phi\frac{d}{dt}\left[\frac{\alpha}{\gamma}J_N'(\alpha)\right] - \frac{\alpha}{\gamma}J_N'(\alpha)\frac{d\phi}{dt}\sin\phi\right\}$$

$$<\frac{dJ_p}{dt}> = \frac{en_o\Omega_o}{k_t}J_{m-N}(k_tR_o)$$

$$\left\{<\frac{\alpha}{\gamma}J_N'(\alpha)\frac{d\phi}{dt}\sin\phi> - <\cos\phi\frac{d}{dt}\left[\frac{\alpha}{\gamma}J_N'(\alpha)>\right]\right\}$$

$$<\frac{dJ_p}{dt}> = P\left[<\frac{d\phi}{dt}\sin\phi> - \frac{1}{2}a(D_o - \frac{A_o\omega}{\omega^2 - k^2c^2})\right] \qquad (B.29)$$

Since

$$\frac{d\phi}{dt}\sin\phi = - \Delta\omega\sin\phi - a\Delta\omega J_N(\alpha)\sin^2\phi - aD_o\sin^2\phi$$

We have

$$<\frac{d}{dt}\sin\phi> = - <\Delta\omega\sin\phi> - \frac{1\phi}{2}aD_o$$

$$= - \Delta\omega_o<\sin\phi> - \frac{1}{2}A_o\int_o^t dt'a'\sin<\phi - \phi'> - \frac{1}{2}aD_o$$

which yields

$$\langle \sin\phi \rangle = - \frac{\langle \frac{d\phi}{dt} \sin\phi \rangle}{\Delta\omega_O} - \frac{1}{2}\frac{A_O}{\Delta\omega_O} \int_0^t dt' a' \sin\langle \phi - \phi' \rangle - \frac{1}{2}\frac{aD_O}{\Delta\omega_O}$$

(B.30)

Using equations B.29 and B.30, we get the following

expression

$$\langle \sin\phi \rangle = - \left[\frac{\frac{dJ_p}{dt}}{P} + \frac{1}{2}(D_O - \frac{A_O\omega}{\omega^2 - k^2 c^2}) \right] \frac{1}{\Delta\omega_O} - \frac{1}{2}\frac{aD_O}{\Delta\omega_O} - $$

$$\frac{1}{2}\frac{A_O}{\Delta\omega_O} \int_0^t dt' a' \sin\langle \phi - \phi' \rangle$$

(B.31)

We also have from equation B.13

$$\langle \cos\phi \rangle = - \frac{J_p}{P}$$

(B.32)

Substituting equations B.31 and B.32 into equation

B.28, we get

$$\langle \frac{d^2 J_p}{dt^2} \rangle + \frac{3}{4}\frac{a}{\Delta\omega_O}\frac{A_O^2 \omega}{\omega^2 - k^2 c^2} I_c \langle \frac{dJ_p}{dt} \rangle + \left[\Delta\omega_O^2 + \frac{3}{4}a\frac{A_O^2 \omega}{\omega^2 - k^2 c2} I_s \right.$$

$$- a^2(D_0{}^2 + D_1{}^2) + 3a^2 \frac{A_0\omega}{\omega^2 - k^2c^2}(D_0 - \frac{3}{4}\frac{A_0\omega}{\omega^2 - k^2c^2})\Big] J_p$$

$$= -\frac{3}{8}a\frac{A_0{}^2\omega}{\omega^2 - k^2c^2}\frac{P}{\Delta\omega_0}\Big[(D_0 - \frac{A_0\omega}{\omega^2 - k^2c^2}) + A_0 I_s + aD_0\Big]I_c +$$

$$\frac{1}{2}PA_0(\Delta\omega_0 + \langle\Delta\omega\rangle)I_c - P\frac{da}{dt}(D_0 - \frac{1}{2}\frac{A_0\omega}{\omega^2 - k^2c^2}) \quad (B.33)$$

where

$$I_c = \int_0^t dt'a'\cos\langle\phi - \phi'\rangle$$

$$I_s = \int_0^t dt'a'\sin\langle\phi - \phi'\rangle$$

If we let

$$C_0 = P(D_0 - \frac{1}{2}\frac{A_0\omega}{\omega^2 - k^2c^2})$$

$$2S = \frac{3}{4}\frac{aA_0{}^2\omega}{\Delta\omega_0(\omega^2 - k^2c^2)}I_c$$

$$\Delta\omega_1{}^2 = \Delta\omega_0{}^2 - a^2\Big[D_1{}^2 + (D_0 - \frac{3}{2}\frac{A_0\omega}{\omega^2 - k^2c^2})^2\Big] +$$

$$\frac{3}{4}a\frac{A_0{}^2\omega}{\omega^2 - k^2c^2}I_s$$

equation B.33 becomes

$$\left\langle \frac{d^2 J_p}{dt^2} \right\rangle + 2S\frac{dJ_p}{dt} + (\Delta\omega_1)^2 J_p =$$

$$- C_o\frac{da}{dt} - SP\left[aD_o + \left(D_o - \frac{A_o\omega}{\omega^2 - k^2 c^2}\right) + \right.$$

$$\left. A_o I_s \right] + \frac{1}{2}PA_o I_c (\langle\Delta\omega\rangle + \Delta\omega_o) \tag{B.34}$$

Equation B.14 relates the polarization current density and the radiation field intensity. Using this, and the fact that $\Delta\omega$ plays a role similar to the population inversion function in a two-level system which allows us to define a population inversion function

$$W = \frac{n_o \gamma_o m_o c^2}{2\hbar\omega_o^2}(\langle\Delta\omega\rangle + \Delta\omega_o) \tag{B.35}$$

where $\hbar$ is Planck's constant.

We finally get a single equation that governs the non-linear evolution of the radiation field intensity

$$\left[\frac{d_3}{dt^3} + 2S\frac{d^2}{dt^2} + (\Delta\omega_1^2 + c_1)\frac{d}{dt}\right]E_o =$$

$$a_O\left\{1 - \frac{\sigma\varepsilon_O(\omega - kv_z)}{2\gamma_O\Delta\omega_O n_O m_O c^2}\left[E_O^2(t) - E_O^2(0)\right]\right\}$$

$$\int_O^t E_O(t')\cos\langle\phi - \phi'\rangle dt' - S\left[2c_1 E_O +\right.$$

$$\left. + \frac{a_O}{\Delta\omega_O}\int_O^t E_O(t')\sin\langle\phi - \phi'\rangle dt'\right] \qquad (B.36)$$

$$\langle\phi - \phi'\rangle = -\Delta\omega_O\int_{t'}^t\left\{1 - \frac{\sigma\varepsilon_O(\omega - kv_z)}{2\gamma_O n_O m_O c^2}\right.$$

$$\left[E_O^2(\tau) - E_O^2(0)\right]\right\}d\tau$$

$$a_O = GA_O\Delta\omega_O$$

$$\Delta\omega_O = \omega - \omega_O$$

$$\omega_O = N\frac{\Omega_O}{\xi} + kv_{zo}$$

$$G = \frac{\omega_p^2}{\sigma\omega}\frac{a_O}{\gamma_O} J_N'(\alpha) J_{m-N}^2(k_t R_O)$$

$$\omega_p^2 = \frac{n_O e^2}{\varepsilon_O m_O}$$

$$A_O = \left(\frac{\Omega_O}{\gamma_O k_t c}\right)^2 (\omega^2 - k^2 c^2)\alpha_O J_N'(\alpha_O)$$

$$\alpha_O = k_t R_L$$

$$c_1 = G\left[D_O - A_O\frac{\omega}{2(\omega^2 - k^2 c^2)}\right]$$

$$D_O = (\omega - kv_{zo})\frac{1}{\alpha_O}\frac{d}{d\alpha_O}\left[\alpha_O J_N{}'(\alpha_O)\right]$$

$$\Delta\omega_1{}^2 = \Delta\omega_O{}^2 - a^2\left\{D_1{}^2 + \left[D_O - 3A_O\frac{\omega}{2(\omega^2 - k^2c^2)}\right]^2\right\} +$$

$$\frac{3}{4} a(A_O{}^2 \frac{\omega}{\omega^2 - k^2c^2})I_s$$

$$a = (-1)^N \frac{B_{zo}}{B_O} J_{m-N}(k_tR_O)$$

$$D_1{}^2 = (\omega - kv_{zo})^2 J_N{}'(\alpha_O)\frac{d}{d\alpha_O}\left\{\frac{1}{\alpha_O}\frac{d}{d\alpha_O}\left[\alpha_O J_N{}'(\alpha_O)\right]\right\}$$

$$S = \frac{3}{8}\frac{aA_O{}^2\omega}{\Delta\omega_O(\omega^2 - k^2c^2)}I_c$$

$$I_c = \int_0^t dt'\ a(t')\ \cos<\Delta\phi(t - t')>$$

$$I_s = \int_0^t dt'\ a(t')\ \sin<\Delta\phi(t - t')>$$

$$\sigma = (1 - \frac{m^2}{k_t{}^2R_w{}^2})J_m{}^2(k_tR_w)$$

BIBLIOGRAPHY

[1] The gyrotron
V.A. Flyagin, A.V. Graponov, M.I. Peletin, and V.K. Yulpatov.
IEEE-MTT, Vol. MTT-25, #6, June 1977

[2] The Electron cyclotron maser. An historical survey
J.L. Hirschfield and V.L. Granatstein.
IEEE-MTT, Vol. MTT-25, #6, June 1977

[3] Comparative study of the axial and azimuthal bunching mechanisms in electromagnetic cyclotron instabilities
K.R. Chu and J.L. Hirschfield.
Physics of Fluids, Vol. 21, #3, March 1978

[4] Simple macroscopic theory of cyclotron maser instabilities
Y.Y. Lau.
IEEE-Electron Devices, Vol ED-29, #2, February 1982

[5] A unified theory of diocotron, cyclotron maser, and negative-mass instabilities
Y.Y. Lau.
IEEE-Electron Devices, Vol. ED-31 #3, March 1984

[6] Relativistic effect in electron cyclotron transverse wave devices
G.J. Sehn and R.E. Hayes.
IEEE-Electron Devices, December 1969

[7] Enhanced microwave emission due to the transverse energy of a relativistic electron beam
M. Friedman, D.A. Hammer, W.M. Manhelmer and P.S. Sprangle.
Physical Review Letters, Vol. 31 #12, September 1973

[8] Stimulated emission of radiation by relativistic electrons in a magnetic field
J. Schneider.
Physical Review Letters, Vol. 2 #12, June 1959

[9] Radiation transfer and the possibility of negative absorbtion in radio astronomy
R.Q. Twiss.
Austrian Journal of Physics, Vol. 11 pp. 564-579, 1958

[10] The gyrotron : high power source of millimeter and submillimeter waves
A.A. Andronov, V.A. Flyagin, A.V. Gaponov,
A.L. Goldenberg, M.I. Peletin, V.G. Osof, and
V.K Yulpatov.
Infrared Physics, Vol 18 pp. 385-395, 1978

[11] Cyclotron autoresonance masers of millimeter-wave range
V.L. Bratman, G.G. Denisov, and M.M. Ofitserov.
Relativistic H.F. Electronics (Institute of Applied Physics, Gorky), 1983

[12] Spatial and temporal coherence of a 35 GHz gyro-monotron using the TE_{o1} circular mode
M.E. Read, R.M. Gilgenbach, R.F. Lucay Jr., K.R. Chu, A.T. Drobot, and V.L. Granatstein.
IEEE-MTT, Vol. 28 #8, August 1980

[13] A high power gyrotron operating in the TE_{o41} mode
B. Arfin, K.R. Chu, D. Dialetis, and M.E. Read.
IEEE-Electron Devices, Vol. ED-29 #12, december 1982

[14] A Gyrotron study program
G. Boucher, P. Boulanger, P. Charbit, G. Faillon,
A. Herscovici, E. Kammerer, and G. Mourier. Infrared and Millimeter waves, Vol. 9, 1983

[15] The problems of increase in power, efficiency and
     frequency of gyrotrons for plasma investigation
     A.S. Fix, V.A. Flyagin, A.L. Goldenberg,
     V.I. Khizhnyak, S.A. Malygin, S.E. Tsimring, and
     V.E. Zapevalov.
     International Journal of Electronics, Vol. 57 #6,
     1984

[16] Gyrotrons for high power millimeter wave genera-
     tion
     H.R. Jory, F. Friedlander, S.J. Hegji,
     J.F. Shively, and R.S. Symons.

[17] Cyclotron resonance devices
     R.S. Symons, and H.R. Jory.
     Advances in Electronics and ElectroPhysics, Vol.
     55, 1981

[18] Gyrotron-TWT operating characteristics
     P.E. Ferguson, G. Valier, and R.S. Symons.
     IEEE-MTT, Vol MTT-29 #8, August 1981

[19] An experimental gyro-TWT
     R.S. Symons, H.R. Jory, S.J. Hegji, and P.E. Ferguson.
     IEEE-MTT, Vol. MTT-29 #3, March 1981

[20] Measurements of gain for slow cyclotron waves on an
     annular electron beam
     H. Guo, L. Chen, H. Keren, J.L. Hirschfield, S.Y. Park,
     and K.R. Chu.
     Physical Review Letters, Vol. 49 #10, September 1982

[21] An experimental wide-band gyrotron traveling wave
     amplifier
     L.R. Barnett, Y.Y. Lau, K.R. Chu. and V.L. Granatstein.
     IEEE-Electron Devices, Vol. ED-23 #7, July 1981

[22] Theory of a wide-band distributed gyrotron traveling
     wave amplifier
     K.R. Chu, Y.Y. Lau, L.R. Barrett, and V.L. Granatstein.
     IEEE-Electron Devices, Vol. ED-28 #7, July 1981

[23] Large Signal theory of a two-stage wide band gyro-TWT
A.K. Ganguly and S. Ahn.
IEEE-Electron Devices, Vol. ED-31 #4, April 1984

[24] An active circulator-gyrotron traveling wave amplifier
Y.Y. Lau, L.R. Barnett, and J.M. Baird
IEEE-Electron Devices, Vol. ED-31 #3, March 1984

[25] The helically wrapped circular waveguide
K.J. Bunch and R.W. Grow.
IEEE-Electron Devices, Vol. ED-34 #8, August 1987

[26] Theory of gyrotron amplifiers in disc or helix loaded
waveguides
J.Y Choe and H.S. Uhm.
International Journal of Electronics, Vol. 53 #6, 1982

[27] The theory of disc-loaded waveguides
E.L. Chu and W.W. Hansen.
Journal of Applied Physics, Vol. 18, November 1947

[28] Multimode oscillation and mode competition in high
frequency gyrotrons
K.E. Kreischer, R.J. Temkin, H.R. Fetterman, and
W.J. Mulligan.
IEEE-MTT, Vol. MTT-32 #5, May 1984

[29] Analysis of the electron cyclotron maser instability
S.P. Kuo and B.R. Cheo.
Physics Letters, Vol. 103A #9, July 1984

[30] Analysis of the harmonic gyrotron traveling wave ampli-
fier
S.P. Kuo, S.C. Kuo, B.R. Cheo, and M.C. Lee.
International Journal of Infrared and Millimeters
Waves, Vol. 7 #4, 1986

[31] Theory and simulation of the gyrotron traveling wave
amplifier operating at cyclotron harmonics
K.R. Chu, A.T. Drobot, H.H. Szu, and P. Sprangle.
IEEE-MTT, Vol. MTT-28 #4, April 1980

[32] Waveguide handbook
Edited by N. Marcuvitz.
McGraw Hill, 1951

[33] The reflection of an electromagnetic plane wave by an
infinite set of plates
J.F. Carlson and A.E. Heins.
Quarterly of Applied Mathematics, Vol 4 #4, January
1947

[34] Self-consistent large signal theory of the gyrotron
traveling wave amplifier
A.K. Ganguly and S. Ahn.
International Journal of Electronics, Vol. 53 #6, 1982

[35] Electromagnetic slow wave systems
P.M. Bevensee.
Wiley, 1964

[36] General mode analysis of a gyrotron dispersion equation
J.Y. Choe and S. Ahn.
IEEE-Electron Devices, Vol. ED-28 #1, Jnuary 1981

[37] The linear and self consistent non-linear theory of the
electron cyclotron maser instability
P. Sprangle and A.T. Drobot.
IEEE-MTT, Vol. MTT-25 #6, June 1977

[38] Coherent non-linear theory of a cyclotron instability
P. Sprangle and W. M. Manheimer.
Physics of fluids, Vol. 18 #2, February 1975

[39] A note on gyrotron traveling wave amplifiers using
rectangular waveguides
Y.Y. Lau and L.R. Barnett.
IEEE-Electron Devices, Vol. ED-30 #8, August 1983

[40] AC Space charge effects in gyrotrons
G. Dohler.
International Journal of Electronics, Vol. 56 #4, 1984

[41] The lasing mechanism in fast-wave devices
G. Dohler.
IEEE-Electron Devices, Vol. ED-31 #3, March 1984

[42] Measured performance of gyrotron oscillators and ampli-
fiers
V.L. Granatstein, M.E. Read, and L. Barnett.
Infrared and Millimeter Waves, Vol. 5, 1982

[43] Status review of research on millimeter wave tubes
J. Feinstein and K. Felch.
IEEE-Electron Devices, Vol. ED-34 #2, February 1987

[44] Study of noise amplification mechanism in Gyrotrons
K.R. Chen and K.R. Chu.
IEEE-MTT, Vol. MTT-34 #1, January 1986

[45] Field theory of guided waves
R. Collins.
McGraw Hill

[46] A flush-mounted leaky-wave antenna with predictable
patterns
R.C. Honey.
I.R.E. Trans. on Antennas and Propagation, October 1959

[47] Theory and numerical modeling of a compact low field
high frequency gyrotron
P. Vitello, W.H. Miner, and A.T. Drobot.
IEEE-MTT, Vol. MTT-32 #4, April 1984

[48] Realization of a stable and highly efficient gyrotron
for controlled fusion research
Y. Carmel, K.R. Chu, M. Read, A.K. Ganguly,
D. Dialetis, R. Seeley, J.S. Levine, and
V.L. Granatstein.
Physical Review Letters, Vol. 50 #2, January 1983

[49] Multimode analysis of quasi-optical gyrotrons and
gyroklystrons
A. Bondeson, W.M. Manheimer, and E. Ott.
Infrared and Millimeter Waves, Vol. 9

[50] Practical considerations in the design of a higher
     power 1mm gyromonotron
     J.D. Silverstein, M.E. Read, K.R. Chu, and A.T. Drobot.
     IEEE-MTT, Vol. MTT-28 #9, September 1980

[51] A 125-260-GHz gyrotron
     G.F. Brand, N.G. Douglas, M. Gross, J.Y.L. Ma,
     L.C. Robinson, and C. Zhiyi.
     IEEE-MTT, Vol. MTT-32 #1, January 1984

[52] Methods of efficiency enhancement and scaling for the
     gyrotron oscillator
     K.R. Chu, M.E. Read, and A.K. Ganguly.
     IEEE-MTT, Vol. MTT-28 #4, April 1980

[53] Experimental examination of the enhancement of gyrotron
     efficiencies by use of profiled magnetic fields
     M.E. Read, K.R. Chu, and A.J. Dudas.
     IEEE-MTT, Vol. MTT-30 #1, January 1982

[54] Loaded Q's and field profiles of tapered axisymetric
     gyrotron cavities
     H. Derfler, T.J. Grant, and D.S. Stone.
     IEEE-Electron Devices, Vol. ED-29 #12, December 1982

DATE
FILMED
8